

Suppression of turbulence and transport by sheared flow

P. W. Terry

Department of Physics, University of Wisconsin-Madison, Madison, Wisconsin 53706

The role of stable shear flow in suppressing turbulence and turbulent transport in plasmas and neutral fluids is reviewed. Localized stable flow shear produces transport barriers whose extensive and highly successful utilization in fusion devices has made them the primary experimental technique for reducing and even eliminating the rapid turbulent losses of heat and particles that characterize fusion-grade plasmas. These transport barriers occur in different plasma regions with disparate physical properties and in a range of confining configurations, indicating a physical process of unusual universality. Flow shear suppresses turbulence by speeding up turbulent decorrelation. This is a robust feature of advection whenever the straining rate of stable mean flow shear exceeds the nonlinear decorrelation rate. Shear straining lowers correlation lengths in the direction of shear and reduces turbulent amplitudes. It also disrupts other processes that feed into or result from turbulence, including the linear instability of important collective modes, the transport-producing correlations between advecting fluid and advectants, and large-scale spatially connected avalanche-like transport events. In plasmas, regions of stable flow shear can be externally driven, but most frequently are created spontaneously in critical transitions between different plasma states. Shear suppression occurs in hydrodynamics and represents an extension of rapid-distortion theory to a long-time-scale nonlinear regime in two-dimensional stable shear flow. Examples from hydrodynamics include the emergence of coherent vortices in decaying two-dimensional Navier-Stokes turbulence and the reduction of turbulent transport in the stratosphere.

CONTENTS

I. Introduction	109	C. Reversed-field pinch	147
II. Phenomenology and Physics	113	D. Linear magnetic configurations	147
A. Background concepts	113	VII. Transition to Enhanced-Confinement States	148
1. Basic turbulence properties	113	A. Bifurcation of plasma state	148
2. Confinement of turbulent plasmas	113	B. Transition modeling	148
B. Scaling theory for suppression of turbulence	116	1. Two-step transition models	149
1. Dimensional analysis	116	2. First-order critical transition theory	150
2. Relative motion of fluid parcels	117	3. Second-order critical transition theory	151
3. Asymptotic analysis	119	C. Transient phenomena	153
C. Role of flow shear in linear instabilities	120	VIII. Generalization to Related Systems	153
D. Observations of transport barriers in plasmas	121	A. Coherent vortices in Navier-Stokes turbulence	153
E. Experimental and numerical tests	122	B. Transport of stratospheric constituents	155
III. Related Hydrodynamic Phenomena and Concepts	125	1. Meridional transport across zonal flows	155
A. Stable shear flow	125	2. β -plane model of meridional transport	156
B. Rapid-distortion theory	126	C. Shear flow in self-organized criticality	158
C. Geostrophic flows and other examples	128	IX. Conclusions	158
IV. Generation of Sheared $E \times B$ Flow	130	A. Summary	158
A. Radial force balance	130	B. Open questions	160
B. Mean ion flows	131	C. Future directions	161
1. Reynolds stress	132	Acknowledgments	161
2. External biasing	133	References	161
3. Injected radio-frequency waves	134		
4. Orbit loss	134		
5. Nonsymmetric transport	135		
C. Miscellaneous processes	136		
V. Suppression in Toroidal Plasmas	136		
A. Plasma geometry and magnetic topology	136		
1. Shear flow stability with magnetic shear	137		
2. Instabilities in a nonuniform magnetic field	138		
3. Shear straining in a torus	140		
B. Effect of flow shear on transport fluxes	141		
VI. Flow Shear and Enhanced Plasma Confinement	143		
A. Tokamak	143		
1. Spontaneous edge transport barrier	143		
2. Externally induced edge transport barrier	144		
3. Spontaneous internal transport barriers	145		
4. Externally induced internal transport barrier	146		
B. Stellarator	146		

I. INTRODUCTION

Turbulent transport can be greatly reduced in the presence of stable shear flow. The mechanism (Biglari, Diamond, and Terry, 1990) is quite simple. When a fluid eddy is placed in a stable laminar background flow whose speed varies transverse to the flow direction, the eddy is stretched and distorted as different fluid parcels in the eddy are advected (carried along) at different speeds. If the eddy is isolated, it can be stretched to many times its original scale length. When the eddy is part of a turbulent flow, however, it loses coherence when stretched to the eddy coherence length along the direction of the background flow (see Fig. 1). The eddy coherence length is the distance over which the eddy flow remains correlated and can be thought of as roughly the distance between two adjacent eddies of

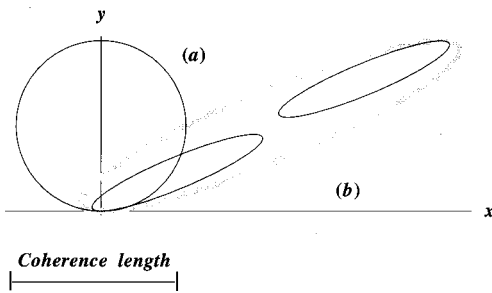


FIG. 1. A reference eddy [(a), no shear flow] sheared by unidirectional plane shearing (b) with $u_x(y) = \alpha y$. If the eddy is isolated it stretches into the shape indicated by the gray shaded curve. In turbulence, the eddy loses coherence in a coherence length, represented as a breakup into two eddies. The loss of coherence reduces the y scale relative to that of the reference eddy.

comparable scale, a distance on the order of the eddy diameter in fully developed turbulence. Fluid parcels that move an eddy coherence length become subjected to the advecting flows of other eddies and are no longer identifiable with their original eddy motion. In the absence of the background shear flow, the time scale for this loss of coherence defines the eddy lifetime. Dimensionally, the eddy lifetime is the eddy rotation period, commonly called the eddy turnover time.

In the presence of a background shear flow whose rate of differential advection exceeds the eddy turnover rate, eddies stretch to a flow-wise eddy coherence length in a fraction of the time they would normally take to turn over were there no shear. Consequently, the eddy lifetime is shortened. Assuming turbulence whose driving source is unaffected by flow shear (such a source might be external stirring, or an instability associated, for example, with a thermal gradient), the decrease in the correlation time implies a decrease in turbulent intensity (eddy velocity). This follows because the rate of turbulent energy dissipation, given roughly by the turbulent energy divided by the correlation time, temporarily exceeds the forcing rate when the correlation time is reduced. This leads to a transient decay of turbulent energy until a new balance is established with lower energy. Also, because of the rapid flow-wise stretching (along the direction of the flow), fluid parcels traverse only a fraction of the original eddy diameter in the shear-wise direction (across the flow in the direction of the gradient of flow speed) before the eddy loses coherence. Eddy scales in the shear-wise direction are thus reduced as a consequence of the background shear flow. If an advected scalar is present, its rate of turbulent transport across the background shear flow is also reduced. This follows because the turbulent intensity and shear-wise eddy coherence length are reduced, thus reducing the speed and step size of a random-walk transport process.

In magnetically confined fusion plasmas, the reduction of cross-flow transport by shear flow is often localized to a region identifiable as a transport barrier. Such barriers are now widely utilized in fusion plasmas. Before the

discovery of the first robust and reproducible transport barrier by Wagner *et al.* (1982), plasma confinement and fusion energy production were seriously limited by small-scale turbulent fluctuations. These had long seemed irreducible, because they are driven by the steep gradients of temperature and density needed to confine and insulate hot fusion plasmas away from material surfaces. With shear suppression, the heat loss caused by these fluctuations has been controlled for the first time. Recent results underscore the impact of shear suppression. Record values of confinement time, fusion power output, fusion neutron yield, and the ratio of fusion power output to input heating power have been achieved using flow-shear-induced transport barriers in the plasma edge [in the hot ion H mode of the Joint European Torus (JET), Gibson *et al.*, 1998], or in plasmas inferred to have a large sheared flow and significant suppression of turbulence (in the supershot of the Toroidal Fusion Test Reactor; Ernst *et al.*, 1998). In other experiments shear suppression in the plasma core has led to the reduction of transport in tokamak plasmas by orders of magnitude to the minimum level set by thermal, collisional motion (Levinton *et al.*, 1995; Strait *et al.*, 1995). A variety of measurements have confirmed the role of flow shear in impeding the transport and diminishing the intensity of turbulence.

This review is intended to present the basic physics of flow-shear-induced transport barriers, to outline the extensive developments in fusion plasma physics pertaining to such barriers, to examine related phenomena in hydrodynamics, and to explore wider applications of these ideas. Prior reviews¹ have been written for specialists and have given little or no discussion of applications outside the subject of magnetically confined plasmas. Moreover, whereas prior reviews have emphasized experimental phenomenology (Groebner, 1993; Burrell, 1994, 1997; Moyer *et al.*, 1995) or the theory of electric fields in plasmas as applied to collisional transport (Itoh and Itoh, 1996; Ida, 1998), this review treats turbulence as a fundamental feature of the systems of interest and develops key theoretical concepts of relevance to experimental phenomena. The level of presentation assumes expertise in neither plasma physics nor turbulence, but a knowledge of general physics at the level of a practitioner in any physics specialty area. This review emphasizes the striking robustness and universal character of flow-shear-induced transport reduction in plasmas. As described in Sec. VI, flow shear reduces transport and turbulence in a variety of magnetic confinement configurations and in different regions of the plasma ranging from the hot core to the cold edge. In contrast, the fluctuations themselves lack such universality, changing character from device to device (Liewer, 1985; Wootton *et al.*, 1990) and within any given device in different regions of the plasma (Durst *et al.*, 1993). The

¹These include Stambaugh *et al.*, 1990; Groebner, 1993; Burrell, 1994, 1997; Moyer *et al.*, 1995; Itoh and Itoh, 1996; Carreras, 1997; Ida, 1998.

universality of shear suppression in plasmas and the dynamical similarities between plasmas and ordinary non-ionized fluids strongly suggest that shear suppression should occur in nonionized fluids and in other types of dynamic media. Section VIII provides a few examples that have been examined to date. These examples are intended to be suggestive, not exhaustive, and hopefully will stimulate further exploration of this topic. The review is structured so that Sec. II provides a self-contained, brief overview of the basic physics and phenomenology, with development, detail, and applications reserved for the remaining sections.

After a brief presentation of underlying concepts, Sec. II describes the basic scaling theory for shear suppression (Biglari, Diamond, and Terry, 1990), using both simple dimensional arguments and more rigorous mathematical analyses. Collective instabilities in plasmas can also be stabilized by flow shear (that is not itself unstable), as illustrated by a heuristic criterion (Hassam, 1991; Waltz, Kerbel, and Milovich, 1994). Turning to experiment, we describe the basic features of the type of barrier first observed and studied in plasmas (Wagner *et al.*, 1982). The presence of flow shear was not initially detected, but the features that were observed, specifically, a localized steepening of gradients of density and temperature, and improved confinement, indicated a localized barrier to transport. Later measurements, including those of fluctuation levels, transport fluxes, and spatial profiles of mean flows, confirmed that flow shear suppresses turbulence and transport in this type of barrier. Specific experimental tests of the theory are described by Ritz *et al.* (1990), La Haye *et al.* (1995), and Moyer *et al.* (1995). These include measurements of the correlation time, shear-wise correlation length, amplitude reduction, and the criterion for significant reduction, and a comparison with the predictions of the scaling theory.

Suppression of turbulence and transport by flow shear occurs in nonionized fluids but is not a familiar hydrodynamic phenomenon. The reason stems from three additional requirements for suppression, beyond the criterion that the shearing rate exceed the eddy turnover rate. These requirements are routinely met in fusion plasmas, but are difficult to satisfy in nonionized fluids. They stipulate that the shear flow must be stable, that turbulence must remain in the domain of flow shear for longer than an eddy turnover time, and that the dynamics should be two dimensional. In nonionized fluids, shear flows are typically unstable, shear is often present only for a short time in the frame of the flow, and the dynamics are usually three dimensional. As discussed in Sec. III, under these conditions turbulence is driven by shear instead of suppressed, is advected into and out of the region of shear before the nonlinearity can decorrelate fluctuations, or its vorticity may be amplified. When turbulence is advected through a region of strong flow shear in a time shorter than the eddy turnover time, rapid-distortion theory, a widely used technique in hydrodynamics, can be applied to trace out fluid motions (for recent reviews see Savill, 1987; Hunt and Carruth-

ers, 1990; Hunt, Carruthers, and Fung, 1991). In Sec. III.B, rapid-distortion theory is shown to be the short-time, linear counterpart of the long-time, nonlinear scaling theory described in Sec. II.B. Section III.C introduces stratospheric geostrophic flow, a type of hydrodynamic flow that satisfies the three requirements stated above. (Geostrophic flows are flows whose time scale exceeds the planetary rotation rate.) In simulations, suppression of geostrophic turbulence in the strong-shear regions of a stable, large-scale jet has been noted, although the mechanism was not elucidated (Shepherd, 1987). Other hydrodynamic examples that relate to the scaling theory and underlying physics are also briefly discussed in Sec. III.C.

In plasma transport barriers, the flow shear is produced by forces in the plasma that respond both to conditions in the plasma and to external forces. The creation of transport barriers in plasmas thus involves the suppression of turbulence by a given shear flow (as described in Sec. II) and the generation of flow. These two processes can be linked in complicated ways. The physics of flow generation in plasmas is presented in Sec. IV by examining momentum balances for plasma flows and the individual forces that contribute to the balances. The flow responsible for plasma transport barriers is the $E \times B$ drift, a motion common to all plasma charge species, so named because its magnitude and direction are proportional to the cross product of the local electric and magnetic fields. Section IV describes how this flow is affected by the equilibrium ion pressure, ion rotation rates, turbulent Reynolds stresses (Carreras, Lynch, and Garcia, 1991; Diamond and Kim, 1991), externally manipulated electric fields (Taylor *et al.*, 1989), preferential loss of a plasma charge species (Itoh and Itoh, 1988; Shaing and Crume, 1989), and anisotropies in transport fluxes (Hassam *et al.*, 1991). The relationships between flow-shear-induced suppression and flow generation are developed in Sec. VII.

The basic theoretical notion of flow-shear-induced transport reduction was formulated for a straight plasma in a uniform magnetic field. In Sec. V the theory is extended to account for the complications of toroidal plasma confinement geometry and magnetic-field inhomogeneity. The toroidal configuration and the spatial variation of the confining magnetic field impart a particular structure to the turbulence and to plasma flows. Consequently, the scaling theory of Sec. II continues to serve as a paradigm for the effect of flow shear in turbulent plasmas, but the specifics of its predictions are modified for toroidal geometry (Hahn and Burrell, 1995).

A critical feature of the spatial variation of the magnetic field in magnetic confinement systems is magnetic shear, a measure of the degree of field-line twist at different locations within the plasma. Typically magnetic shear localizes fluctuations to the vicinity of special surfaces within the plasma. This property imposes a constraint on the way in which flow shear affects fluctuations (Carreras *et al.*, 1992). Magnetic shear likewise affects the stability of sheared flows, significantly raising

the threshold of basic flow-shear-driven instabilities such as the Kelvin-Helmholtz instability (Chiueh *et al.*, 1986). In Sec. V.B, the effect of flow shear on the fluctuation correlations that underlie transport is introduced in the context of a simple model that includes magnetic shear (Ware *et al.*, 1996, 1998). This question is revisited in Sec. VIII.C, where the effect of flow shear on transport in systems with self-organized dynamics is examined (Diamond and Hahm, 1995).

Since the first observation of transport barriers in magnetically confined plasmas, significant progress has been made in controlling and manipulating these barriers. These efforts are reviewed in Sec. VI. Historically, flow-shear-induced transport barriers were first produced spontaneously in the edge of a type of toroidal plasma known as a tokamak (Wagner *et al.*, 1982). Later it was found that the edge flow shear region in such barriers could be externally induced by charging the plasma edge with a biased probe (Taylor *et al.*, 1989). It was also discovered that under certain conditions, the edge flow shear region extended itself inward toward the center of the plasma, producing a core transport barrier (Jackson *et al.*, 1991). Recently, transport barriers have been initiated in the core, independently of edge barrier formation (Levinton *et al.*, 1995; Strait *et al.*, 1995; Kimura *et al.*, 1996; Mazzucato *et al.*, 1996). In these plasmas, the turbulent transport is reduced to the point where loss rates are governed by particle collisions. The spontaneous core barriers are often produced in conjunction with certain magnetic-shear configurations, but otherwise exhibit common features of edge transitions. It has been predicted that core barriers can also be induced externally using injected rf waves (Craddock and Diamond, 1991). Experimental efforts to induce core barriers in this fashion have been limited and have produced mixed results (LeBlanc *et al.*, 1995; 1999). The above results pertain to the tokamak, the most developed magnetic confinement device. Alternative magnetic confinement approaches to the tokamak have also achieved enhanced confinement operation in connection with the formation of regions of strong flow shear. Work done in stellarator, reversed-field pinch (RFP), tandem mirror, and Z-pinch configurations is reviewed in Secs. VI.B–D.

Flow-shear-induced transport barriers in plasmas are created as part of a transition in which mean quantities transiently undergo an adjustment to new values in response to an internally or externally driven change within the plasma. Prior to the transition, the $E \times B$ flow is not strongly sheared, and the fluctuations are large. After the transition there is a large shear in the $E \times B$ flow, and the fluctuations have diminished. Other quantities involved in momentum balances, such as ion rotation rates, can also change dramatically at the transition. Because the plasma state undergoes a fundamental change in properties as it passes through the transition, the transition is generally labeled as a bifurcation process. Section VII presents transition phenomenology as observed in experiment and reviews theoretical models of the transition. The theoretical models generally fall

into two categories, dictated in part by which flow-shear-generating force is treated as dominant, an issue not yet fully resolved. In the first step of two-step transition theories (Itoh and Itoh, 1988; Shaing *et al.*, 1990), conditions within the plasma or an external force (such as the force produced by an electrically biased probe), charge up the plasma and create a sheared $E \times B$ flow. In the second step, turbulence and transport are reduced in response to the flow shear. In single-step transitions (Hinton, 1991; Hinton and Staebler, 1993; Diamond *et al.*, 1994; Terry *et al.*, 1994), flow generation and turbulence suppression evolve as integrated elements of the transition and cannot be separated. Single-step theories are analogous to first- and second-order phase transitions in continuous media. Mathematically, the plasma states before and after transition are fixed points of turbulent fluid closures that model the key forces involved in the transition.

Section VIII is devoted to the application of flow-shear-induced transport reduction to nonplasma systems. Efforts in this area are in their infancy. Section VIII.A reviews work that shows that certain vorticity fluctuations in two-dimensional Navier-Stokes turbulence become coherent (McWilliams, 1984) as a result of the strong flow shear in their periphery (Terry, 1989; Terry *et al.*, 1992). This flow shear suppresses ambient turbulence, composed of the eddy motions of lower-amplitude vorticity, enabling the vortex to escape being mixed. For a vorticity fluctuation to become coherent it must exceed an amplitude threshold. The threshold is consistent with the evolution of the vorticity probability distribution function in spatially intermittent turbulence, and with the spatial structure of coherent vortices in the simulations. Flow shear has also been speculated to play a role in atmospheric and oceanic transport barriers, as described in Sec. VIII.B. Transport barriers in the stratosphere have been detected through satellite observations and *in situ* measurements, and have generally been attributed to other mechanisms (McIntyre and Palmer, 1984). Theoretical and numerical modeling of the transport of atmospheric constituents in two-dimensional stratospheric turbulence (Ware *et al.*, 1995, 1999) indicates that there is suppression of turbulent transport by the flow shear associated with polar jets and zonal flow (flows along a fixed latitude). The role this process plays in observed transport barriers, which involve other complex geophysical processes, is an open question. Section VIII.C examines dynamical media in which transport is governed by a process with self-organized criticality (Bak, Tang, and Wiesenfeld, 1987). The presence of wind shear incident on sand pile automata suppresses the excitation of large-scale avalanche-like transport events (Diamond and Hahm, 1995; Newman *et al.*, 1996).

The discussion of Sec. VIII.C completes an elucidation of four distinct effects of stable flow shear on fluctuations. These are (1) the fundamental process of direct reduction of scales and amplitude in turbulence (Sec. II.B), (2) the stabilization of collective modes that are otherwise linearly unstable (Sec. V.A.2), (3) the disrupt-

tion of correlation between the fluctuations of an advectant and the advecting flow, resulting in a reduction of transport beyond that accounted for by decreased fluctuation amplitudes (Sec. V.B), and (4) the disruption of the extended correlation of large-scale avalanche-like transport events (Sec. VIII.C). This review concludes with a brief summary in Sec. IX, followed by a discussion of open questions and current research directions.

II. PHENOMENOLOGY AND PHYSICS

A. Background concepts

1. Basic turbulence properties

Flow shear affects turbulence because it modifies the time required for correlated fluid motion of a given scale to lose coherence. The loss of correlation arises from the nonlinearity of turbulent advection, which acts both to scramble fluid motion and to spread its energy from one scale to another. This process can be readily appreciated from the Navier-Stokes equation,

$$\left[\frac{\partial \mathbf{u}}{\partial t} + (\mathbf{u} \cdot \nabla) \mathbf{u} \right] = -\frac{1}{\rho} \nabla p + \mu \nabla^2 \mathbf{u}, \quad (2.1)$$

where ρ is the mass density, \mathbf{u} is the flow field, p is the pressure, and μ is the kinematic viscosity. For incompressible flow ($\nabla \cdot \mathbf{u} = 0$) the Laplacian of the pressure is related to the divergence of the advective term $\{\rho^{-1} \nabla^2 p = \nabla \cdot [(\mathbf{u} \cdot \nabla) \mathbf{u}]\}$ and therefore can be incorporated into the advective derivative (Kraichnan, 1959). The evolution of the flow is governed by two forces, each with a characteristic time scale. These are the inertial force, represented by the advective term (with pressure included through the identity just mentioned), and the dissipative force, represented by the viscous term. The inertial force describes self-advection of the flow. From the second term of Eq. (2.1), the time scale of the inertial force is

$$\frac{1}{\tau_e} = \frac{u}{l}, \quad (2.2)$$

where u and l are characteristic flow and length scales. Turbulence consists of a hierarchy of such scales. Because turbulent flow possesses vorticity, $\boldsymbol{\omega} = \nabla \times \mathbf{u}$, it is useful to think of the flow as a hierarchy of eddies of different scales. Consequently, if u is the characteristic flow velocity of eddies of scale l , τ_e is the time scale of that eddy. At each position, the flow is a superposition of many eddies of different scales all contributing to the advection process. The flow is random because the transfer of energy between scales is constantly changing the configuration of eddies. Motion at a given scale loses coherence, i.e., any given eddy decays, due to advection by other eddies. The decay time is τ_e because that is the unique characteristic time of the advection process. This time is called the eddy turnover time. By the time an eddy rotates, its energy has been transferred to other eddies and it has decayed. The energy transfer process is

conservative, i.e., in the absence of viscosity, advection causes no loss of energy, only transfer of energy from motion on one scale to motion on another. The invariance of energy leads to self-similar spectral energy transfer. The turbulent flow velocity at each scale adjusts itself so that the energy transfer rate u^2/τ_e is invariant for all scales in which viscosity has a negligible effect on the dynamics (Kolmogorov, 1941).

The effect of viscosity is quantified by the viscous dissipation rate, $\tau_d^{-1} = \mu/l^2$, the rate at which the energy of fluid motion is dissipated and converted to heat. Because viscous dissipation is diffusive (giving the l^2 factor in the denominator of τ_d^{-1}), the dissipation rate increases at smaller scales faster than the turbulent decorrelation (eddy turnover) rate. Therefore, at large scales, $\tau_d^{-1} < \tau_e^{-1}$, and energy is transferred between scales with negligible dissipation, establishing the self-similar energy cascade. At smaller scales, $\tau_d^{-1} > \tau_e^{-1}$, and energy is dissipated before advection can pass it to other scales, terminating the cascade. In three-dimensional (3D) Navier-Stokes turbulence, energy injected at large scale, where $\tau_d/\tau_e \gg 1$, is transferred to successively smaller scales by the cascade. This process continues until reaching the Kolmogorov scale at which $\tau_d = \tau_e$, whereupon the cascade ceases and energy is converted to heat. The ratio of τ_d/τ_e for the flow U at the largest scale L defines the Reynolds number $\text{Re} = UL/\mu$, which for turbulent motion is necessarily much larger than unity. Scales between L and the Kolmogorov scale are referred to as the inertial range. The turbulence considered in this review is dominated by the inertial force, i.e., $\tau_d/\tau_e > 1$, so that the decorrelation rate is governed by turbulent advection and is given by the eddy turnover rate, Eq. (2.2).

2. Confinement of turbulent plasmas

In magnetically confined fusion plasmas it is necessary to contain and isolate from material surfaces ionized gases whose temperatures and densities exceed 10 keV (10^8 K) and 10^{13} particles/cm³. Moreover, confinement must be of sufficient duration for fusion interactions to replenish the heat lost from neutron fluxes, radiation, and transport. In most devices, the plasma is toroidal. By design, the current and magnetic field lie on nested tori within the plasma called magnetic-flux surfaces. Together, the current and magnetic field exert a bulk force on the plasma given by their vector cross product. This force is normal to the flux surfaces and can therefore contain the pressure of the plasma, as indicated in Fig. 2. For simplicity of presentation we treat only the case for which the flux surfaces have circular cross sections and are concentric. In this case, the normal direction is radially outward. The balance of magnetic force and pressure specifies a steady state of the mean ideal magnetohydrodynamics (MHD) equations (Freidberg, 1982). Experience has established that ideal MHD adequately reflects the force balance as measured in plasmas, with the magnetic field determined from the current density through Ampère's law. The mean states of ideal MHD

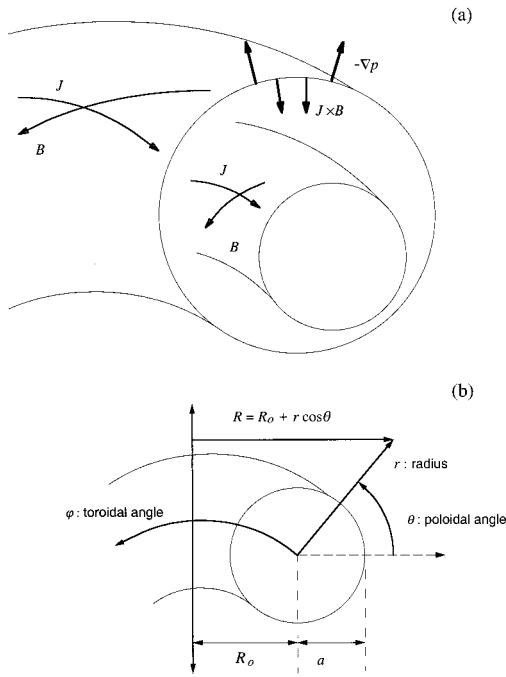


FIG. 2. Flux surfaces of a magnetically confined toroidal plasma. In (a), the currents and magnetic-field lines lie on nested tori. The $J \times B$ force balances the plasma pressure. In (b), simple toroidal coordinates used for flux surfaces with circular cross section are shown.

are often referred to as equilibria. These are not equilibria in the thermodynamic sense, and they are steady only over the short time scales of plasma motion for which the resistivity is negligible, i.e., for motions in which the magnetic field is carried by the plasma with negligible resistive diffusion (Jackson, 1975). Over longer time scales, slower processes, such as two-body collisions and resistive instabilities, cause the plasma to evolve from one ideal equilibrium to another and set the radial variation of pressure and current.

For the plasma to remain stationary on the ideal time scale, the equilibrium must be stable to collective motions whose evolution occurs on the ideal time scale. Stable, confining equilibria generally require that the magnetic field possess helicity, i.e., that it have components in both toroidal (the long way around the torus) and poloidal directions (the short way around). These directions are indicated in Fig. 2. It is also common for the field-line pitch, or the ratio of the toroidal component to the poloidal component, to vary in specified ways from one toroidal surface within the plasma to the next. A magnetic field with this radial variation is said to have magnetic shear. The magnetic field can be created by currents in external coils, which themselves must be helical if this is the sole source of the magnetic field, or by a combination of external windings and internal plasma current. In the most common toroidal configuration, known as the tokamak, external windings produce the toroidal field, and plasma current flowing toroidally produces the poloidal field. The toroidal field typically exceeds the poloidal field by an order of magnitude.

On the slower nonideal time scale, the pressure gradient and other inhomogeneities of the equilibrium drive slow-time-scale turbulent fluctuations. Together with two-body collisions, these fluctuations produce a flux of heat and particles out of the plasma. A class of slow-time-scale fluctuations characterized by spatial scales that are small compared to the dimensions of the plasma generally dominates the losses of heat and particles (Liewer, 1985; Wootton *et al.*, 1990). Although it has not been possible to attribute the dominant losses to fluctuations associated with a specific collective plasma mode, measurements have confirmed that the losses are due to fluctuations and not collisions (for example, see Ritz *et al.*, 1989). In some cases fluctuation-driven loss rates exceed those due to collisions by orders of magnitude.

Energy and particle loss rates are measured and employed as a figure of merit for confinement. In steady state, the energy loss rate is balanced by injected power, and the energy confinement time τ_E is defined as the ratio of thermal energy stored in the plasma to input power P :

$$\tau_E = \frac{\frac{3}{2} \int n_o (T_i + T_e) d^3x}{P}, \quad (2.3)$$

where T_i and T_e are ion and electron temperatures multiplied by the Boltzmann constant, and a neutral plasma with equal ion and electron number densities n_o is assumed. The energy confinement time τ_E is global, i.e., it is sensitive to losses occurring throughout the plasma. Physically, τ_E represents the rate of exponential decay of plasma energy when power sources are shut off. In the definition of confinement time, the loss mechanism is arbitrary, but in practice losses are dominated by fluctuations.

The fluxes that quantify fluctuation-driven losses depend on quadratic correlations of particular fluctuating fields. For example, the flux of electrons is governed by the continuity equation for the electron number density n_e :

$$\frac{\partial n_e}{\partial t} + \nabla \cdot (\mathbf{u}_e n_e) = 0, \quad (2.4)$$

where \mathbf{u}_e is the electron flow, specified either in a fluid description by a continuum equation for the flow, or in the kinetic description by the velocity moment of the single-particle probability distribution in the phase space of electron position and velocity. Toroidal and poloidal flows effectively lie on nested tori and therefore lead to no loss, provided the torus of interest intersects no material surface. Net losses are consequently governed by a radial derivative of the product of density and radial flow. Separating the density into ensemble-averaged and fluctuating components $\langle n_e \rangle$ and \tilde{n}_e , and considering equilibria in which the average radial flow is zero, $\langle u_{re} \rangle = 0$, we find that the average density is governed by

$$\frac{\partial \langle n_e \rangle}{\partial t} + \frac{\partial \Gamma_e}{\partial r} = 0, \quad (2.5)$$

where the fluctuation-induced particle flux Γ_e is

$$\Gamma_e = \langle \tilde{u}_r \tilde{n}_e \rangle. \quad (2.6)$$

In a turbulent flow, the advection of random density perturbations by the random motions of turbulent flow must be correlated; otherwise blobs of density are moved in all directions with equal probability. Such correlations naturally occur when density perturbations are produced by the random advection of a gradient of the average density $\langle n_e \rangle$. If the density perturbations are proportional to the gradient, substitution of the proportionality relationship into the flux yields an expression of Fick's law (i.e., $\Gamma_e = -D_e d\langle n_e \rangle / dr$, where D_e is the electron diffusion coefficient).

This review deals with fluctuating flows produced by $E \times B$ motion: in a plasma with magnetic and electric fields, individual particles (Krall and Trivelpiece, 1973) undergo circular rotation about magnetic-field lines and drift across the field with a velocity

$$\mathbf{u}_E = \frac{\mathbf{E} \times \mathbf{B}}{B^2}. \quad (2.7)$$

The $E \times B$ drift is independent of charge and identical for all charge species. It therefore represents a fundamental plasma flow. Under fairly general conditions the $E \times B$ flow is the sole advecting flow for fluctuations of density, temperature, and flow (Kim *et al.*, 1991). In a tokamak, the mean magnetic field B_0 is primarily toroidal, and the electric field is approximately an electrostatic fluctuation, i.e., $\mathbf{E} = -\nabla \tilde{\phi}$. The radial component of the fluctuating $E \times B$ drift is therefore $\tilde{u}_{E_r} = -B_0^{-1} \nabla_\theta \tilde{\phi}$, where ∇_θ is the derivative in the poloidal direction. If a Fourier transform is introduced for the coordinates in the toroidal and poloidal directions, the real part of the flux becomes

$$\text{Re } \Gamma_e = -B_0^{-1} \sum_{\mathbf{k}} k_\theta \text{Im} \langle \tilde{\phi}_{-\mathbf{k}} \tilde{n}_{\mathbf{k}} \rangle, \quad (2.8)$$

where $\tilde{\phi}_{-\mathbf{k}}$ and $\tilde{n}_{\mathbf{k}}$ are Fourier amplitudes, \mathbf{k} is the wave vector composed of poloidal k_θ and toroidal k_ϕ components, and the ensemble average is an average over toroidal and poloidal angles. In Eq. (2.8), the turbulent advection of density is represented as a sum over scales, $k = l^{-1}$, with each component describing the advection of a blob of scale k^{-1} by an eddy of the same scale. The nonzero correlation required for a net flux here imposes a constraint on the phase angle between the two complex Fourier amplitudes. The flux is maximal when the relative phase is $\pi/2$. Physically, the maximal case can be visualized as a blob being carried radially across the eddy diameter in exactly the eddy lifetime, whereupon the correlation has decayed and an increment of transport is complete. Nonlinear interactions create a new correlation and the process continues. There is also an ion flux, given by an identical relation, with \tilde{n} representing the ion density.

A similar procedure shows that the heat flux depends on the product of $\tilde{\phi}_{-\mathbf{k}}$ and $\tilde{p}_{\mathbf{k}}$,

$$\text{Re } Q_\alpha = -B_0^{-1} \sum_{\mathbf{k}} k_\theta \text{Im} \langle \tilde{\phi}_{-\mathbf{k}} \tilde{p}_{\alpha \mathbf{k}} \rangle, \quad (2.9)$$

where Q_α and $\tilde{p}_{\alpha \mathbf{k}}$ are the heat flux and Fourier pressure amplitude for charge species α . The heat flux, Eq. (2.9), contains both a conductive component, arising from the temperature contribution to the pressure, and a convective component, arising from the density contribution. These fluxes are classified as electrostatic because the electric field is specified solely by a scalar potential gradient. Magnetic fluctuations also produce transport. The transport is due to the motion of particles along magnetic fields having a radial component due to an instability or turbulence (Callen, 1977; Rechester and Rosenbluth, 1978; Terry *et al.*, 1996). Magnetic-fluctuation-induced fluxes of particles and heat involve correlations between the radial magnetic-field component and either the field-aligned current or the field-aligned heat flux (Prager, 1990).

Just as advection in the density continuity and energy equations leads to particle and heat transport through fluxes constructed from appropriate quadratic correlations, advection in the momentum equation leads to transport of momentum through a momentum flux with its corresponding quadratic correlation. Turbulent momentum transport was first studied for neutral fluids described by the Navier-Stokes equation. The i th component of the mean flow $\langle u_i \rangle$ satisfies

$$\frac{d\langle u_i \rangle}{dt} = \frac{1}{\rho} \frac{\partial}{\partial x_j} \Theta_{ij} = \frac{1}{\rho} \frac{\partial}{\partial x_j} (-p \delta_{ij} + 2\mu S_{ij} - \rho \langle \tilde{u}_i \tilde{u}_j \rangle), \quad (2.10)$$

where $d/dt = \partial/\partial t + \langle u_j \rangle \partial/\partial x_j$ is the advective derivative of the mean flow; $u_i = \langle u_i \rangle + \tilde{u}_i$ is the incompressible flow, Θ_{ij} is the total mean momentum flux or total mean flux; $S_{ij} = \frac{1}{2} (\partial \langle u_i \rangle / \partial x_j + \partial \langle u_j \rangle / \partial x_i)$ is the mean rate of strain; and

$$\tau_{ij} = \rho \langle \tilde{u}_i \tilde{u}_j \rangle \quad (2.11)$$

is the Reynolds stress. Equation (2.10) is known as the Reynolds momentum equation (Tennekes and Lumley, 1972). According to this equation, the mean momentum may change because of a gradient in the mean pressure, a gradient in the mean flow leading to viscous losses, or the mean transport (advection) of fluctuating momentum, as described by the Reynolds stress. A similar equation, Eq. (4.4), describes the transport of mean momentum in a plasma.

In the absence of dissipation or external driving, total momentum is conserved. Therefore the Reynolds stress describes the *exchange* of momentum between the mean flow and the turbulence. Because the turbulent velocity fluctuations have zero mean, $\langle \tilde{u}_i \rangle = 0$, the net mean momentum exchanged is also zero. Turbulence thus rearranges mean momentum, modifying its profile (spatial variation), without changing the total (spatially integrated) momentum. Turbulent momentum transport is characteristic of nonuniform flows, and the Reynolds stress is therefore nonzero. Like the particle and heat fluxes of Eqs. (2.8) and (2.9), the Reynolds stress re-

quires a correlation between two fluctuations, in this case, two flow components. Mean flow gradients tilt turbulent eddies, thereby making the Reynolds stress non-zero, just as mean density and temperature gradients distort turbulence to make the correlations of the particle and heat fluxes nonzero.

B. Scaling theory for suppression of turbulence

The first theory to examine the suppression of turbulence by stable flow shear sought an explanation for robust transport barriers observed in fusion experiments. The theory, which assumes a given shear flow, identifies a universal feature of advection of turbulence by stable shear flow. This feature is more general than the experiments and experimental conditions that motivated the theory, applying to neutral fluids as well as plasmas. By the same token, suppression of turbulence by flow shear does not address every aspect of observed barriers, which also involve the creation of the flow in a complex, turbulent fluid and in complicated geometries. These more specialized issues are examined in later sections. Of two early theories, one focused on the role of flow velocity (Shaing, Crume, and Houlberg, 1990); the other (Biglari, Diamond, and Terry, 1990) focused on the role of flow shear. The latter followed up on earlier work (Chiueh *et al.*, 1986) that had addressed the behavior of turbulence in the localized flow shear layer at the edge of a particularly well-diagnosed device (Ritz *et al.*, 1984). Subsequent measurements on that device (Ritz *et al.*, 1990) established many of the qualitative features of the flow shear theory.

1. Dimensional analysis

The physics of the flow shear theory is most transparent as an exercise in dimensional scaling analysis (DSA; Terry, Newman, and Mattor, 1992; Ware *et al.*, 1999). The effect of flow shear on the inertial interactions of turbulent eddies and advected scalars is described in the advective derivative, which accounts for eddy decorrelation under advection by random eddy motion and a mean flow with shear. A scalar quantity ξ , advected in a two-dimensional (2D) incompressible turbulent flow with a sheared mean component, is governed by the following equation:

$$\frac{\partial \xi}{\partial t} + \bar{u}(y) \frac{\partial \xi}{\partial x} + \bar{u} \frac{\partial \xi}{\partial x} + \bar{v} \frac{\partial \xi}{\partial y} = \sigma_\xi, \quad (2.12)$$

where \bar{u} is a mean flow in the x direction and \bar{u} and \bar{v} are fluctuating flows in the x and y directions. The mean flow has shear in the y direction, which hereafter is referred to as the shear-wise direction. The flow is assumed stable. At the present level of specificity, ξ could itself be a component of the turbulent flow, the magnitude of turbulent vorticity, or a scalar such as density or temperature. Terms other than the advective derivative are lumped with any source term into the right-hand side of Eq. (2.12). Turbulence in plasmas is typically two dimensional. Rapid streaming of the highly mobile elec-

trons along the direction of the magnetic field (here, the z direction) smoothes fluctuations along the field and thus restricts significant variations to the xy plane. Large-scale turbulence in the atmosphere is also two dimensional due to planetary rotation (Pedlosky, 1979). As an incompressible flow in 2D, the flow can be written in terms of a stream function ϕ with $\bar{u} = -\partial\phi/\partial y$ and $\bar{v} = \partial\phi/\partial x$.

In a mean flow with shear, the inertial dynamics have two time scales. One is the eddy turnover rate [Eq. (2.2)], $\tau_e^{-1} \approx \bar{u}/\delta x \approx \bar{v}/\delta y \approx \phi/\delta x \delta y$, which describes the rate at which eddies decay. The second time scale τ_s arises from the sheared mean flow and opens the possibility that the turbulent dynamics are altered from the simple picture of Sec. II. A. Consider an eddy whose shear-wise extent is δy . It undergoes a differential stretching along the flow by an amount δx in a time

$$\tau_s = \frac{\delta x}{\delta y \bar{u}_y}, \quad (2.13)$$

where \bar{u}_y is the derivative of \bar{u} with respect to y , and $\delta y \bar{u}_y$ is therefore the difference of mean flow speeds across the eddy. When the stretching length δx along the flow is equal to the coherence length, or distance to the next eddy of comparable size, the eddy loses coherence due to the random advection by other eddies. With δx specified as the coherence length, τ_s^{-1} is the shear strain rate. When the shear strain rate is smaller than the eddy turnover rate τ_e^{-1} , eddies are only slightly distorted by the flow shear in an eddy turnover time. In this limit there is essentially no effect on the turbulent dynamics, apart from a small geometrical distortion of the eddy flow pattern.

In the opposite limit when $\tau_s < \tau_e$, the differential flow stretches an eddy to its coherence length in a fraction of an eddy turnover time, making this shortened time the new eddy lifetime. In this time, fluid parcels within the eddy have moved across the flow only a fraction of the cross-flow eddy size δy . Since the eddy has now lost coherence, this new shear-wise scale,

$$\delta y_s = \tau_s \bar{v} = \frac{\tau_s \phi}{\delta x}, \quad (2.14)$$

becomes the shear-wise coherence length or eddy scale. Substituting for τ_s from Eq. (2.13), with the new eddy scale δy_s replacing δy , we find that this eddy scale is

$$\delta y_s = \left[\frac{\phi}{\bar{u}_y} \right]^{1/2}. \quad (2.15)$$

In terms of this new shear-wise eddy scale δy_s , the new eddy turnover time $\tau_e^{(s)} = \delta y_s / \bar{v}_s$ is equal to the shear time, defining a shortened coherence time $\tau_c^{(s)}$:

$$\tau_c^{(s)} \equiv \tau_e^{(s)} = \frac{\delta y_s}{\bar{v}_s} = \frac{\delta x}{\bar{u}_y \delta y_s} = \tau_s^{(s)}. \quad (2.16)$$

Therefore, in a strongly sheared flow, turbulence adjusts itself via the accelerated decorrelation to shorten the shear-wise correlation length, bringing the eddy turn-

over time into parity with the shear straining time. The threshold criterion for this effect defines the strong-shear limit.

$$\varepsilon_s \equiv \frac{\tau_s}{\tau_e} = \frac{\bar{u}}{\delta y \bar{u}_y} < 1, \quad (2.17)$$

where τ_e is the eddy turnover time *defined with respect to the original shear-wise scale* δy , or equivalently, defined in a region away from the flow shear. Note that in terms of the ambient time scales τ_e and τ_s , the reduced correlation time $\tau_c^{(s)}$ can be written as the geometric mean,

$$\tau_c^{(s)} = \delta x / \delta y_s \bar{u}_y = \delta x / \bar{u}_y^{1/2} \phi^{1/2} = \tau_e^{1/2} \tau_s^{1/2}. \quad (2.18)$$

When an eddy is introduced into a region with flow shear, its shear-wise coherence length decreases in the time $\tau_c^{(s)}$. On a longer time scale the eddy velocity decreases because shear increases the advective derivative,

$$\frac{\partial}{\partial t} + \bar{u}(y) \frac{\partial}{\partial x} + \bar{u} \frac{\partial}{\partial x} + \bar{v} \frac{\partial}{\partial y} \approx \frac{1}{\tau_c^{(s)}} + \frac{\delta y_s \bar{u}_y}{\delta x} + \frac{\phi_s}{\delta y_s \delta x}, \quad (2.19)$$

relative to its value in regions with no shear. The turbulent energy cascade rate, which is governed by the advective derivative, now becomes greater than the energy input rate σ_ξ . (If the latter changes, it also changes on a slower time scale.) The enhanced rate of energy cascade (and therefore the enhanced rate of dissipation at the Kolmogorov scale, as explained in Sec. II. A. 1) decreases the turbulence level, or magnitude of ξ , until a balance between σ_ξ and the left-hand side of Eq. (2.12) is reestablished. Final steady-state values of the shear-wise eddy coherence length, fluctuation amplitude, and correlation time can be obtained from Eqs. (2.15) and (2.16) and the balance of the turbulent cascade rate with the source

$$\frac{\phi_s \xi_s}{\delta y_s \delta x} = \sigma_\xi^{(s)}. \quad (2.20)$$

In these expressions the amplitudes ϕ , \bar{v} , ξ , and source σ_ξ must be written as ϕ_s , \bar{v}_s , ξ_s , and $\sigma_\xi^{(s)}$, indicating their self-consistent values in the regions of localized strong flow shear. As a concrete example, consider the shear-wise turbulent flow \bar{v} as the quantity ξ . In terms of a source $\sigma_v^{(s)}$ whose dependence on shear remains unspecified, the eddy coherence length, stream-function amplitude, and correlation time are

$$\begin{aligned} \frac{\delta y_s}{\delta y_o} &\approx \varepsilon_s^{2/3} \left[\frac{\sigma_v^{(s)}}{\sigma_v^{(o)}} \right]^{1/3}, \\ \frac{\phi_s}{\phi_o} &\approx \varepsilon_s^{1/3} \left[\frac{\sigma_v^{(s)}}{\sigma_v^{(o)}} \right]^{2/3}, \\ \frac{\tau_c^{(s)}}{\tau_c^{(o)}} &\approx \varepsilon_s^{1/3} \left[\frac{\sigma_v^{(s)}}{\sigma_v^{(o)}} \right]^{-1/3}. \end{aligned} \quad (2.21)$$

Each quantity has been normalized with respect to its value determined by ambient turbulence alone, and ϕ_o

and $\sigma_v^{(o)}$ are related by the balance of the ambient turbulence cascade rate and ambient source $\phi_o^2 / \delta y_o \delta x^2 = \sigma_v^{(o)}$. Further simplification requires specification of the nature of the driving source and therefore depends on the details of the turbulence. Because the source can also depend on the flow shear, the response of each quantity in Eq. (2.21) to the flow shear can differ. For example, in a self-similar energy cascade driven by stirring at some scale (Ware *et al.*, 1999), the amount of energy transferred per unit time in every scale is constant, implying $\phi^3 / \delta x \delta y^3 = \text{const}$. Under this arrangement, $\phi_s / \phi_o = \delta y_s / \delta y_o$, and $\sigma_v^{(s)} / \sigma_v^{(o)} = (\phi_s / \phi_o)^2 (\delta y_s / \delta y_o)^{-1} = \phi_s / \phi_o = \delta y_s / \delta y_o$. The ratios of Eq. (2.21) then become $\delta y_s / \delta y_o = \varepsilon_s$, $\phi_s / \phi_o = \varepsilon_s$, and $\tau_c^{(s)} / \tau_c^{(o)} = 1$. In this case there is no change in the correlation time because of the manner in which the source is decreased by the constraint of constant energy injection rate.

In the above discussions, it has been assumed that δx is invariant inside and outside the region of flow shear. For the closed flow patterns characteristic of fusion plasmas this is equivalent to assuming that the number of eddies along the path traced by the flow remains unchanged as the eddies are distorted by the shear. In such a case there is a scaled reduction in the cross-shear direction for each scale δx along the flow, i.e., eddies on a range of scales are affected by the shear as described above. For eddies whose scales are sufficiently small, the shear time ceases to be smaller than the eddy turnover time for ambient turbulence, and Eq. (2.17) is no longer satisfied. Representing δx with the Fourier wave number k_x , there is therefore a spectrum subrange at lower wave number over which shear suppression occurs self-similarly, and a subrange over higher wave numbers where flow shear has a negligible effect on the turbulent dynamics. If there are inhomogeneities in the x direction (arising, for example, from the equilibrium, which in turn affects the turbulence sources), the scale δx may itself change in the flow shear. From Eq. (2.14), it is apparent that if δx increases in a region of flow shear, the shear strain time becomes larger, weakening the effect of flow by slowing down the shear-enhanced decorrelation. Conversely, if δx decreases in a region of flow shear, the tendency of flow shear to reduce the cross-shear eddy scale and eddy amplitude is enhanced.

2. Relative motion of fluid parcels

The results of dimensional scaling analysis can be recovered from more rigorous analyses that invert the differential operator describing advection. The inverted operator obviously combines the fundamental time scales τ_s and τ_e . The analysis of this and the next subsection establishes the basic conjecture of DSA: that the eddy turnover time and shear straining time are brought into parity by the reduction of the shear-wise eddy scale. The inversion of the advective operator was originally done for a two-point description of the fluid motion (Biglari, Diamond, and Terry, 1990; Shaing, Crume, and Houlberg, 1990). In this case the inversion yields the

relative trajectory of two fluid parcels in the turbulent flow. This method determines eddy scales and the eddy coherence time from the difference in the character between relative trajectories of fluid parcels that are in the same eddy and whose motion is correlated, and fluid parcels that are in different, comparable-sized eddies, and whose motion is therefore uncorrelated.

The evolution equation of the two-point correlation $\langle \xi(1)\xi(2) \rangle$ is constructed by taking the product of $\xi(2)$ with Eq. (2.12) written for $\xi(1)$, adding it to the product of $\xi(1)$ with Eq. (2.12) written for $\xi(2)$, and taking an ensemble average. If the equation is expressed in terms of relative ($-$) and center-of-mass ($+$) coordinates defined by $(x_{\pm}, y_{\pm}) = (x_1 \pm x_2, y_1 \pm y_2)$, its form is given by

$$\left[\frac{\partial}{\partial t} + \bar{u}_y y_- \frac{\partial}{\partial x_-} - \frac{\partial}{\partial y_-} D_- (x_-, y_-) \frac{\partial}{\partial y_-} \right] \langle \xi(1)\xi(2) \rangle = \zeta, \quad (2.22)$$

where $\bar{u}_y = \delta \bar{u} / \delta y_+$, $\zeta = \langle \xi(1)\sigma_{\xi}(2) + \xi(2)\sigma_{\xi}(1) \rangle$ is the two-point source, and D_- is a nonuniform eddy diffusivity whose precise form (Terry and Diamond, 1985) is obtained by application of a systematic procedure known as a statistical closure. Under the statistical closure, the eddy diffusivity and the eddy decorrelation rate on which it depends are functions solely of quadratic correlations. The diffusivity is dimensionally equivalent to the eddy turnover rate ($D_- / \delta y^2 \approx \bar{v} / \delta y$) in a strong-turbulence (high-Reynolds-number) regime. In a two-point description, the diffusion describes the scattering apart of fluid parcels under advection by the random flow. The relative diffusion process is dominated by diffusion in the y direction, because it is the direction of inhomogeneity. Both the equilibrium flow and the equilibrium profile of $\langle \xi \rangle$ (which contributes to the source) are nonuniform in this direction. The usual difficulty with eddy diffusivities, i.e., that they destroy invariance symmetries of the original evolution equation, is averted in the two-point closure used in Eq. (2.22) (Dupree, 1972; Boutros-Ghali and Dupree, 1981). Specifically, the inertial range conservation of the energy $\langle |\xi|^2 \rangle$ under turbulent advection is guaranteed by the variation of D_- with relative separation: $D_- \sim D_o (x_-^2 / \delta x^2 + y_-^2 / \delta y^2)$ as $x_-^2 \rightarrow 0$ and $y_-^2 \rightarrow 0$. For $x_-^2 > \delta x^2$ and $y_-^2 > \delta y^2$, D_- approaches the constant D_o asymptotically. The vanishing of D_- as x_-^2 and y_-^2 go to zero reflects the coherent flow pattern within the eddy, i.e., fluid parcels separated by a fraction of the eddy scales δx and δy essentially move together. Parcels whose separation is greater than the eddy scale diffuse apart with a random walk whose rate is governed by D_o . These properties of the relative motion of parcels emerge from the solution of Eq. (2.22) when $\bar{u}_y = 0$. The scales δx and δy are natural coherence lengths for the relative motion. In the presence of flow shear, coherence lengths for relative motion change: a new shorter scale emerges as the shear-wise separation at which fluid parcels move apart in an uncorrelated fashion.

To compare the results of two-point theory with the heuristic dimensional scaling analysis predictions of the

prior section, it is necessary to formulate the DSA predictions for a statistical closure model, which contains a diffusivity instead of the advective derivative $\mathbf{u} \cdot \nabla \mathbf{u}$. The predictions of DSA take a slightly different form for statistical closure theory than for the primitive equation because different powers of δy appear in the turbulent decorrelation rate: in closure theory, the turbulent decorrelation rate has the diffusivity D_o divided by the shear-wise scale squared, while in the primitive equation the decorrelation rate is the velocity \bar{v} divided by the shear-wise scale to the first power. In the closure model the shear straining time is unchanged and is given by $\omega_s^{-1} = \delta x / \delta y \bar{u}_y$. (Here, time scales are expressed as rates, i.e., $\omega_s = \tau_s^{-1}$, in order to distinguish the DSA predictions of this and the prior section.) The turbulent decorrelation time is $\omega_e^{-1} = \delta y^2 / D_o$. The contracted shear-wise scale is obtained from $\omega_e = \omega_s$, yielding $\delta y_{D_s} = (D_o \delta x / \bar{u}_y)^{1/3}$. With the equality $v' / \delta y_s = \phi / \delta x \delta y_s = D_o / \delta y_{D_s}^2$, Eq. (2.14) is recovered. The shortened correlation time in regions of flow shear is

$$\omega_c^{(s)-1} = \frac{\delta y_{D_s}^2}{D_o} = \frac{(D_o \delta x / \bar{u}_y)^{2/3}}{D_o} = \left(\frac{\delta y^{2/3}}{D_o^{1/3}} \right) \left(\frac{\delta x^{2/3}}{\delta y^{2/3} \bar{u}_y^{2/3}} \right) = \omega_e^{-1/3} \omega_s^{-2/3}. \quad (2.23)$$

The corresponding expression from the prior section, Eq. (2.18), involves the geometric mean. The extra factor of δy in the diffusion term leads here to a stronger weighting on the shear term.

Returning to the two-point calculation, the trajectories of relative motion are extracted from the Green's function $G(x_-, y_-, t | x'_-, y'_-, t')$ that inverts the spatiotemporal operator of Eq. (2.22) (Dupree, 1972; Terry and Diamond, 1985). Spatial moments of the Green's function define stochastic trajectories. The $\langle y_-^2 \rangle$ trajectory, for example, is given by $\langle y_-^2 \rangle = \int dy'_- dx'_- dt' y'^2_- G(x_-, y_-, t | x'_-, y'_-, t')$. Evolution equations for these moments are derived from the operator and can be solved for $\omega_c^{(s)} t < 1$ in terms of initial separations y_- and x_- , yielding

$$\langle x_-^2 \rangle \approx \frac{1}{3} [2 \varepsilon_s^{-2/3} (\delta x / \delta y)^2 y_-^2 + x_-^2 - 2 \varepsilon_s^{-1/3} (\delta x / \delta y) x_- y_-] \exp[\omega_c^{(s)} t], \quad (2.24)$$

$$\langle y_-^2 \rangle \approx \frac{1}{3} [(1 + 2^{1/3} \cdot 3 \varepsilon_s^{2/3}) y_-^2 + 2^{1/3} \varepsilon_s^{2/3} (\delta y / \delta x)^2 x_-^2 - 2^{-1/3} \cdot 6 (\delta x / \delta y) y_- x_-] \exp[\omega_c^{(s)} t], \quad (2.25)$$

where $\varepsilon_s = \omega_e / \omega_s$ as before, and $\omega_c^{(s)} = (2 \omega_e \omega_s^2)^{1/3}$. Apart from the factor of $2^{1/3}$ this expression is identical with the results of dimensional scaling analysis.

Fluid parcels become decorrelated when the relative separation reaches the eddy scales δy and δx . This defines the parcel correlation time τ_{pc} , which can be obtained by inverting the trajectory expressions,

$$\tau_{pc} \approx \omega_c^{(s)-1} \ln \left[\left(\frac{y_-}{\varepsilon_s^{1/3} \delta y} \right)^2 - \frac{2}{3} (1 + 2^{1/3}) \frac{x_- y_-}{\varepsilon_s^{1/3} \delta x \delta y} + \frac{1 + 6 \cdot 2^{1/3}}{3} \left(\frac{x_-}{\delta x} \right)^2 \right]. \quad (2.26)$$

From this it is clear that the shear-wise coherence length is

$$\delta y_s = \varepsilon_s^{1/3} \delta y = (D_o \delta x / \bar{u}_y)^{1/3} \quad (2.27)$$

while the coherence time is

$$\tau_{pc} \approx \omega_c^{(s)-1} = (2\omega_e \omega_s^2)^{-1/3} = (D_o / \delta y_{D_s}^2)^{-1} = (\delta y_{D_s} \bar{u}_y / \delta x)^{-1}. \quad (2.28)$$

The coherence length along the flow remains δx in the presence of strong flow shear, as postulated in the previous section. The above analysis reproduces the results of the DSA, to wit, the shear-wise scale contracts, bringing the turbulent correlation time and shear straining time into parity. From the expression $\omega_c^{(s)} = (2\omega_e \omega_s^2)^{1/3}$, and from other expressions of the two-point theory, it is apparent that fluctuation suppression by flow shear is independent of the sign of the flow shear or the flow. This is confirmed experimentally by varying the sign in a single device (Weynants *et al.*, 1991) or by comparing barriers in two devices having opposite signs (Levinton *et al.*, 1995; Strait *et al.*, 1995).

3. Asymptotic analysis

The advective derivative with strong flow shear, under a statistical closure, has also been inverted using asymptotic analysis to construct the leading-order contribution to the Green's function in the asymptotic limit $\varepsilon_s \ll 1$ (Terry, Newman, and Mattor, 1992). Asymptotic analysis allows determination of the unique combination of terms that dominates the advective operator in the asymptotic limit and therefore controls the spatiotemporal structure of the turbulence in the presence of the inhomogeneity of the background shear flow. Terry *et al.* (1992) consider an incompressible vortical 2D mean flow with symmetry in the azimuthal direction, defined with reference to a polar coordinate system whose origin is the center of the vortex. Adopting this coordinate system, we specify (r, ϑ) as the radius and angle, and (v, u) as the flow velocities in the radial and azimuthal directions. The mean flow $\bar{u}(r)$ is stable and purely azimuthal, with radial shear. For simplicity, the shear is treated as linear in the region of interest.

As in the previous section, a statistical closure is applied to the advective derivative. The quantity ξ satisfies

$$\begin{aligned} & [\gamma_n - i(r - r_o)n(\bar{u}/r)_r] \xi_{n,\gamma} - \frac{1}{r} \frac{\partial}{\partial r} \left(r D_n \frac{\partial \xi_{n,\gamma}}{\partial r} \right) \\ & + \frac{n^2}{r^2} D_n \xi_{n,\gamma} = \sigma_\xi - \xi_n(t=0), \end{aligned} \quad (2.29)$$

where the $\xi_{n,\gamma}$ is the amplitude of the Fourier-Laplace transformation of ξ ,

$$\xi_{n,\gamma} = \int_0^\infty dt \exp(-\gamma t) \int_0^{2\pi} d\vartheta \exp(in\vartheta) \xi(r, \vartheta, t).$$

Here $\xi_n(t=0)$ is the Fourier amplitude at the initial time, $(\bar{u}/r)_r = \partial(\bar{u}/r)/\partial r|_{r_o}$ is the shear of differential rotation near some position r_o , $\gamma_n = \gamma + in\bar{u}/r|_{r_o}$ is the Laplace frequency Doppler shifted by the mean vortical flow at r_o , and D_n is the turbulent diffusivity. As before, D_n is dimensionally consistent with turbulent advection ($D_n \partial^2 / \partial r^2 \approx v \partial / \partial r$). Note that in this calculation there is diffusion in both the radial and the azimuthal directions. The quantity n/r_o is the azimuthal wave number. Its inverse is the azimuthal eddy size, with n being the number of same-sized eddies that can be placed adjacent to one another in the circle of radius r_o .

Equation (2.29) is formally inverted using a Green's function $\xi_{n,\gamma} = \int r' dr' G_n(r|r') D_n^{-1} [\sigma_\xi - \xi_n(t=0)]$, where $G_n(r|r')$ is the impulse response of the left-hand operator of Eq. (2.29) and with the source describes the spatiotemporal structure of turbulence in the presence of the differential rotation of the mean flow. To determine this structure, it is sufficient to examine the properties of the eigenmodes $\psi_{n,\gamma}$ of the Sturm-Liouville problem corresponding to the homogeneous equation

$$\begin{aligned} & \frac{\partial^2 \psi_{n,\gamma}}{\partial \hat{r}^2} + \frac{1}{\hat{r} + r_o} \frac{\partial \psi_{n,\gamma}}{\partial \hat{r}} - \frac{\gamma_n}{D_n} \psi_{n,\gamma} \\ & + \frac{in}{D_n} (\bar{u}/r)_r \hat{r} \psi_{n,\gamma} - \frac{n^2}{(\hat{r} + r_o)^2} \psi_{n,\gamma} = 0, \end{aligned} \quad (2.30)$$

where $\hat{r} = r - r_o$. The limit of arbitrarily strong flow shear is particularly useful. In this limit, asymptotic analysis (Bender and Orszag, 1978) reveals the dominant balance between terms of Eq. (2.30) responsible for the structure of the advected field. The asymptotic limit of strong shear is parametrized by $\varepsilon_s^{-1} = n(\bar{u}/r)_r r_o^3 / D_n \rightarrow \infty$, i.e., by the limit in which the shear straining time becomes arbitrarily short relative to the turbulent diffusion time at the scale r_o of the mean flow.

In the strong-shear limit there are two possible balances among the terms of Eq. (2.30). For stationary turbulence ($\gamma \rightarrow 0$), Eq. (2.30) becomes singular in the reference frame of the flow at r_o as $\varepsilon_s^{-1} \rightarrow \infty$. Here singularity refers to the fact that the highest derivative of Eq. (2.30) drops out of the equations unless a singular layer develops allowing ψ_{rr} to become as large as $n\psi_{\hat{r}}(\bar{u}/r)_r D_n^{-1}$. Other potential balances lead to inconsistencies and therefore do not dominate. Note that this balance implies a shrinkage of the radial (shear-wise) scale to make ψ_{rr} of the same order as the shear term. If advection in the sheared mean flow has started as an initial-value problem, this balance is established only after an eddy turnover time. Prior to that time the advectant responds transiently to the flow shear and $\gamma_n \psi / D_n$ balances the shear term. This second balance represents the initial response of the advectant during

the first eddy turnover time, or for situations in which the advectant is carried through a localized zone of strong flow shear and out before an eddy turnover time. The latter does not apply in the present case of a vortical mean flow that closes on itself, but does apply to other types of flows, for example, the flow inside a nozzle. For this short time response the diffusivity can be ignored, i.e., the problem can be linearized. This is the domain of rapid-distortion theory (RDT; Hunt, Carruthers, and Fung, 1991). For the longer-time response, linearization is not possible and the balance of the diffusive term and shear straining term must be considered. Because the turbulence is also distorted under this balance, analysis in the longer time limit can be called balanced-distortion theory.

The solution of Eq. (2.30) in the limit of balanced distortion is obtained systematically using a WKB expansion and a formal ordering in terms of the large parameter $\varepsilon_s^{-1} = n(\bar{u}/r)_r r_o^3 / D_n = \omega_s / \omega_e$. In order to determine the time scale over which the dominant asymptotic balance is established we also take γ_n as order ε_s^{-1} . The WKB expansion is $\psi_{n,\gamma} = \exp[\delta^{-1} \sum_m \delta^m S_m(\hat{r})]$, where S_m is the WKB eikonal of order m in the expansion. The dominant balance occurs in a singular layer of width $\delta = \varepsilon_s$. Substituting this form into Eq. (2.30) and solving for the eikonals to second order, we find the eigenfunctions to be Airy functions modified by the cylindrical geometry,

$$\begin{aligned} \psi_{n,\gamma} \sim (\pm 1)^{-1/2} (\hat{r} + r_o)^{-1/2} \left(\frac{\gamma_n}{D_n} - \frac{i\hat{r}(\bar{u}/r)_r}{d_n} \right)^{-1/4} \\ \times \exp \left[\pm \frac{2}{3} \left(\frac{-in(\bar{u}/r)_r}{D_n} \right)^{1/2} \left(\hat{r} + \frac{i\gamma_n}{(\bar{u}/r)_r} \right)^{3/2} \right], \\ (\varepsilon_s^{-1} \rightarrow \infty). \end{aligned} \quad (2.31)$$

The Airy function behavior is a direct reflection of the essential balance between the diffusion ψ_{rr} and the linear profile of differential rotation assumed in this model. From the argument of the exponential in Eq. (2.31) the shear-wise variation occurs on a spatial scale

$$\delta r = \left[\frac{D_n}{n(\bar{u}/r)_r} \right]^{1/3}. \quad (2.32)$$

Note that this is equivalent to the shear-wise coherence length [Eq. (2.27)] of the previous section. Equation (2.31) also indicates that the response is maximum when $|\gamma_n| \approx rn(\bar{u}/r)_r \approx \delta rn(\bar{u}/r)_r = \omega_s^{2/3} \omega_e^{1/3}$, in accordance with Eq. (2.28).

The eigenfunction ψ describes the response of the advectant ξ in the sheared turbulence subject to the constraints of the formal asymptotic ordering analysis. The balances and scalings of dimensional scaling analysis are recovered here from the unique dominant asymptotic balance in the limit of large shear. This analysis has also illustrated the distinction between rapid and balanced-distortion theories, a topic to which we return in Sec. III.

C. Role of flow shear in linear instabilities

The suppression of turbulence by stable flow shear appears to be robust and quasiuniversal in magnetized plasmas, a property stemming from the central role of advection in 2D turbulence. It is tempting to examine linear instabilities using heuristic arguments like those of the section on dimensional scaling analysis. The term linear instability refers to a collective plasma mode whose amplitude e folds at the weak intensities under which linearization of the governing equations is permissible. Although linear instabilities are widely investigated, there is not always a simple connection between the properties of turbulence and those of an underlying instability. The spatial and temporal scales of a linear instability often change once growth is arrested at finite amplitude by nonlinear effects and turbulence (for example, see Garcia *et al.*, 1985). Notwithstanding these caveats, heuristic treatments of linear stability have been formulated, yielding estimates for the level of flow shear required to modify instabilities (Hassam, 1991; Waltz, Kerbel, and Milovich, 1994).

Flow shear enters the advective derivative as a shear strain rate. The simplest hypothesis for linear stabilization is that the shear strain rate exceeds the inverse time scale of the instability,

$$\tau_s^{-1} > |\omega|, \quad (2.33)$$

where ω is the larger of the real mode frequency or the growth rate (Hassam, 1991). In a variant of this criterion, $|\omega|$ is the linear growth rate, calculated assuming no shear flow, regardless of the magnitude of the real frequency (Waltz, Kerbel, and Milovich, 1994). These criteria suppose that a large shear strain rate deforms the advective pattern of the normal mode faster than the rate at which free energy is released into the instability, thus inhibiting its release. A simple test of this hypothesis is the Rayleigh-Taylor mode, an instability of a stratified atmosphere. This mode develops for unstable stratification, i.e., for higher-density fluid above (higher gravitational potential) lower-density fluid. The growth rate γ is given by the dimensional combination of the gravitational acceleration and density-gradient scale length $L_n = n(dn/dz)^{-1}$: $\gamma = (g/L_n)^{1/2}$. Here, n is the density. A flow U transverse to gravity with linear variation of flow speed in the vertical direction stabilizes perturbations whose wave vector is in the direction of the flow, provided the Richardson number, $J = -(g/L_n) \times (dU/dz)^{-2}$, is greater than -2 (Kuo, 1963; Brown, 1980). For the flow U the shear strain rate is $\tau_s^{-1} = k_y \delta z dU/dz$, where k_y is the wave number of the perturbation and δz is the scale of the perturbation in the direction of inhomogeneity. For this instability, $\delta z \sim k_y^{-1}$ and the criterion of Eq. (2.33) approximately reproduces the Richardson number criterion. Wave numbers transverse to the flow and gravity are not stabilized, but if there is a magnetic field in this direction, the mode is completely stabilized (Lehnert, 1966).

Comparison with careful calculations of the growth rates of several instabilities that are considered impor-

tant in limiting the confinement of fusion plasmas indicates that Eq. (2.33) is not generally valid.² Strong flow shear often stabilizes collective modes driven by gradients of pressure or other equilibrium quantities, but weaker shear can be either stabilizing or destabilizing, depending on the collective mode. Moreover, the mechanisms involved are varied. In some cases, flow shear enhances the extraction of free energy by modifying eigenmode structure. In general, proper stability criteria must account for the effect of flow shear on eigenmode structure. This involves the combined effect of flow shear and other plasma inhomogeneities, introducing complications that are not included in Eq. (2.33). This issue is revisited in Sec. V. A. Despite these difficulties, simulation studies show the criterion of Waltz *et al.* (1994) to be a reasonable predictor to within a factor of 50% for the quenching of ion-temperature-gradient turbulence by flow shear (Waltz, Dewar, and Garbet, 1998).

D. Observations of transport barriers in plasmas

The first observations of a transport barrier in plasmas were made by Wagner *et al.* (1982), several years before it was realized that flow shear was present in the barrier. The appearance of the barrier coincided with a sudden increase in confinement time, typically by a factor of 2, and the steepening of the radial variation of temperature and density in a narrow layer 1–2-cm thick at the edge of the tokamak plasma. Direct measurement showing reduction of turbulence in the region of steepened gradients was not made until several years later in other devices. [It is evident in Fig. 2 of Taylor *et al.* (1989), and was reported in Burrell *et al.* (1990).] Barrier formation was triggered by the application of additional heating power during a distinct temporal transition. After the transition, the plasma energy and confinement time rose to higher values, the density and temperature gradients steepened in the barrier region, and emissions of hydrogen Lyman alpha (H_α) radiation promptly dropped, indicating a significant decrease in particle losses. The H_α emission was easily measured and, because its intensity was observed to undergo the most precipitous change of any quantity, it was adopted as the indicator of the transition time. The pre- and post-transition conditions were called *L* mode and *H* mode, for low and high confinement, respectively. Transitions were observed when the input power exceeded a threshold. The threshold was found to depend on a variety of plasma conditions, often in a complicated way. Through experiments in which the transition was triggered by a heat pulse propagating into the barrier region from a disturbance in the plasma core (Wagner *et al.*, 1984), it was established that power or

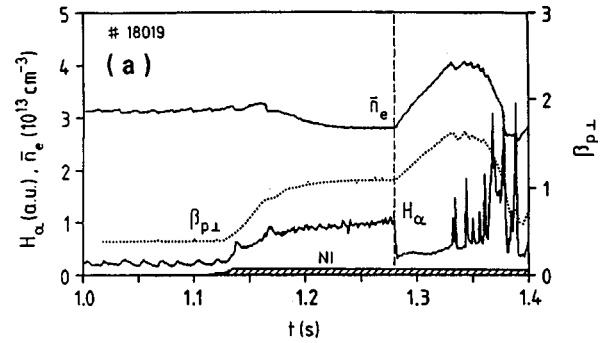


FIG. 3. Evolution of plasma properties through the transition from *L* mode to *H* mode. The transition is marked by the dashed line at $t=1.28$ s. The density \bar{n}_e and plasma energy $\beta_{p\perp}$ begin increasing abruptly at the transition, while hydrogen Lyman alpha radiation H_α decreases. From ASDEX Team, 1989.

heat flux into the barrier region was a critical parameter and might therefore be equivalent to a critical temperature in this region.

Figure 3 shows time traces of plasma energy and the intensity of H_α emissions with the transition marked. Figure 4 displays the radial variation, or profile, of density and temperature before and after the transition. The region of steepened gradients, about 1 cm in extent, is clearly evident. The *H* mode represents a fundamental change in the plasma, as indicated by changes in the empirical scaling of confinement time with plasma parameters (ITER Confinement Database and Modelling Working Group, 1997) and a reduction of radial correlation lengths (Costley *et al.*, 1993). In the *L* mode, the local diffusivity is governed by large global (machine-size) scales, whereas in the *H* mode the diffusivity is governed by the smaller scales of charged-particle gyromotion around magnetic-field lines (Petty *et al.*, 1995).

The evolution of the plasma energy and the profiles in the *H* mode is consistent with a local transport process in which heat and particle fluxes are proportional to local temperature and density gradients (Fick's law) and the barrier is created by a reduction in the diffusivities. Consider, for example, an equation for radial ion energy transport,

$$\frac{\partial p_i}{\partial t} + \frac{\partial}{\partial r} Q_i = \hat{P}_i, \quad (2.34)$$

where the heat flux Q_i is related to the pressure gradient through a diffusivity χ_i :

$$Q_i = -\chi_i \frac{\partial}{\partial r} p_i, \quad (2.35)$$

and \hat{P}_i is the external power supplied to the ions. In steady state the input power and energy loss balance. If the energy loss (and therefore the diffusivity) diminishes suddenly at some radial position, the input power will exceed the loss, and the pressure will increase, thereby increasing the plasma energy. As the pressure increases inside the radius where χ_i has diminished, the gradient of p_i steepens. Eventually the product of the reduced χ_i and increasing pressure gradient grows until a balance is

²See, for example, Chen and Morrison, 1990; Hassam, 1991; Staebler and Dominguez, 1991; Sugama and Wakatani, 1991; Carreras *et al.*, 1992; Hamaguchi and Horton, 1992; Wang, Diamond, and Rosenbluth, 1992; Waltz *et al.*, 1995.

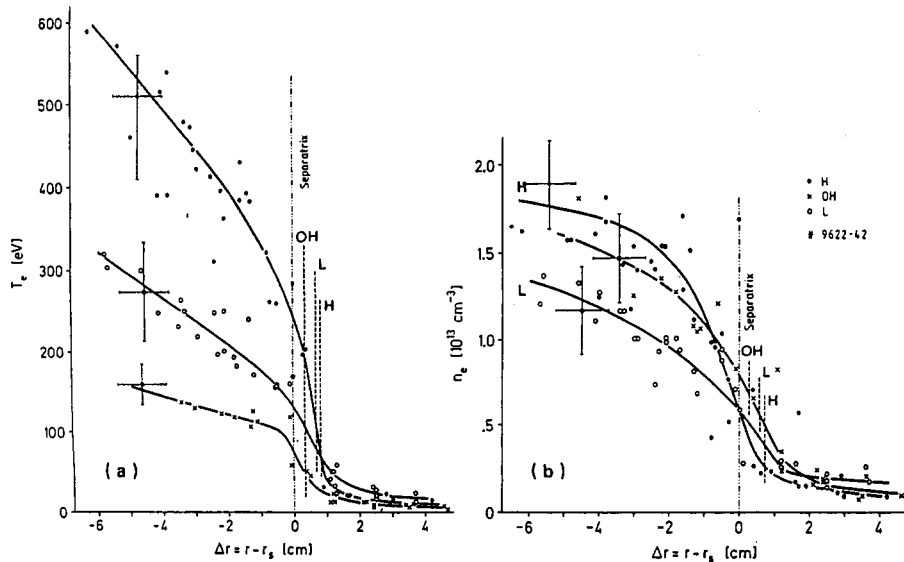


FIG. 4. Radial profiles of temperature and density in ohmic, L -mode, and H -mode discharges. The H -mode discharge has steeper gradients than the ohmic and L -mode plasmas, neither of which have a transport barrier. From ASDEX Team, 1989.

reestablished. Although the loss rate reaches its original value in this example, the plasma energy and confinement time have increased. If \hat{P}_i is switched off, the pressure will decay more slowly because χ_i is smaller.

The creation of this type of transport barrier has been widely reproduced and studied in a large number of devices. Subsequent observations have established that sheared flows are spun up at the transition. The earliest observations showed that the radial profiles of the poloidal velocity of different ion species change dramatically at the transition (Groebner *et al.*, 1989). Subsequently it was shown that similar changes occur in the main ion flow, whose direction need not be the same as the flow of impurity species (Kim *et al.*, 1994), and in the $E \times B$ flow. As discussed in Sec. IV, the $E \times B$ flow is of primary interest as the flow that suppresses turbulence. Plasma flows are of secondary interest as contributors to the $E \times B$ flow. The $E \times B$ flow exhibits rapid radial variation in the barrier region where steepened gradients are present, with variations of 20 km/s over a centimeter. The radial variation of the radial electric field, which determines the $E \times B$ flow, is shown in Fig. 5, before and after the transition. For reference, the ion temperature profile is also displayed, demonstrating that the large gradient forms in the same location as the region of strong flow shear. Measurement of fluctuation intensities shows a decrease in the level of potential, density, and magnetic-field fluctuations in the H mode. The decrease commences with the transition and is localized to the region of strong flow shear and gradient steepening. Note that if fluctuations dominate the transport losses, a decrease in fluctuations leads to a decrease in the transport fluxes, as is apparent in Eq. (2.9), for example, which in turn leads to a decrease in diffusivities and thermal conductivities.

E. Experimental and numerical tests

Shortly after the development of the scaling theory for shear suppression, detailed measurements of turbu-

lence properties in a plasma flow shear layer were made on a device known as the Texas Experimental Tokamak (TEXT; Ritz *et al.*, 1990). This device utilized a material surface inserted in the plasma edge to keep the plasma from the walls of the containment vessel. Near this surface there was a region of localized flow shear in which a poloidal $E \times B$ flow changed sign from -3×10^5 km/s to 3×10^5 km/s in a radial layer about 1.5 cm in thickness. This region of strong flow shear occurred in the cold edge plasma, making it accessible to electrostatic probes. These probes provided measurements of radial profiles of the $E \times B$ flow, the mean density gradient, profiles of fluctuation amplitudes in the density and electrostatic potential (the latter relates to the fluctuating flow through the fluctuating $E \times B$ drift), correlation lengths, and the correlation time.

The measurements showed that the mean density gradient steepened noticeably in the region of strong flow

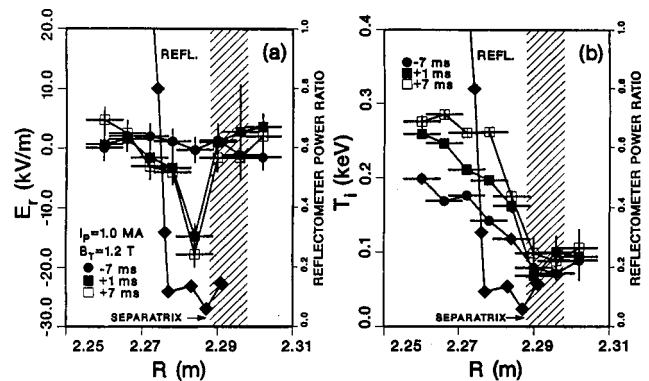


FIG. 5. Radial electric field and ion temperature profile before (negative times) and after (positive times) the transition from L mode to H mode. (a) In H mode the radial electric field is seen to develop large radial variation in a narrow layer. (b) The ion temperature profile steepens in the region of the large variation. The reflectometer data indicate the decrease in fluctuation activity within the transport barrier. From Doyle *et al.*, 1993.

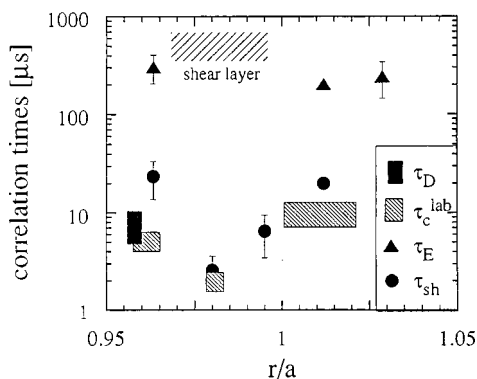


FIG. 6. Turbulent correlation and shear straining times at positions inside and outside a localized shear layer. Outside the layer the turbulent correlation time τ_D is smaller than the shear straining time τ_{sh} . Inside the layer both times decrease and become equal, as predicted by theory [Eq. (2.16)]. From Ritz *et al.*, 1990.

shear. The magnitude of fluctuations in the electrostatic potential and density were observed to decrease as probes were moved from the central plasma region through the flow shear layer toward the plasma boundary. Both observations are consistent with a flow-shear-induced transport barrier. Of more direct significance to the theoretical predictions were observations that the radial (shear-wise) correlation decreased in the shear layer. Ritz *et al.* (1990) also saw indications of a decrease in the flow-wise correlation length. The shear straining and turbulent correlation times of the experiment, labeled as τ_{sh} and τ_D to distinguish them from their theoretical counterparts τ_s and τ_e , were measured inside and outside the shear layer. Outside, $\tau_{sh} > \tau_D$, indicating weak shear. The shear straining time dropped by an order of magnitude in the shear layer to a value below τ_D as measured outside. The turbulent correlation time also dropped in the shear layer to the same value as the shear straining time, making $\tau_c^{(s)} = \tau_s$, as predicted by theory. The comparison of τ_D and τ_{sh} is plotted in Fig. 6. The time τ_c^{lab} in Fig. 6 is the turbulent correlation time measured in the laboratory frame. It represents a lower bound on the turbulent correlation time in the plasma frame. In the shear layer the flow goes through zero, and τ_c^{lab} is the same as the plasma frame correlation time τ_D .

Moyer *et al.* (1995) measured the suppression of turbulent fluctuations in the *H*-mode flow shear layer of the Doublet III-D tokamak (DIII-D), examining the scaling of the density fluctuation amplitude with flow shear strength and comparing with theory. As a probe was moved through the shear layer from an interior position toward the boundary, a decrease in density fluctuations was registered. The fact that fluctuations were low in the extreme edge, where the shear became zero, probably reflects a change in the turbulence source that is coupled to boundary effects and the steep-gradient transport barrier region further in. The data were compared with the density suppression prediction of Biglari, Diamond, and Terry (1990), where $n_s/n_o \sim \epsilon_s^{2/3}$, and an interpolation fit (Zhang and Majahan, 1992) between the strong-

shear scaling of $\epsilon_s^{2/3}$ and a weak-shear scaling of ϵ_s^2 derived by Shaing, Crume, and Houlberg (1990) for the regime $\epsilon_s > 1$. In the negative-shear region on the inner side of the shear layer the predicted strong-shear scalings are in close agreement with the observations for strong flow shear strengths that vary by a factor of 5. In the outer, positive-shear part of the shear layer the data are in disagreement with the suppression theory. With increasing shear, there is little change, or even an increase, in the density fluctuations. Moyer *et al.* (1995) speculate that this behavior may be caused by a local change of the plasma state from *L* mode to *H* mode or by an instability driven by the flow curvature.

Numerous experiments have probed the relationship between the observed confinement enhancements of *H* mode and the theoretical threshold for induced suppression of turbulence $\epsilon_s < 1$ (Burrell *et al.*, 1992; Matsumoto *et al.*, 1992; Doyle *et al.*, 1993; Ohdachi *et al.*, 1994; Tynan *et al.*, 1994). In these experiments the shear strain rate $\omega_s = \tau_s^{-1}$ increases significantly as the plasma goes from *L* mode to *H* mode. (The shear strain rate is modified by toroidal geometry, as discussed in Sec. V.) In the *H* mode, ω_s becomes considerably larger than ω_e , indicating that $\epsilon_s < 1$. In a novel series of experiments, a technique referred to as magnetic braking (La Haye *et al.*, 1993) was used to apply an external torque to the plasma that slowed down the rotation and decreased the flow shear. The experiments showed a marked increase in the fluctuation-driven thermal conductivity in regions where the flow shear had been decreased by the magnetic braking (Burrell *et al.* 1995; La Haye *et al.*, 1995). Because the flow shear was manipulated externally, it could be concluded that there was a cause-and-effect relationship between the decreased flow shear and the increased thermal transport. The conclusion of a causal connection between the flow shear as agent and the decrease of turbulence and transport as response is more difficult to demonstrate in *L-H* transitions. There the spontaneous transition to a different plasma equilibrium brings numerous, nearly simultaneous changes affecting not just the magnitude of flow shear, but the profiles of mean quantities that enter the turbulence sources and the transport fluxes. The causality issue was further examined in *L-H* transitions that show an increase in flow shear prior to the transition. In these transitions the flow shear changed before the turbulence and transport, which in turn changed before the transition and its further modifications of both the equilibrium and the turbulence (Burrell *et al.*, 1995, 1996; Moyer *et al.*, 1995). The same conclusion was reached in an experiment in which the transition was induced by biasing the plasma with an inhomogeneous external electric field that grew slowly in time (Jachmich *et al.*, 1998). The slowly growing shear of the resultant $E \times B$ flow led to a steepening of the density profile that began before the transition. Biasing experiments can also reverse the sign of the flow and flow shear. Suppression has been observed in both cases (Weynants *et al.*, 1991), in accordance with theory.

Suppression of turbulence and turbulent transport by flow shear is a common feature of numerical studies.

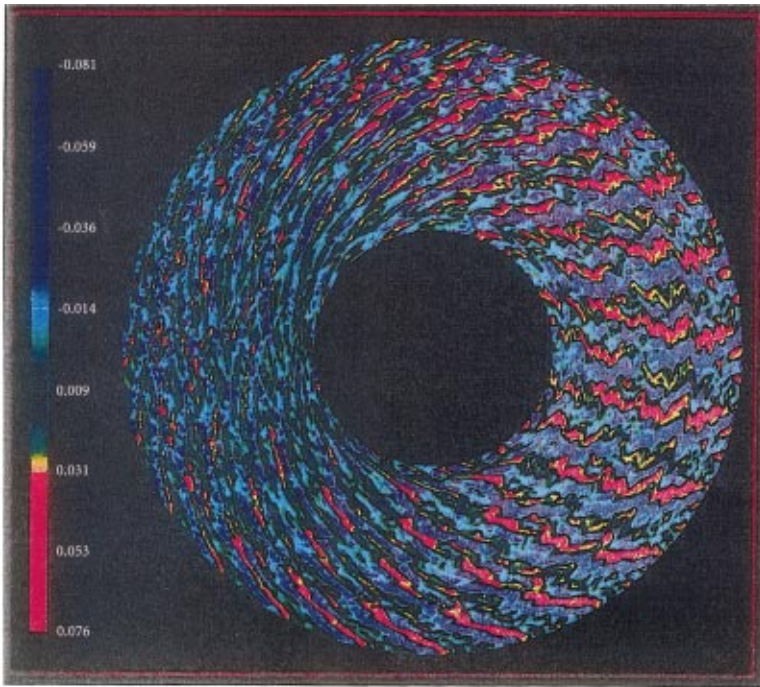
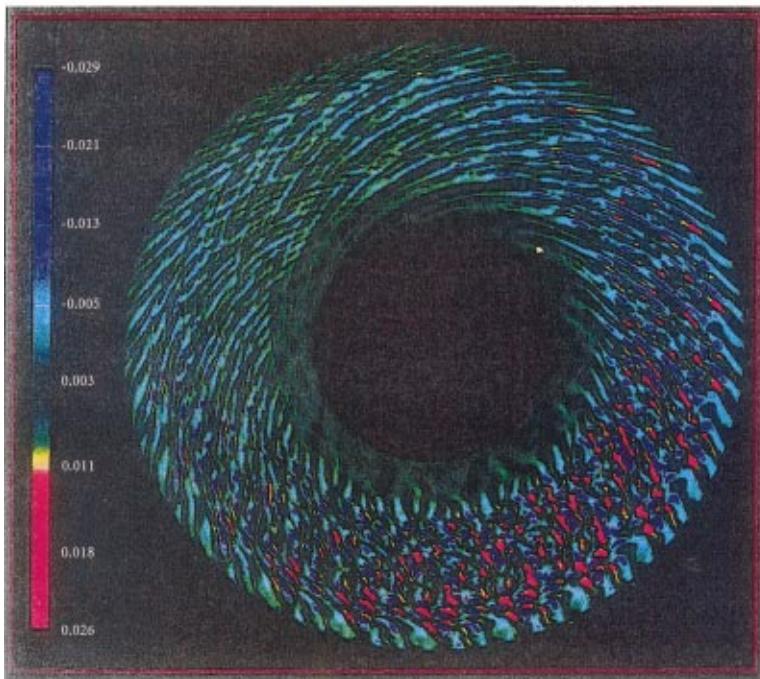


FIG. 7. Fluctuations in simulations of ion-temperature-gradient turbulence in a torus: (a) contours of ion density fluctuation with no rotational shear present, and (b) with rotational shear. Structures have a smaller radial extent in case (b). From Waltz, Kerbel, and Milovich, 1994 [Color].



Such studies, by choice of model, are limited to particular types of collective fluctuations. All, however, show strong suppression at sufficiently large shear. A graphic illustration is provided by simulations of ion-temperature-gradient turbulence in toroidal geometry (Waltz, Kerbel, and Milovich, 1994). Figure 7 shows a cross section of a torus for two cases, one with radially sheared rotation and one without. The structures clearly

have a reduced radial extent when sheared rotation is present. In computations, multiple effects contribute to the suppression, including the balanced-distortion turbulent decorrelation mentioned in Sec. II. C, the stabilization of linear instabilities discussed in Sec. II. E, and the disruption of the transport flux cross phases, to be treated in Sec. V. B. For example, all three processes appear to contribute to the flow-shear-induced suppression.

sion of ion-temperature-gradient-driven turbulence studied by Hamaguchi and Horton (1992). In most numerical studies, flow shear is not a controlled parameter, but is determined self-consistently by the momentum transport dynamics to be discussed in Sec. IV. The Reynolds stress, Sec. IV.B, is a key element in the simulations of Carreras *et al.* (1991), (1992) Ware *et al.* (1992), and Guzdar *et al.* (1993). The nonsymmetry of transport, Sec. IV.B.5, is also a feature of the work of Guzdar *et al.* (1993). Despite these complications, specific aspects of the balanced-distortion theory are evident. The suppression threshold criterion, Eq. (2.17), predicts which fluctuations are suppressed by flow shear (Carreras *et al.*, 1991) and also emerges as the suppression condition when inhomogeneities in the magnetic field are considered (Carreras *et al.*, 1992). The effect of flow shear on the shear-wise eddy scales and the absence of an effect on the flow-wise scales are also observed (Guzdar *et al.*, 1993). Of current interest in simulations is the observed role of unsteady zonal flows in lowering the level of turbulent fluctuations (Das *et al.*, 1997; Lin *et al.*, 1998). Zonal flows are Fourier components of the fluctuating flow field with poloidal and toroidal wave numbers of zero. Analysis indicates that zonal flows are collisionally damped (Diamond *et al.*, 1998; Rosenbluth and Hinton, 1998). Details of the damping are still being investigated.

III. RELATED HYDRODYNAMIC PHENOMENA AND CONCEPTS

There is a close relationship between hydrodynamics and plasma dynamics, the basis of which is the $E \times B$ drift. As a common velocity for all charge carriers, it allows plasma to move as a flow continuum. If one considers a plasma in a magnetic field directed along the \mathbf{z} axis, the charge continuity equation under the $E \times B$ flow is $\partial \rho_q / \partial t + \nabla \cdot (\mathbf{u}_E \rho_q) = \partial \rho_q / \partial t - B_0^{-1} \nabla \tilde{\phi} \times \mathbf{z} \cdot \nabla \rho_q = 0$, where ρ_q is the charge density, $\tilde{\phi}$ is the electrostatic potential, and B_0 is a constant magnetic field. Substitution of the Poisson equation, $\nabla^2 \tilde{\phi} = -\epsilon_0^{-1} \rho_q$, then yields

$$\frac{\partial \nabla^2 \tilde{\phi}}{\partial t} - \frac{1}{B_0} \nabla \tilde{\phi} \times \mathbf{z} \cdot \nabla \nabla^2 \tilde{\phi} = 0, \quad (3.1)$$

an equation that is isomorphic to the vorticity evolution equation of 2D incompressible Navier-Stokes turbulence with a stream-function representation for the flow, $\mathbf{u} = -B_0^{-1} \nabla \tilde{\phi} \times \mathbf{z}$. It is thus possible to identify the electrostatic potential, charge density, and charge continuity equation with the scalar stream function, vorticity, and vorticity evolution equation of 2D Navier-Stokes turbulence. This simple picture is modified if the fluctuation scale exceeds the Debye length, the scale over which thermal electrons short out potential differences (Krall and Trivelpiece, 1973). In that case $\rho_q = 0$, but the continuity of ion density n_i under the polarization drift (a finite inertia correction to the $E \times B$ flow) recovers Eq. (3.1) with the addition of $\partial n_e / \partial t$ from the neutrality condition $n_i = n_e$ (Hasegawa and Mima, 1977). The $E \times B$

flow thus possesses vorticity by virtue of the ion polarization drift. Additional effects, particularly those due to electron dynamics, complicate Eq. (3.1) but do not supplant the basic dynamics of vorticity advection by the $E \times B$ flow (Terry and Horton, 1982; Newman *et al.*, 1993).

Such similarities lead to the question of why suppression of turbulence by flow shear is not a familiar phenomenon in hydrodynamics. The answer is provided by three basic conditions for simple observation of the suppression effect: (1) the shear flow should be stable; (2) the turbulence should remain in the region of shear for longer than an eddy turnover time; (3) the dynamics should be 2D. These conditions are generally met in fusion plasmas but, as illustrated in the remainder of this section, are satisfied in neutral flows only under special circumstances. Shear flow stability is discussed in Sec. III.A, where it is shown that unstable shear flows, such as jets, can be stabilized by a rotation gradient. The condition is mathematically analogous to the condition for stabilization of shear flow in plasmas by the equilibrium magnetic-field inhomogeneity, as will be discussed in Sec. V.A.1. Section III.B considers rapid-distortion theory, a theory widely used in hydrodynamics for strong-shearing regimes ($\tau_s < \tau_e$), but only valid in the short time limit when τ_e exceeds the time that turbulence remains in the region of shearing. Strongly sheared hydrodynamic flows are frequently well modeled by rapid-distortion theory, hence they do not satisfy the second condition. Rapid-distortion theory also illustrates why 2D dynamics are desirable for suppression, showing that common 3D shear flows lead to vortex tube stretching, which amplifies components of the vorticity instead of suppressing them. Two-dimensional turbulent flows are unusual in hydrodynamics, except under strong stratification or rotation. Section III.C introduces geostrophic flow, a hydrodynamic flow that satisfies the three conditions given above. Further examples are given in Sec. VIII.

A. Stable shear flow

In hydrodynamics shear flows are often unstable, generating turbulence instead of suppressing it. A simple example is the Kelvin-Helmholtz instability. The instability problem is analytically tractable for a piecewise continuous mean flow with oppositely directed uniform flows connected by a region of linear shear: $\bar{u}(y) = U_0$ for $y > L$, $\bar{u}(y) = -U_0$ for $y < -L$, and $\bar{u}(y) = U_0 y / L$ for $-L < y < L$ (Chandrasekhar, 1961). Assuming homogeneity in the z direction, the evolution equation for vorticity governs the temporal growth of vorticity fluctuations,

$$\left(\frac{\partial}{\partial t} + \bar{u}(y) \frac{\partial}{\partial x} + \nabla \tilde{\phi} \times \mathbf{z} \cdot \nabla \right) \nabla^2 \tilde{\phi} - \frac{d^2 \bar{u}}{dy^2} \frac{\partial \tilde{\phi}}{\partial x} = \frac{\mu}{\rho} \nabla^4 \tilde{\phi}, \quad (3.2)$$

where the fluctuating flow $\mathbf{u} = \nabla \tilde{\phi} \times \mathbf{z}$ is expressed in terms of the stream function $\tilde{\phi}$, and $\mathbf{z} \nabla^2 \tilde{\phi} = \nabla \times \mathbf{u}$ is the vorticity. The last term on the left-hand side is required

for instability, i.e., the flow must have a second derivative, usually referred to as the curvature of the mean flow. For the piecewise continuous flow this is provided by the discontinuities in slope at $x = \pm L$. Fluctuations centered at the vorticity maximum $y=0$ are unstable if $k_x L \lesssim 1$, where k_x is the Fourier wave number for the x direction. The growth rate (neglecting viscosity) is

$$\gamma_k = U_o k_x \left(\frac{1}{k_x L} - 1 - \frac{1}{2k_x^2 L^2} \frac{\sinh(2k_x L)}{\exp(2k_x L)} \right)^{1/2}. \quad (3.3)$$

For this and more general flow profiles, a necessary condition for instability is the existence of a vorticity maximum at the point of inflection of the mean flow (Lin, 1955).

Many flows are unstable, including jets, flow past objects, and wall flows (Poisueille and Couette flows). Certain flows, however, are stable. Localized vortices in 2D with azimuthal symmetry and appropriate vorticity profiles are an example. An isolated 2D vortex strip is unstable, but if there is a background shear flow with a uniform shear of sufficient strength opposing the shear of the isolated vortex strip, the strip is stabilized (Dritschel, 1989). One realization of the background flow is the differential rotation of a circular vortex. More generally, rotation tends to stabilize flow-shear-driven instabilities (Lesieur, 1997). Geostrophic flows in rotating planetary atmospheres can be stabilized by planetary rotation. Two types of large-scale instability are thought to be important in the Earth's stratosphere (Andrews, Holton, and Leovy, 1987). Barotropic instability arises from large horizontal curvature of a zonal (east-west) flow, $\partial^2 \bar{u} / \partial y^2$, where positive \bar{u} is an eastward flow and y is the northward direction. Baroclinic instability basically arises from vertical curvature $\partial^2 \bar{u} / \partial z^2$, but also involves buoyancy and the vertical density stratification of the atmosphere. These instabilities require the curvature forces to exceed the stabilizing effect of rotation. Instability is governed by a quantity S_R representing the difference between the rotational and curvature effects:

$$S_R = \beta - \frac{\partial^2 \bar{u}}{\partial y^2} - \frac{1}{\rho_o} \frac{\partial}{\partial z} \left(\rho_o \epsilon \frac{\partial \bar{u}}{\partial z} \right), \quad (3.4)$$

where β is the gradient of the projection of the planetary vorticity on the local vertical, ρ_o is the mass density at a reference height, ϵ accounts for stratification and buoyancy effects, and S_R is the northward gradient of a quantity known as the potential vorticity. A necessary condition for instability is that S_R must change sign in the flow domain (Andrews, Holton, and Leovy, 1987). The barotropic part of this criterion is derived in Sec. III. C. Large-scale shear flows in the stratosphere, such as the equatorial jet (Treppe and Hitchman, 1992) and the Antarctic and Arctic polar vortices (Tuck, 1989; Tuck *et al.*, 1992), are stable most of the time. Occasionally they become unstable due to an episodic disturbance called a wave-breaking event (McIntyre and Palmer, 1984). This event redistributes the flow curvature, and stability is reestablished.

B. Rapid-distortion theory

Rapid-distortion theory describes the evolution of turbulence that transits through a region of strong mean flow shear. A typical application of this theory is the advection of turbulence into and through a region of strong shear, as occurs for example in a nozzle, or a constriction or bend in a pipe. Because rapid-distortion theory linearizes the evolution equations, its validity criterion is that the domain time, or the time during which turbulent structures are advected through the domain of sheared flow, be shorter than the time scale of the turbulent interactions (or eddy turnover time) for the largest eddies (Hunt, Carruthers, and Fung, 1991). When this holds, the nonlinearity has insufficient time to modify the flow, and the flow retains features of the initial state. Under the linearization, turbulence entering the region of strong flow shear is taken as an initial state and mapped under a kinematic ray tracing transformation to the evolving configuration at later times. The mapping is applied to quantities such as fluctuation intensities and scales, energies, and Reynolds stresses. Because the domain time is the time over which the strong flow shear interacts with turbulence, it is the shear straining time for finite-length domains. The criterion for rapid distortion theory therefore resembles the threshold condition for shear suppression, Eq. (2.17). However, plasma flows in fusion devices are circular, and the domain time becomes much longer than both the shear straining time and the nonlinear interaction time. In this situation linearization is not valid.

A lucid discussion of rapid-distortion theory is given by Townsend (1976). Following Batchelor and Proudman (1954), he treats the mean flow variation as linear and uses the method of characteristics to transform the inhomogeneity to a characteristic equation for Fourier wave numbers. With mean and fluctuating flow components U_i and u_i , the linearized Navier-Stokes equation is

$$\frac{\partial u_i}{\partial t} + U_l \frac{\partial u_i}{\partial x_l} + u_l \frac{\partial U_i}{\partial x_l} = - \frac{1}{\rho} \frac{\partial p}{\partial x_i} + \mu \frac{\partial^2 u_i}{\partial x_l^2}, \quad (3.5)$$

where for incompressible flow the pressure and flow are related via $2\rho(\partial U_l / \partial x_m)(\partial u_m / \partial x_l) = -\partial^2 p / \partial x_m^2$, enabling Eq. (3.5) to be expressed solely in terms of the flows. The mean flow variation is linear, $U_l = x_j(\partial U_l / \partial x_j)$, where $\partial U_l / \partial x_j$ is a constant. Introducing a Fourier expansion $u_i = \sum_k a_i(k, t) \exp(i\mathbf{k} \cdot \mathbf{x})$, one can transform the inhomogeneity to a derivative of a_i with respect to k_j ,

$$U_l \frac{\partial u_i}{\partial x_l} = x_j \frac{\partial U_l}{\partial x_j} \frac{\partial u_i}{\partial x_l} = - \sum_k \frac{\partial U_l}{\partial x_j} \frac{\partial a_i}{\partial k_j} k_l \exp(i\mathbf{k} \cdot \mathbf{x}). \quad (3.6)$$

The amplitude evolution equation is solved by the method of characteristics, writing $da_i/dt \equiv \partial a_i / \partial t + (\partial a_i / \partial k_j)(dk_j/dt)$. The characteristic equation for wave-number evolution is obtained from the coefficient of $\partial a_i / \partial k_j$ in the Fourier-transformed Navier-Stokes equation, yielding

$$\frac{da_i}{dt} = -\mu k^2 a_i - \frac{\partial U_i}{\partial x_l} a_l + \frac{2k_i k_l}{k^2} \frac{\partial U_l}{\partial x_m} a_m, \quad (3.7)$$

$$\frac{dk_j}{dt} = -\frac{\partial U_l}{\partial x_j} k_l. \quad (3.8)$$

The amplitude a_i evolves from an initial value according to $a_i(\mathbf{k}, t) = a_i[\mathbf{k}_0(\mathbf{k}, t), t_0]$, where $\mathbf{k}_0(\mathbf{k}, t)$ is the time-inverted solution of Eq. (3.8), with \mathbf{k}_0 the initial value at t_0 and \mathbf{k} the value at time t .

Two examples of simple mean flow configurations illustrate how flow shear modifies intensities and scales for short times. The first is an irrotational flow $U_1 = \alpha_1 x_1$, $U_2 = \alpha_2 x_2$, $U_3 = \alpha_3 x_3$, where α_l can vary in time but not in space. This is a 3D flow that illustrates how vorticity is amplified by vortex tube stretching. Incompressibility constrains α_l so that $\alpha_1 + \alpha_2 + \alpha_3 = 0$. This type of flow occurs in ducts with changing cross section. The clearest indication of the distortion is obtained by applying the method of characteristics to the vorticity equation,

$$\frac{\partial \omega_i}{\partial t} + U_l \frac{\partial \omega_i}{\partial x_l} = \omega_l \frac{\partial U_i}{\partial x_l}, \quad (3.9)$$

where $\omega = \nabla \times \mathbf{u}$ is the vorticity, and viscosity has been assumed to be negligible. Under the Fourier expansion $\omega_i = \sum_k \Omega_i(k, t) \exp(i\mathbf{k} \cdot \mathbf{x})$, the characteristic procedure yields

$$\frac{d\Omega_l}{dt} = \alpha_l \Omega_l, \quad \frac{dk_1}{dt} = -\alpha_1 k_1, \quad (3.10)$$

with similar equations for the other two components. It is evident that along directions in which the flow moves outward from the origin, the vorticity intensifies and the wave number decreases. The opposite is true along directions in which the flow moves inward. This is a simple manifestation of a basic process known as vortex tube stretching (Tennekes and Lumley, 1972). The outward-directed flow velocity increases with distance from the origin and thereby stretches vortex tubes whose axes align with the flow velocity. The increase of vortex tube length requires a decrease of cross-sectional area because the vortex volume must remain invariant. The smaller cross-sectional area requires an increase in vorticity to maintain the invariance of circulation ($\int \mathbf{u} \cdot d\mathbf{l} = \text{const}$ for inviscid flow). In a flow with $\alpha_1 = -\alpha_3 = \text{const}$, $\alpha_2 = 0$, vorticity in the x_1 direction increases while its cross-sectional area, parametrized by k_3 , decreases. This means that the wave number k_3 increases. Similarly, Ω_3 and k_1 decrease. Note that the intensification of vorticity is a 3D phenomenon. If the turbulence is 2D, the vorticity is solely in the x_2 direction. With $\alpha_2 = 0$, the vorticity is unchanged. In this case only the scales are modified. In 3D flows, the intensification of vorticity aligned with the mean flow is a competing effect to the reduction of vorticity perpendicular to the flow, making suppression of turbulence, even in the long-time domain, difficult to detect.

A second example is unidirectional plane shearing, with $U_1 = \alpha x_3$, $U_2 = U_3 = 0$. This flow can be viewed as

the superposition of an irrotational plane straining flow $U_1^{(i)} = 1/2 \alpha x_3$, $U_3^{(i)} = 1/2 \alpha x_1$, and a rotation about the x_2 axis $U_1^{(r)} = 1/2 \alpha x_3$, $U_3^{(r)} = -1/2 \alpha x_1$. The irrotational flow is like that of the previous example, but the axes of outward and inward flows are turned through 45° . The tendency of the irrotational flow to align and intensify vortex tubes along angles of 45° and 225° with respect to the x_1 axis is counteracted by the rotational part of the flow, which turns vortex tubes away from these directions. Plane shear flow is therefore less efficient at transferring energy to turbulence than irrotational flow. Townsend (1976) examines rapid-distortion theory for unidirectional plane shearing of turbulence with an eddy viscosity, such as the diffusivity of statistical closure theory used in Eq. (2.29). It is tempting to view the presence of the eddy viscosity as an extension of rapid-distortion theory away from its traditional linearization of the dynamics. However, examination of wave-number evolution shows that rapid-distortion theory remains linear, even with an eddy viscosity in the model. The wave-number evolution, specified by

$$\frac{dk_1}{dt} = \frac{dk_2}{dt} = 0, \quad \frac{dk_3}{dt} = -\alpha k_1, \quad (3.11)$$

does not depend on the eddy viscosity and is strictly reversible. The solutions,

$$k_1 = k_{10}, \quad k_2 = k_{20}, \quad k_3 = k_{30} - \alpha k_1 (t - t_0), \quad (3.12)$$

have secular evolution, implying no loss of correlation. The k_3 solution describes the unbounded stretching of an eddy along the x_1 axis. If some feature of the turbulence has an initial structure

$$s(k_1, k_3, t_0) = \exp[-(k_1^2 + k_3^2)/2\Delta k^2], \quad (3.13)$$

at later times the envelope (irrespective of amplitude changes) becomes

$$s(k_1, k_3, t) = \exp(-[k_1^2 + [k_3 + \alpha k_1 (t - t_0)]^2]/2\Delta k^2). \quad (3.14)$$

It is apparent that the width of the structure $\langle k_1^2 \rangle$ in the k_1 direction of wave-number space shrinks in time as $\langle k_1^2 \rangle \approx \Delta k^2 / [\alpha^2 (t - t_0)^2 + 1]$. The stretching with time along the x_1 axis thus continues without bound. The eddy viscosity contributes to amplitude decay, but the extended structure maintains coherence indefinitely, both temporally and spatially.

The secularity and reversibility of the wave-number solution, Eq. (3.12), with its direct dependence on initial state, are striking given the presence of eddy viscosity and the essentially identical content of Eq. (3.5) and the models of the prior section, e.g., Eq. (2.29). Returning to Eq. (2.29), the rapid-distortion wave-number solution can be obtained by retaining the initial state in the Laplace transform, taking the turbulent diffusivity to zero and inverting the spatially inhomogeneous operator. The dominant asymptotic balance in Eq. (2.29) with $D_n = 0$ is

$$-\gamma_n \psi_{n,\gamma} + i n (\bar{u}/r) {}_r \hat{r} \psi_{n,\gamma} = \psi_n(\hat{r}, t=0). \quad (3.15)$$

Converting this equation to the Cartesian geometry of

the plane shearing example, with $(\bar{u}/r)|_{r_0}=0$, $\hat{r} \rightarrow x_3$, and $in(\bar{u}/r)_{r \rightarrow i} \alpha k_1$, this balance is

$$-\gamma \psi_{k_1, \gamma}(x_3) + i \alpha k_1 x_3 \psi_{k_1, \gamma}(x_3) = \psi_{k_1}(x_3, t=0). \quad (3.16)$$

If the initial state is given by $\psi_{k_1}(x_3, t=0) = \exp[-1/2 x_3^2 \Delta k^2 - k_1^2 / 2 \Delta k^2]$ [the equivalent of Eq. (3.13)], the solution of Eq. (3.16) is

$$\psi(x_1, x_3, t) = \exp\{-1/2[x_3^2 + (x_1 - \alpha x_3 t)^2] \Delta k^2\}, \quad (3.17)$$

where the inverse Laplace transform has been used. Equation (3.17) is the Fourier transform of Eq. (3.14), up to a normalization factor, confirming the statement made in Sec. II.B.3 that rapid-distortion theory is the short-time asymptotic balance for the strong-shearing limit. For longer times, specifically when the elapsed time from the initial moment exceeds the eddy turnover time or turbulent correlation time, $\gamma \psi$ becomes smaller than the turbulent diffusivity term neglected in Eq. (3.15), and it enters the balance that determines spatial structure.

The validity criterion given for rapid-distortion theory by Hunt, Carruthers, and Fung (1991) should thus be modified. They stipulated that $\tau_D < \tau_N$, where the domain time τ_D is the time during which flow is advected through the domain of strong flow shear, and τ_N is the turbulent correlation time of the largest eddies. The modified rapid-distortion criterion is

$$\tau_S \leq \tau_D < \tau_N. \quad (3.18)$$

The distinction between the domain time and the shear time, which are normally equal in rapid-distortion theory, is introduced because the two times become distinct in fusion plasma transport barriers where the sheared flow is circular. The shear suppression criterion of balanced-distortion theory is therefore

$$\tau_S < \tau_N < \tau_D. \quad (3.19)$$

In this limit turbulent diffusivity enters asymptotic balances and affects both scales and intensities.

It is instructive to examine why the eddy diffusivity appears only in the amplitude evolution of rapid-distortion theory but never enters the wave-number evolution, while in the Green's-function techniques of the previous section, it affects both amplitudes and wave numbers for sufficiently long times. Eddy diffusivities are a dissipative representation of the energy lost at a given scale due to turbulent energy transfer, which in reality is a conservative process. If a conservative model of the turbulent transfer process is used, the characteristic method of Batchelor and Proudman (1954) leads to an eddy diffusivity dependence in the wave-number evolution equation. Conservative closures, such as the direct-interaction approximation (Kraichnan, 1959), which are derived in a Fourier space representation, produce spatially inhomogeneous diffusivities in real space (Boutros-Ghali and Dupree, 1981; Terry and Diamond, 1985). As described in Sec. II.B.2, the diffusivity vanishes quadratically as the separation of fluid parcels goes to zero. Using a method of characteristics to sepa-

rate out the evolution of wave numbers, we see that the quadratic spatial variation of the diffusivity enters the wave-number evolution as an effective force that drives the second temporal derivative of the wave number. The analysis of Sec. II.B establishes that this force increases the shear-wise wave number (reduces the shear-wise scale), consistent with dimensional scaling analysis.

Balanced-distortion theory is thus an extension of rapid-distortion theory into a nonlinear regime. The extension, however, is for the simplest of situations and does not address many complexities that arise even in the linearized theory. These complexities include 3D behavior and boundary conditions. In fusion plasmas the magnetic field generally imposes 2D motion, and boundary conditions are often ignored for small-scale fluctuations because the inhomogeneity of the equilibrium magnetic field localizes fluctuations away from boundaries. In applications of rapid-distortion theory, there is also frequently a need to achieve highly accurate flow modeling, which requires mappings that preserve key symmetries of Reynolds stresses and other tensoral quantities (Reynolds and Kassinos, 1995).

C. Geostrophic flows and other examples

Hydrodynamic flows that satisfy the three conditions required for simple observation of turbulence suppression by flow shear do not usually include common types of shear flow. One that does is geostrophic flow. Consider the Earth's stratosphere, where mean geostrophic flows, such as the equatorial jet and the Arctic and Antarctic polar vortices, run zonally (east-west) and have shear in the meridional (north-south) direction. Provided that planetary rotation is sufficiently strong relative to the meridional curvature to prevent barotropic instability [Eq. (3.5)], these mean flows are stable. Because of planetary rotation, large-scale geostrophic turbulence is approximately 2D. As zonal flows, the mean flows close on themselves, making the domain time larger than any nonlinear time.

The simplest model for geostrophic turbulence is the quasigeostrophic β -plane model. The β plane is a tangent plane to the planetary surface. Fluid motions are 2D in this plane, provided that their eddy turnover time is larger than the local planetary rotation time, i.e., $\Omega \sin \theta \tau_e \equiv Ro^{-1} \gg 1$. Here Ω is the planetary rotation rate, θ is the latitude, τ_e is the eddy turnover time, and Ro is the Rossby number. The total vorticity perpendicular to the β plane, which includes the planetary vorticity component $2\Omega \sin \theta$, is approximately conserved under these conditions, yielding $d/dt(2\Omega \sin \theta - \nabla^2 \Phi) = 0$. The total flow vorticity $\nabla^2 \Phi$ is the curl of the incompressible 2D flow \mathbf{u} , which can be expressed in terms of the stream function Φ : $\mathbf{u} = \nabla \Phi \times \mathbf{z}$, where \mathbf{z} is normal to the β plane. The stream function has mean and turbulent components $\Phi = \Phi_0(y) + \phi(x, y)$, yielding flow $\mathbf{u} = \bar{u}(y)\mathbf{x} + \nabla \phi \times \mathbf{z}$ with a zonal mean component with meridional shear $\bar{u}(y) = \partial \Phi_0 / \partial y$ and a turbulent component $\nabla \phi \times \mathbf{z}$. The β -plane coordinates x and y are zonal and meridional displacements from the tangency point of the β plane. In terms of the longitude φ and latitude θ

of any point on the β plane, $x = a \cos \theta_0(\varphi - \varphi_0)$ and $y = a(\theta - \theta_0)$, where φ_0 and θ_0 are the longitude and latitude of the tangency point and a is the planetary radius. Making advection explicit in the total derivative [$d/dt = \partial/\partial t + \bar{u}(y)\partial/\partial x + \nabla\phi \times \mathbf{z} \cdot \nabla$], one finds the vorticity conservation expression

$$\left(\frac{\partial}{\partial t} + \bar{u}(y) \frac{\partial}{\partial x} + \frac{\partial\phi}{\partial y} \frac{\partial}{\partial x} - \frac{\partial\phi}{\partial x} \frac{\partial}{\partial y} \right) \nabla^2 \phi + \beta \frac{\partial\phi}{\partial x} - \frac{\partial\phi}{\partial x} \frac{d^2\bar{u}}{dy^2} = 0, \quad (3.20)$$

where the northward gradient of the locally vertical component of planetary vorticity defines β :

$$\begin{aligned} d/dy[2\Omega \sin(\theta_0 + y/a)] &= 2\Omega a^{-1} \cos \theta_0 + O(y/a) \\ &\equiv \beta + O(y/a). \end{aligned}$$

The stabilizing effect of β is evident in its creation of an effective zero-point shift of the mean flow curvature. If $\beta - d^2\bar{u}/dy^2$ does not change sign, there is no point of inflection. The barotropic instability condition [Eq. (3.5)] is thus a form of the Lin (1955) criterion. The quasigeostrophic β -plane model is closely related to the Hasegawa-Mima (1977) model of magnetized plasma turbulence, a relationship that originates with an isomorphism between the Coriolis force in a rotating neutral fluid and the Lorentz force in a magnetized plasma. From the respective momentum equations, $\rho(d\mathbf{u}/dt + 2\Omega \times \mathbf{u}) = -\nabla p$ and $\rho d\mathbf{u}/dt = e\mathbf{p}m^{-1}(\mathbf{u} \times \mathbf{B}) - \nabla p$, the dynamical equivalence of 2Ω and $e\mathbf{m}^{-1}\mathbf{B}$ is evident. This has two consequences of relevance to present considerations: (1) rotation gradient and magnetic-field inhomogeneity play analogous roles in stabilizing shear flow (the latter is developed in Sec. V.A.1), and (2) rotation and magnetic field enforce 2D dynamics.

The effect on geostrophic β -plane turbulence of a large-scale mean zonal flow with meridional shear has been considered by Shepherd (1987) and Ware *et al.* (1999). Part of Shepherd's analysis employs rapid-distortion theory and describes shear straining of Rossby wave packets in the absence of nonlinear interactions. Wave numbers evolve according to Eq. (3.11), and the unbounded zonal stretching of eddies eventually converts wave energy into the zonal mean flow. The discussion of nonlinear effects focuses on the tendency of the turbulence to isotropize eddies. While the shear suppression mechanism is not identified, it appears to be operating. In a simulation of driven, stationary geostrophic turbulence, the near absence of enstrophy (mean-squared vorticity) in regions of strongest basic shear is pointed out by Shepherd (1987). This is apparent in a plot of contours of constant enstrophy (mean-squared vorticity), shown in Fig. 8. Where the flow shear is zero in horizontal bands at $y = 0, \pi,$ and 2π , enstrophy fluctuations are strong, as indicated by closed contours with three and four contour levels for either positive (solid line) or negative (dotted line) contours. Where the shear is maximum in bands at $y = \pi/2$ and $3\pi/2$, the enstrophy fluctuations are weak, as indicated by the ap-

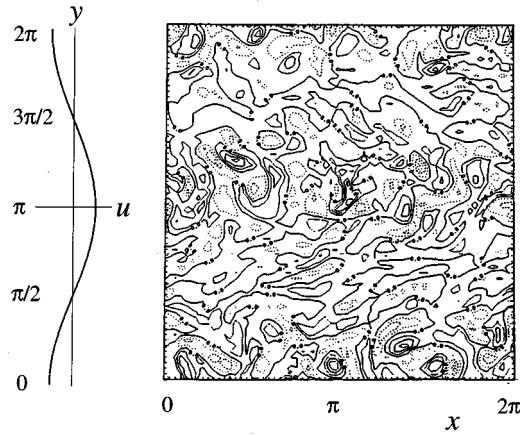


FIG. 8. Enstrophy contours in simulations of geostrophic turbulence in a β plane with a large-scale sheared zonal jet. Enstrophy is reduced in the regions of large shear at $y = \pi/2$ and $3\pi/2$. From Shepherd, 1987.

pearance of few structures with closed contours, and, when such structures do occur, the existence of at most a single contour level. In simulations of decaying turbulence, plots of turbulent energies as a function of the meridional coordinate (Fig. 15 of Shepherd, 1987) also show energy minima where the shear is maximum. The enstrophy contour plots suggest that the ratio of meridional to zonal scale is reduced in regions of strong shear relative to regions of no shear for the larger scales. For smaller scales the fluctuations are isotropic. These tendencies are consistent with a reduction of shear-wise scale for the larger eddies, as indicated by Eqs. (2.15) and (2.17). In the simulations of Shepherd the suppression of turbulence is marginal because the shear is not very strong. In Sec. VII β -plane turbulence is revisited to examine stronger shear and confirm the predictions of balanced-distortion theory.

The β -plane model, Eq. (3.20), also has linear wave solutions called Rossby waves. Linearization of Eq. (3.20) for $\bar{u}(y) = 0$ yields the Rossby wave dispersion

$$\omega_R = \frac{-k_x \beta}{(k_x^2 + k_y^2)}, \quad (3.21)$$

where ω_R is the Rossby wave frequency, and k_x and k_y are wave numbers in the zonal and meridional directions. When a coherent Rossby wave couples to pressure fluctuations to become a thermal Rossby wave and produce a heat flux [Eq. (2.9)], flow shear can suppress the transport (Azouni, Bolton, and Busse, 1986; Or and Busse, 1987). Flow shear changes the complex phase between the fluctuations of pressure and flow, reducing the transport. Flow shear also changes the complex phase between pressure and flow in turbulence, as described in Sec. V.B.

Another class of turbulent flows, referred to as slowly changing turbulence, has the opposite limit, $\tau_N < \tau_D$, and thus involves the nonlinearity (Hunt, Carruthers, and Fung, 1991). Unconfined turbulent flows, such as wakes, jets, and shear layers, lack confining boundaries and nominally belong to this class. Observations for

nearly a dozen cases of unconfined turbulent flows establish that $\tau_N = \tau_D$, suggesting that the turbulence adjusts in some way to achieve this balance. This adjustment is postulated by Hunt, Carruthers, and Fung (1991) to involve an increase in the largest turbulence scales to the size of the inhomogeneity in order to bring the nonlinear time into balance with the domain time. Note that the plasma flows of balanced-distortion theory are unconfined in the sense that the domain time becomes large. However, the domain time and shearing time, unlike rapid-distortion theory, are distinct. The large domain time allows the nonlinearity to force adjustments, but the inhomogeneity originates with the shear straining. The nonlinearity thus adjusts the turbulent flow to bring the nonlinear and shear straining times into balance. In this sense balanced-distortion theory is a hybrid of slowly changing and rapidly changing turbulence, created by the decoupling of the shearing time and domain time.

An example in which shearing and nonlinear times balance is flow over an undulating surface. Changes in the drag force caused by surface undulations are shown by Belcher, Newly, and Hunt (1993) to arise from a thickening of the turbulent boundary layer leeward of the undulation. Sufficiently far above the surface, the flow can be modeled with rapid-distortion theory, but nonlinear interactions become important near the surface in an inner layer. The boundary layer thickening is caused by the turbulent Reynolds stress in a region where it is in balance with the shear straining force, i.e., *where the turbulent correlation time balances the shear straining time*, as in Eq. (2.16); Hunt, Leibovich, and Richards (1988). The shear-wise spatial variation consistent with this balance differs from Eq. (2.15) only in its details, which reflect the structure of the boundary layer and the asymptotic matching analysis used to solve the problem. The scalings, however, evince the same general features as those of Eq. (2.15): the layer width is proportional to a positive power of the turbulence strength and a negative power of flow shear strength. Leeward of the undulation, the shear strength diminishes relative to the turbulence strength, and the layer thickens.

IV. GENERATION OF SHEARED $E \times B$ FLOW

Although a variety of flows appear in plasma continuum descriptions, the $E \times B$ flow is responsible for the observed suppression of turbulent fluctuations in plasmas. This statement is rooted in empirical observations and theoretical calculations that show that the $E \times B$ flow is the sole advectant of fluctuations in density, temperature, and flow. For example, the diamagnetic flow $\mathbf{u} = (B^2 en)^{-1} \nabla p \times \mathbf{B}$ does not advect fluctuations because it is canceled by a part of the gyroviscous tensor (see Kim *et al.*, 1991; Chang and Callen, 1992; and the references to earlier work cited therein). Given the unique status of $E \times B$ flow in plasmas, it is essential to understand its generation. It involves processes that differ dramatically from those of shear-driven hydrodynamic turbulence. In the turbulent boundary layer of a

nonionized fluid, for example, the flow shear is determined by the momentum input and the transverse-momentum transport arising from the Reynolds stress. Flow shear drives turbulence, which greatly increases the drag relative to that of a laminar boundary layer by increasing the momentum transport to the wall. This transport regulates the momentum gradient and therefore feeds back on the turbulence drive. Increases in free energy cause an increase in fluctuation energy, enabling momentum transport to keep pace with the momentum input.

In plasmas, an increase in free energy can lead to a *decrease* in fluctuation energy because the free energy that normally drives turbulence can drive flow shear instead. The result is a decrease in turbulence and turbulent transport, which leads to a further increase in the gradients providing the free energy (the free energy itself does not necessarily increase because of the suppressing and stabilizing effect of the flow shear). The generation of mean $E \times B$ flow shear involves any of a number of processes affecting momentum, including external momentum sources from the injection of energetic beams of neutral particles or intense rf waves, the Reynolds stress, mean electric and magnetic fields through the Lorentz force, the pressure, and dissipative processes. Turbulence directly participates in the momentum balance governing the generation of $E \times B$ flow shear through the Reynolds stress, but also enters indirectly, because turbulent transport affects the pressure profile and fields.

A. Radial force balance

The problem of determining the mean $E \times B$ flow in most plasmas is essentially the problem of determining the radial component of the mean electric field. The mean magnetic field can generally be treated as a known and fixed parameter, because most of the field is produced by external windings or is part of a relaxed state with a known and robust magnetic field. The electric field is specified by a mean radial force balance. The radial component is the relevant component because for the plasma to be radially confined, both the magnetic field and the $E \times B$ flow must lie on the nested tori of Fig. 2, i.e., they must be perpendicular to the radial direction.

The fundamental equation governing the electric field is the Poisson equation, $\nabla \cdot \mathbf{E} = \rho_q / \epsilon_0$. The large polarizability of a plasma and the difficulty of directly measuring charge density in fusion plasmas have led to the development of other methods for inferring the electric field. The Poisson equation is closely related to the momentum, as illustrated in Eqs. (3.1) and (3.2), because flow is the primary arbiter of charge density through the charge continuity equation. Consequently, to determine the radial electric field, it is often sufficient to specify and solve the radial force balance. It is the ion radial force balance that is of interest. Ions dominate the plasma momentum because of their large mass relative to electrons. The equilibrium radial force balance for ions is given by

$$E_r = \frac{1}{Z_i e n_i} \frac{\partial}{\partial r} p_i + \frac{m_i}{Z_i e} \frac{\partial}{\partial r} \langle \tilde{u}_{r i} \tilde{u}_{r i} \rangle - u_{\theta i} B_\varphi + u_{\varphi i} B_\theta, \quad (4.1)$$

where Z_i is the charge state of the ions, e is the electronic charge, n_i is the ion number density, p_i is the ion pressure, m_i is the ion mass, and the subscripts θ and φ indicate the components of the mean poloidal and toroidal ion flow and magnetic field. In Eq. (4.1) all quantities have been averaged over magnetic-flux surfaces, i.e., the surfaces of Fig. 2. Equation (4.1) is comparable to the Reynolds momentum equation, Eq. (2.10), except for the absence of dissipation, which is negligible for the radial momentum component, and the addition of the electric and Lorentz forces. Two components of the Reynolds stress are fluxes of radial momentum on magnetic-flux surfaces and, for incompressible flow, vanish upon averaging. All terms from the advective derivative of the mean flow vanish because, by design, there is no mean radial flow in magnetically confined plasmas on the time scales of dynamical evolution. (Transport produces mean radial displacements on longer time scales, but the effect enters in higher order.) The diagonal Reynolds stress contribution to the radial force balance appearing in Eq. (4.1) is often neglected. Its ratio with the first term of the Lorentz force is $k_\theta^2 k_r \rho_i^3 (Z_i e \phi / T_e)^2 (T_e / T_i)^2 (u_{T i} / u_{\theta i})$, where $u_{T i} = (T_i / m_i)^{1/2}$ is the ion thermal speed and $\rho_i = (T_i / m_i)^{1/2} / Z_i e B_0$ is the ion radius of gyration in the magnetic field. The poloidal and radial wave numbers k_θ and k_r are typically smaller than ρ_i^{-1} by an order of magnitude; the electrostatic fluctuation amplitude $Z_i e \phi / T_e$ typically ranges from a few to ten percent, but is never larger than 1; the ratio of electron to ion temperature T_e / T_i is of order unity; and the ratio of the ion thermal velocity to the poloidal flow ranges from 10 to 100. The neglect of the Reynolds stress in the radial force balance is justified in most situations, although it could be important in cases in which fluctuations are of large amplitude and short wave length, and the poloidal flow is small. Looking at the ratio of the Reynolds stress to the two other terms on the right-hand side of Eq. (4.1) leads to similar conclusions. For the ratio with the pressure term, the same ratio expression given above applies with $u_{\theta i}$ replaced by the ion diamagnetic flow $u_{*i} (1 + L_n / L_T) = T_i (Z_i e B_0 L_n)^{-1} (1 + L_n / L_T)$, where L_n and L_T are the scale lengths of the ion density and pressure. For the ratio with the toroidal flow term of the Lorentz force, $u_{\theta i}$ is replaced by $u_{\varphi i} B_\theta / B_\varphi$. Reynolds stress components in the toroidal and poloidal force balances are proportionately much more important because parallel forces are weaker than the radial forces, which mediate confinement balances. Parallel force balances are examined in Sec. IV. B.

Ignoring the Reynolds stress in Eq. (4.1), it is evident that the radial electric field is governed by the ion pressure force and, in conjunction with the mean magnetic field through the Lorentz force, by the toroidal and poloidal ion flows. Depending on the circumstance, any of these forces, either individually or jointly, can play an important role in generating and sustaining the large ra-

dial electric fields of transport barriers. Measurements indicate that both the pressure gradient and the poloidal ion flow become large in the H mode (Figs. 4 and 5). From experimental observations the ion pressure gradient is unimportant in the initial stages of the H mode but subsequently becomes the dominant driver of the radial electric field as reduced transport fluxes steepen the pressure profile (Burrell, 1994). In core transport barriers, depending on device, the radial electric field is either negative, consistent with a large pressure gradient, or because of large toroidal rotation it is positive. Observations indicate that poloidal flow is the dominant driver of the electric field in the initial stages of the H mode (Moyer *et al.*, 1995). Poloidal flow is also the dominant driver of the electric field in externally induced transport barriers. In barriers induced by the injection of rf waves, poloidal flow is directly driven by ion Bernstein waves (LeBlanc *et al.*, 1995). In barriers induced with biased electrodes, a radial current responding to an induced voltage drives a poloidal flow, which in turn drives the radial electric field (Cornelis *et al.*, 1994). The toroidal flow is observed to play an important role in core transport barriers (Greenfield *et al.*, 1993; Burrell, 1997) and in the reversed-field pinch (Fiksel, 1998).

The radial force balance represents a constitutive equation for the radial electric field. Other relations must be introduced to determine the pressure gradient and ion flows. As described by Eq. (2.35), the pressure gradient is governed by a balance of an energy source and the heat flux produced by turbulence. The toroidal and poloidal ion flows are specified from toroidal and poloidal momentum balances. Because these flows are key elements of the transition theories that describe the generation of the radial electric field, the momentum balances that govern flows must be considered in detail.

B. Mean ion flows

To describe ion flows let us consider first the momentum equation for particle species α ,

$$m_\alpha n_\alpha \left(\frac{\partial \mathbf{u}_\alpha}{\partial t} + \mathbf{u}_\alpha \cdot \nabla \mathbf{u}_\alpha \right) = q_\alpha n_\alpha (\mathbf{E} + \mathbf{u}_\alpha \times \mathbf{B}) - \nabla \cdot \tilde{\mathbf{p}}_\alpha + \mathbf{R}_\alpha, \quad (4.2)$$

where \mathbf{R}_α is the mean momentum transfer between unlike particles due to the friction of collisions and $\tilde{\mathbf{p}}_\alpha$ is the total pressure tensor, with isotropic and anisotropic pressures p_α and $\tilde{\Pi}_\alpha$ according to $\tilde{\mathbf{p}}_\alpha = \tilde{\Pi}_\alpha + p_\alpha \mathbf{I}$ (Freidberg, 1982). Adding ion and electron momentum equations to eliminate the electric field \mathbf{E} yields

$$m_i \left(\frac{\partial \mathbf{u}_i}{\partial t} + \mathbf{u}_i \cdot \nabla \mathbf{u}_i \right) - \frac{1}{n_i} (\mathbf{J} \times \mathbf{B} - \nabla p) = - \frac{\nabla \cdot \tilde{\Pi}}{n_i} - m_e \left(\frac{\partial \mathbf{u}_e}{\partial t} + \mathbf{u}_e \cdot \nabla \mathbf{u}_e \right), \quad (4.3)$$

where $\mathbf{J} = e(n_i \mathbf{u}_i - n_e \mathbf{u}_e)$ is the plasma current, $p = p_i + p_e$ is the total pressure, $\tilde{\Pi} = \tilde{\Pi}_i + \tilde{\Pi}_e$ is the total aniso-

tropic pressure tensor, and charge neutrality $n = n_i = n_e$ has been assumed. Equation (4.3) is essentially the plasma flow equation of MHD plus an electron inertia term. Electron inertia effects are generally neglected because of the smallness of the ratio of the electron-to-ion mass. The three remaining terms, the Reynolds stress, the Lorentz force, and the pressure force (isotropic and anisotropic), drive mean ion flows. The Reynolds stress is the primary arbiter of momentum redistribution in neutral fluid turbulence. In plasmas it plays a central role in second-order critical theories of the L - H transition (Sec. VII. B. 3). Because measurements of the Reynolds stress in plasmas have been limited, its contribution to flows in fusion experiments is poorly understood. When mean flow is driven by injected rf waves, the Reynolds stress of the fluctuating wave field drives the flow. There is a mean Lorentz force due to mean current when a radial current is driven in the plasma by a biased electrode. The resulting mean flow triggers a transition to the externally driven H mode (Sec. VII. B. 1). The Lorentz force due to the fluctuating current and magnetic field is important in rf-driven flow and in the transition to the enhanced confinement mode of the reversed-field pinch (Sec. VI. C). The anisotropic pressure tensor involves the most complicated effects in mean flow drive. It includes viscous damping (Hirshman and Sigmar, 1981) of mean flows driven by radial pressure gradients in tokamaks (Hinton and Hazeltine, 1976) and the flow drive associated with differential loss of charge near plasma boundaries. In the following subsections, flow drive associated with the forces of Eq. (4.3) is discussed in more detail.

1. Reynolds stress

If the isotropic pressure is constant on a flux surface, the flux-surface-averaged toroidal and poloidal pressure forces vanish. (The case of pressure with poloidal variation is considered in Sec. IV. B. 5.) For incompressible flow, the toroidal and poloidal components of $\mathbf{u}_\alpha \cdot \nabla$ vanish upon averaging, and there are no radial components of $\langle \mathbf{u}_\alpha \rangle$, $\langle \mathbf{J} \rangle$, or $\langle \mathbf{B} \rangle$ to lowest order. The only surviving components of the advective derivatives are Reynolds stresses. If there are no external currents (external currents are considered in Sec. VII. B. 1), the resulting form of the poloidal flow equation (Craddock and Diamond, 1991; Diamond *et al.*, 1994) is

$$\frac{\partial \langle u_{\theta i} \rangle}{\partial t} = - \frac{\partial}{\partial r} \left[\langle \tilde{u}_{ri} \tilde{u}_{\theta i} \rangle - \frac{1}{m_i n_i \mu_0} \langle \tilde{b}_r \tilde{b}_\theta \rangle \right] - \mu_\theta \langle u_{\theta i} \rangle, \quad (4.4)$$

where μ_0 is the magnetic permeability, μ_θ is the poloidal flow-damping rate, and the fluctuating current has been expressed in terms of the fluctuating magnetic field using Ampère's law. In Eq. (4.4), the Reynolds stress,

$$\tau_{r\theta} = \langle \tilde{u}_{ri} \tilde{u}_{\theta i} \rangle - \frac{1}{m_i n_i \mu_0} \langle \tilde{b}_r \tilde{b}_\theta \rangle, \quad (4.5)$$

is generalized to include the effect of the Lorentz force. The poloidal flow damping originates with the anisotropic pressure force; in a torus with toroidal symmetry,

there is no viscous damping of toroidal flow. The poloidal flow damping, called the neoclassical viscosity or magnetic pumping, arises from ion-ion collisions and the asymmetry of poloidal variation in a torus (Shaing and Hirshman, 1989). The poloidal asymmetry is evident in the variation with poloidal angle of the length of a toroidal arc subtended by a toroidal angle. The arc length is larger at the outside of a torus ($\theta=0$) than the inside ($\theta=\pi$). There is no asymmetry in the toroidal angle. The form and magnitude of the neoclassical viscosity depends sensitively on kinetic effects, and its representation in a fluid description is an area of current investigation (Morris, Haines, and Hastie, 1996; Rosenbluth and Hinton 1998). Equation (4.4) indicates that, in a toroidal plasma, the balance of Reynolds stress and neoclassical viscous drag determines the radial transport of poloidal momentum. Clearly it is important to identify the circumstances under which the Reynolds stress is nonzero and therefore produces changes in the mean momentum.

This question has been extensively studied in the stratosphere, where the Reynolds stress $\rho \langle \tilde{u}_i \tilde{u}_j \rangle$ frequently plays an important role in the structure of large-scale mean flows. A particularly useful form of the turbulent momentum flux in the stratosphere is the Eliassen-Palm flux (1961). It is a form of the Reynolds stress valid for geostrophic flows. Its meridional component in a β plane is simply $F_\theta = -\rho_0 \langle u_x u_y \rangle$, where ρ_0 is the mean density. The vertical component accounts for vertical momentum transport from the meridional advection of temperature fluctuations in a rotating atmosphere. The divergence of the Eliassen-Palm flux has a direct relationship to the properties of large-scale linear wave disturbances: for linear wave action that is steady, frictionless, and adiabatic, and for conservative mean flow, the Eliassen-Palm flux divergence vanishes and there is no acceleration of the mean flow (Andrews, Holton, and Leovy, 1987). An example of mean flow acceleration by wave disturbances occurs at a critical surface, where a mean flow $\bar{u}(y)$ with transverse variation is equal to the phase velocity ω/k of a propagating wave. At such a surface the total derivative of the flow, $\omega - k\bar{u}$, vanishes. This allows transience, dissipation, or nonlinearity, effects that are generally smaller than $\omega - k\bar{u}$ away from the critical surface, to become important and violate the nonacceleration conditions of the Eliassen-Palm theorem. The result is a conversion of wave momentum into mean flow. The momentum deposition can change $\bar{u}(y)$ and alter the position of the critical surface. This process is believed responsible for generation of mean zonal flow from vertically propagating Kelvin waves and Rossby-gravity waves in models of an observed periodic zonal flow in the stratosphere known as the quasibiennial oscillation (Holton and Lindzen, 1972; Plumb, 1977). It also figures in the generation of the seasonal easterly and westerly flow regimes of the stratosphere (Andrews, Holton, and Leovy, 1987).

In plasmas a similar set of conditions governs the acceleration of mean poloidal flow by the radial derivative of the Reynolds stress $\partial/\partial r \langle \tilde{u}_{ri} \tilde{u}_{\theta i} \rangle$. To have net mean

flow, acceleration, radial wave propagation, and radial asymmetry are required. This is readily apparent for fluctuating $E \times B$ flow, in which case $\tilde{u}_{ri} = B_0^{-1} i k_\theta \phi_k$ and $\tilde{u}_{\theta i} = B_0^{-1} \partial \phi_k / \partial r$. With radial propagation, $\partial / \partial r \rightarrow i k_r$, and the Reynolds stress is real; otherwise, it is purely imaginary. Radial asymmetry is required for the radial momentum convergence that drives acceleration in a region of interest. Both conditions have corresponding constraints in the Eliassen-Palm theorem. The plasma case has been analyzed to delineate circumstances under which these conditions are met (Diamond and Kim, 1991). In a plasma, radial asymmetry is assured for large-scale waves, which sample the variation of equilibrium density and temperature on the largest scale (Hasegawa and Wakatani, 1987; Carreras, Lynch, and Garcia, 1991), for wave structures within a radial correlation length of the plasma boundary or some other significant boundary (Diamond and Kim, 1991) and for waves in regions where there is strong variation of the mean density, temperature, or flow. The full plasma Reynolds stress $\tau_{r\theta}$ has been examined for electromagnetic Alfvén waves (Craddock and Diamond, 1991). In analogy with flow acceleration in the atmosphere at the critical surface, the wave number of radially propagating Alfvén waves goes to zero at the resonant surface defined by $\omega = k_\parallel v_A$, where $k_\parallel = \mathbf{k} \cdot \mathbf{B}$ is the wave vector along the equilibrium magnetic field, and $v_A = B / (\mu_0 m_i n_i)^{1/2}$ is the Alfvén velocity. In this region there is strong resonant absorption of the wave energy and strong radial variation or asymmetry. The two components of the Reynolds stress nearly cancel for electromagnetic waves. For kinetic shear Alfvén waves an imbalance is provided by ion inertia in the form of the polarization drift (Craddock and Diamond, 1991).

The radial asymmetry required for finite Reynolds stress can arise from flow shear through its distortion of fluctuations (Diamond *et al.*, 1994; Terry *et al.*, 1994) or from other inhomogeneities such as the pressure. For example, turbulence in an infinite, homogeneous medium has a zero Reynolds stress because advection across any surface is equally likely to carry both signs of momentum. This property is traceable to the lack of a gradient in mean flow, i.e., the lack of an asymmetry in some direction. Likewise, the Reynolds stress of global magnetic turbulence in the reverse-field pinch edge is measured to be zero under most conditions (Fiksel, 1998), a property that can be attributed to the lack of radial propagation of simple resistive MHD instabilities when there is no background shear flow (Diamond and Kim, 1991). The notion of eddy viscosity follows directly from the dependence of the Reynolds stress on flow shear. The eddy viscosity is derived from the Reynolds stress using Prandtl's mixing-length hypothesis to model the turbulent flow as linearly proportional to the flow shear (for a simple derivation, see Tennekes and Lumley, 1972). Eddy viscosity is an oversimplification of the dynamics, but it illustrates the property that flow shear leads to mean flow acceleration by turbulence. This is an important element of second-order phase transitions, as discussed in Sec. VII.B.3. From the above discussion,

note that the conditions for acceleration under wave action essentially carry over to the turbulent case, in which the motions need not satisfy any collective resonance or have wavelike features.

The Reynolds stress is difficult to measure in fusion plasmas and consequently has figured more prominently in theory than in the interpretation of experiment. Measurements in stellarators (Matthews *et al.*, 1993; Hidalgo *et al.*, 1997) indicate that the Reynolds stress in those plasmas is of comparable magnitude to mean flow accelerations. These measurements provide insufficient detail to establish a causal relationship. Reynolds stresses are easily measured in simulations and are found to produce flows of sufficient magnitude to decrease turbulence levels in accord with the principles of Sec. II (Carreras, Lynch, and Garcia, 1991). The generation of flows by the Reynolds stress is particularly noticeable in simulations of ion-temperature-gradient-driven turbulence in tokamak plasmas (Waltz, Kerbel, and Milovich, 1994). Reynolds-stress-driven flows play a significant role in saturating the instability. A like process associated with an instability of flow parallel to the equilibrium magnetic field is also illustrated in Fig. 16 of Charlton *et al.* (1994).

2. External biasing

In external biasing experiments, the Lorentz force drives flows through the balance in Eq. (4.3) of $\mathbf{J} \times \mathbf{B} = \nabla \cdot \vec{\Pi}$, where \mathbf{J} is the radial current injected by the probe. The flow is proportional to the current when the anisotropic pressure force is dominated by viscous dissipation (e.g., $\mathbf{B} \cdot \nabla \cdot \vec{\Pi} \propto n_i m_i \mu_\theta u_\theta$). The radial current flows in response to an applied voltage difference between the vessel wall and a surface inside the plasma (Sakai, Yasaka, and Itatani, 1993) or an electrode inserted into the plasma (Taylor *et al.*, 1989; for a review see Weynants and Oost, 1993). When the current from the electrode to the wall is plotted as a function of the voltage between these points, a bifurcation of the plasma equilibrium is evident, manifested as an abrupt change in the effective radial plasma resistance (Taylor *et al.*, 1989). The bifurcation occurs at a critical value of the current. Above the critical current the plasma resistance increases sharply, allowing a larger radial electric field for a given radial current. The current-voltage response for a biased plasma is shown in Fig. 9, along with the inferred plasma resistance. The jump to a larger field yields a jump in the magnitude of the $E \times B$ flow and flow shear, with concomitant reductions in fluctuations and transport (Taylor *et al.*, 1989; Weynants *et al.*, 1991; Tynan *et al.*, 1992; Askinazi *et al.*, 1993). The bifurcation produces changes in plasma transport and equilibrium profiles that are similar to those that occur in the H -mode transition (Sec. II.B). This behavior is consistent with a simple model of the flow dynamics that balances the external poloidal force of the biasing with a nonlinear flow-damping process that, as a function of flow speed, first increases to a maximum (at a flow speed of order the relevant sound speed) and then strongly

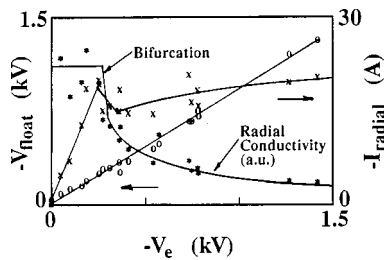


FIG. 9. Electrode current vs bias voltage in plasma biasing experiment. The current has a linear response until the point labeled bifurcation, after which the current actually decreases and then rises slowly. The inferred plasma resistance is also plotted. From Taylor *et al.*, 1989.

decreases (Weynants *et al.*, 1991). This allows for two markedly different flows for the same forcing or external current. The neoclassical viscosity has a nonlinear form with a peak near $u_\theta = u_{Ti} B_\theta / B_\phi$ (Shaing and Crume, 1989). Above this critical speed, ions rarely suffer Coulomb collisions and the dissipation of poloidal momentum becomes weak. It is not known if the Reynolds stress contributes to the force balance or is overwhelmed by the external poloidal force in biasing experiments. Biasing experiments also have been conducted in a variety of nontokamak devices, including the stellarator (Isler *et al.*, 1992), reversed-field pinch (Craig *et al.*, 1997), and tandem mirror (Sakai, Yasaka, and Itatani, 1993). All observe reduced transport, but a bifurcation has not been observed in the reversed-field pinch. Features of bias-induced transport barriers are discussed in Sec. VI. A. 2.

3. Injected radio-frequency waves

Earlier in this section it was noted that the fields of electromagnetic waves can generate flow through the Reynolds stress, Eq. (4.5), where it is understood that the fluctuating flow \tilde{u} of the Reynolds stress is the $E \times B$ flow created by the electric field of the wave. Such waves can be externally injected into a plasma using an rf antenna. Fluid analyses of the rf force arising from kinetic shear Alfvén waves (Craddock and Diamond, 1991) and ion Bernstein waves (Biglari *et al.*, 1991) suggest that it may be feasible to excite flow shear in this fashion. A recent kinetic treatment of the rf force finds that ion Bernstein waves are less efficient at driving flows than originally thought, but that fast magnetosonic waves can drive significant flows at power levels like those used to heat plasmas (Berry, Jaeger, and Batchelor, 1999). Using rf waves to drive flows is not a simple procedure. Reflection, scattering, dispersion, mode conversion, dissipation, and differing frequency-dependent interactions with electrons and ions all enter the problem.

Evidence that a flow-shear-induced transport barrier can be produced in a core plasma using injected rf waves has been reported by LeBlanc *et al.* (1995). This work, conducted in the Princeton Beta Experiment Modification (PBX-M), involved the resonant absorption of an

ion Bernstein wave (IBW) in the core of a plasma that was already in *H* mode. It was observed that in the region of IBW absorption, steep gradients developed in the electron density and ion and electron temperature profiles. Inside these gradients, the density and temperature reached higher values than those of comparable plasmas without the IBW. These features suggest a transport barrier in the region of wave absorption. The increase of temperature associated with an IBW, and a concomitant increase in neutron production rate, abruptly began some time after the IBW power was applied. This time was labeled as the onset time for the barrier, which was designated as the CH mode (core H mode). The toroidal flow and toroidal flow shear also increased with the IBW. There was no diagnostic for measuring the poloidal flow. (Toroidal flow contributes to the radial electric field and $E \times B$ flow shear, but its contribution is smaller by a factor of B_θ / B_ϕ than that of a poloidal flow of the same magnitude.) Energy balance calculations indicated that the transport of toroidal momentum and ion energy diminished at the *H*-mode transition with a further decrease beginning at the onset of the CH phase. There was no change in electron energy transport with either transition. Values for the ion thermal conductivity, toroidal momentum diffusivity, and particle diffusivity have since been reported as lower than collisional diffusivities calculated for a toroidal plasma (Ono *et al.*, 1997). Other devices have had difficulty producing core barriers with rf flow drive, raising questions as to the robustness of the method. Experiments conducted on the Tokamak Fusion Test Reactor (TFTR) indicated that shear flow was driven by an ion Bernstein wave, but no evidence of a transport barrier was seen, presumably because the flow strength was insufficient to reach the suppression threshold (LeBlanc *et al.*, 1999). The desirability of controlling the location and strength of internal shear layers in plasmas warrants further work on this technique.

4. Orbit loss

In a toroidal plasma, a radial electric field can build up due to differential charge loss (Itoh and Itoh, 1988) and differences in the way ion and electron orbits intercept material surfaces in the edge region (Shaing and Crume, 1989). The latter is referred to as ion-orbit loss and it provides the basic flow drive in the two-step models of the *H*-mode transition described in Sec. VII. Here the physics of the ion-orbit loss mechanism is presented heuristically. Mathematically, the orbit loss drive can be included as part of the anisotropic pressure force $\nabla \cdot \vec{\Pi}$ in certain regions of the plasma, e.g., in the vicinity of a magnetic-field-line separatrix. The separatrix is a flux surface that separates an outer region of the plasma volume, in which diverted magnetic flux intersects material surfaces, from an inner region in which it does not. The separatrix and flux surfaces typical of diverted tokamaks are depicted in Fig. 10. The separatrix geometry is intentionally introduced into fusion plasmas in order to channel the outflow of hot plasma particles. This is achieved with a device known as a divertor, which consists of external magnetic coils to produce the field geometry, the

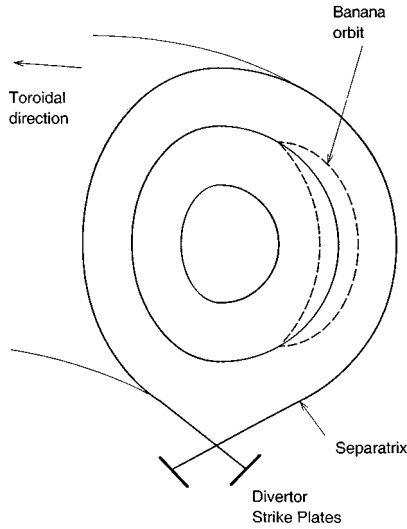


FIG. 10. Cross section of flux surfaces in a diverted tokamak plasma. A surface known as the separatrix crosses itself at a null point of the poloidal field. Particles moving along field lines on the separatrix hit a material surface known as a strike plate. A projection onto a plane of constant toroidal angle of a banana orbit about one of the flux surfaces is indicated for illustration.

strike plates on which field lines terminate, and pumping ducts for edge pressure control.

The loss of particles near a separatrix relates to the average motion of charged particles trapped in the magnetic field well along magnetic-field lines in a torus. If the circular motion of charged particles in planes perpendicular to magnetic-field lines is averaged over, the resultant average motion of charge follows orbits called guiding centers. The curvature and gradient of the magnetic field cause the guiding centers to drift off the field lines (Krall and Trivelpiece, 1977). The projection of the guiding-center orbit onto a cross section at fixed toroidal angle traces out a banana shape (depicted in Fig. 9) whose maximum radial thickness is given by

$$\rho_{\theta} = \frac{2u_{\parallel}m_j}{|e|B_{\theta}}, \quad (4.6)$$

where u_{\parallel} is the guiding-center velocity along the field. u_{\parallel} scales with the thermal velocity, making the ion banana width larger than the electron banana width by the square root of the ion-to-electron mass ratio. The radial gradient of the steady $E \times B$ drift created by a mean electric field significantly reduces the larger ion banana width (Berk and Galeev, 1967). However, the squeezed ion radius remains much larger than the electron radius. A collision between trapped particles on banana orbits shifts a particle on the outside of a banana to the inner side of a new banana whose inner side is at the position of the outer side of the old banana. The collision has thus moved the particle one banana width in the radial direction, i.e., the Brownian motion random-walk step size of trapped particles in a magnetic field is the banana width. Trapped particles within one banana width of the separatrix move across it upon colliding, and onto field

lines that intersect material surfaces. If the collision detraps the particle, it moves out of the mirror and along the field to the strike plate, where it is lost from the plasma. Because the electron banana width is essentially negligible in comparison to the ion banana width, the region within one ion banana width of the separatrix suffers a net loss of ions and becomes negatively charged.

Orbit loss also occurs in nondiverted tokamaks near material surfaces called limiters. The poloidal limiter is an annular disk placed at a particular toroidal position. Its outer edge is fixed to the wall, and its inner edge protrudes radially into the plasma. Because ion banana orbits can reach behind the limiter without hitting it, the region one banana width behind the limiter becomes positively charged (Hazeltine, 1989; Tendler and Rozhansky, 1992), producing a positive sheath potential (Ritz *et al.*, 1984). Orbit loss is only capable of producing a radial electric field within one banana width of a material surface such as a limiter, or of a divertor separatrix, and is therefore intrinsically an edge effect.

5. Nonsymmetric transport

Transport fluxes that are asymmetric in poloidal angle have been postulated to produce poloidal rotation. The original hypothesis (Stringer, 1969) predicted flow acceleration that was too weak to overcome neoclassical flow damping. It has been argued that the fluctuation-driven fluxes of present-day tokamaks are of sufficient magnitude to drive robust poloidal rotation in the presence of neoclassical viscosity (Hassam *et al.*, 1991). There is some evidence of poloidal asymmetries in experiment, inferred from poloidal variations of the edge plasma density (Brower, Peebles, and Luhmann, 1987; LaBombard and Lipschultz, 1987) and the observation of large flows along the equilibrium magnetic field (Vershkov, 1989). Poloidally asymmetric particle transport, poloidal variation of the density, and parallel flows are directly linked in the theory.

Poloidal flow arises as part of a collective plasma mode that couples to the asymmetry of the particle flux and is uncovered in an ordering scheme based on the smallness of the inverse aspect ratio a/R_0 (see Fig. 2). At lowest order there is a poloidally uniform equilibrium density but no steady poloidal flow. Higher order yields an exponentially growing normal mode with poloidally nonuniform perturbations in u_{\parallel} and n , matching the variation of the particle flux, and a uniform perturbation in u_{θ} . The growth rate is proportional to the $\frac{1}{3}$ power of the asymmetric part of the steady parallel flow and is thus proportional to the same power of the asymmetric part of the particle flux. To obtain large poloidal flows it is not sufficient to have a large particle flux; a large asymmetry is required. This process represents a collective excitation coupling multiple equations, and it is more complicated than any single force like the Reynolds stress. It has not been determined from experiment if this collective mode is excited in fusion plasmas.

C. Miscellaneous processes

The time derivative of the Poisson equation and the evolution equations for the average ion and electron densities [e.g., Eq. (2.5)] lead to an expression that may be evaluated for the radial electric field if the radial fluxes of ions and electrons are known (Itoh and Itoh, 1988, 1996). In steady state, the dependence of the fluxes on the electric field must be specified in order to determine the field. The effects of Sec. IV.B may be expressed as contributions to the net difference between electron and ion fluxes. Any additional process that contributes to the difference of fluxes can affect the radial electric field, in principle. One such process is the particle transport induced by a slight variation in magnetic-field strength with toroidal angle. This variation, called magnetic-field ripple, is caused by a corresponding variation in the external current density that produces the toroidal field. It occurs, for example, because the external current is driven in a discrete set of coils surrounding the plasma at different toroidal locations. Another process is charge exchange, i.e., the exchange of an electron between ions and neutrons, or ions and ions. These contributions to the flux difference have been included in general expressions (Itoh and Itoh, 1996). The penetration depth of neutrals has been considered in connection with the location of the H -mode transport barrier (Carreras *et al.*, 1998), and ripple losses have been invoked in a transition model for core transport barriers (Shaing *et al.*, 1998).

V. SUPPRESSION IN TOROIDAL PLASMAS

The basic notion of shear suppression of fluctuations was presented in Sec. II in a simple form, using a model in which the only temporal scales were the shear straining and turbulent decorrelation rates, and the geometry was rectilinear. In this section complications related to magnetically confined plasmas are addressed. The most important of these are the inhomogeneity of the magnetic field and toroidal geometry. These issues allow further examination of several distinct mechanisms by which shear suppresses turbulence, viz., through its effect on turbulent decorrelation, on linear stability, and on the cross phase of transport fluxes.

A. Plasma geometry and magnetic topology

In a toroidal plasma the magnetic field is not uniform. Its magnitude varies both along and transverse to the field lines. The longitudinal variation traps particles (the orbit loss mechanism of Sec. IV.B.4 is caused by trapped particles) while the transverse variation, referred to as magnetic shear, has a strong stabilizing effect on collective instabilities. Hence magnetic shear is utilized to gain stability. Generally, magnetic shear is the most significant inhomogeneity affecting the eigenmode structure of collective instabilities. One component of the magnetic field typically changes its magnitude more

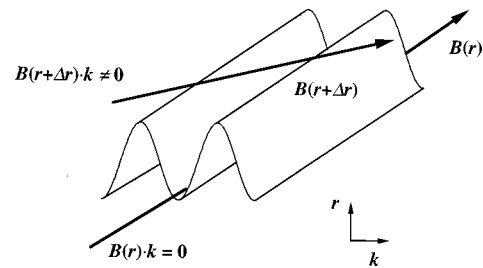


FIG. 11. Magnetic-field lines at two radial locations relative to a radially extended collective plasma eigenmode whose displacement is represented as a sinusoidal sheet. The field line at r is perpendicular to the wave vector k , so there is no projection of k on B . At $r + \Delta r$ magnetic shear has twisted the field line, producing a nonzero projection of k on B .

than the other, so that shear is seen as a change in field-line direction or pitch from one flux surface to another (see Fig. 2).

Magnetic shear is stabilizing because collective motions, which extend radially in order to tap the free energy of gradients, experience enhanced damping from the variation of field-line pitch with radius. This damping is associated with parallel motion, which is efficiently dissipated by collisions because of the ease of motion along the field. To couple to parallel motion, collective modes must have variation along the field, i.e., there must be a nonzero wave number k_{\parallel} along the field. A collective mode cannot avoid parallel damping if there is magnetic shear. The mode can arrange for k_{\parallel} to be zero at one radial location, but it will extend to other radial locations, where k_{\parallel} is nonzero, and there is parallel damping. This is illustrated in Fig. 11, which shows a radially extended sinusoidal fluctuation with a symmetry direction parallel to the magnetic-field line at r [$\mathbf{B}(r) \cdot \mathbf{k} = k_{\parallel}(r) = 0$]. Because of the twist of the field line, $k_{\parallel}(r + \Delta r) \neq 0$, i.e., $\mathbf{B}(r + \Delta r) \cdot \mathbf{k} \neq 0$.

The parallel wave number is calculated from the field-aligned gradient,

$$\frac{\mathbf{B} \cdot \nabla}{|\mathbf{B}|} \equiv \nabla_{\parallel} = \frac{1}{|\mathbf{B}|} \left\{ \frac{B_{\varphi}}{R} \frac{\partial}{\partial \varphi} + \frac{B_{\theta}}{r} \frac{\partial}{\partial \theta} \right\}, \quad (5.1)$$

where the coordinates R , r , θ , and φ are those of Fig. 2(b). Introducing the Fourier transform in toroidal and poloidal angles, $f(r, \theta, \varphi) = \sum_{m,n} f_{m,n}(r) \exp(in\varphi - im\theta)$, we find the parallel wave number, obtained from $(2\pi)^{-2} \int \exp(in\varphi - im\theta) \nabla_{\parallel} f(r, \theta, \varphi) d\theta d\varphi = ik_{\parallel} f_{m,n}(r)$, given by

$$k_{\parallel} = \frac{1}{|\mathbf{B}|} \left\{ \frac{iB_{\varphi}n}{R} - \frac{iB_{\theta}m}{r} \right\}. \quad (5.2)$$

In tokamaks with $a/R_0 < 1$, the variation of B_{φ} and R with r is weak compared to that of B_{θ} . At a certain radius r_s , where $B_{\varphi}n/R = B_{\theta}(r_s)m/r_s$, k_{\parallel} vanishes. The toroidal surface with $r = r_s$ is called a rational surface, because the ratio of the two terms in Eq. (5.2),

$$q(r_s) \equiv \frac{B_{\varphi}r_s}{B_{\theta}(r_s)R} = \frac{m}{n}, \quad (5.3)$$

is a rational number on that surface. The quantity $q(r)$ is the winding number of magnetic-field lines on any given flux surface, i.e., the ratio of displacement in toroidal angle to displacement in poloidal angle between two points on a field line. [The use of polar coordinates for the toroidal cross section and the assumption $a/R_0 < 1$, adopted for simplicity of presentation, make Eq. (5.3) valid only for large-aspect-ratio, circular cross-section flux surfaces. Generalizations of q exist for the finite-aspect-ratio, noncircular cross-section toroidal plasmas in common use.] Away from the rational surface B_θ can be expanded in a Taylor series. Keeping only the lowest-order nonvanishing term,

$$k_\parallel = \frac{(r-r_s)}{L_s} \frac{m}{r_s} = \frac{(r-r_s)}{L_s} k_\theta, \quad (5.4)$$

where k_θ is the poloidal wave number, $L_s = Rq/\hat{s}|_{r_s}$ is the magnetic-shear scale length, and $\hat{s} = rq^{-1}dq/dr$. From Eq. (5.4) the parallel wave number is proportional to the poloidal wave number and has a radial variation away from the rational surface that is linear with a scale length L_s . The scale length is of the order of the major radius R and is large compared to the radial scales of fluctuations.

In the absence of complicating effects such as flow shear, fluctuations tend to have maximum amplitude at the rational surface where the damping of parallel motion is zero. The amplitude decays away from the rational surface on a scale that is set by the tradeoff of enhanced dissipation at finite k_\parallel and the efficient extraction of gradient free energy. Instabilities are often analyzed in the so-called slab reduction of toroidal geometry, where

$$\begin{aligned} r - r_s &\rightarrow x, \\ m/r &= k_\theta \rightarrow k_y, \\ n/R &= k_\phi \rightarrow k_z. \end{aligned} \quad (5.5)$$

Note that x is the direction of inhomogeneity, by the convention of fusion literature. (Up to this point in the review, the convention of fluid dynamics and atmospheric literature has been followed, making y the direction of inhomogeneity. Both conventions will be used hereafter, depending on the context.) The effect of magnetic shear on plasma instabilities is illustrated by the Kelvin-Helmholtz instability, which is driven by flow shear, but can be stabilized by magnetic shear.

1. Shear flow stability with magnetic shear

The Kelvin-Helmholtz instability (Sec. III. A) is flow-shear driven, drawing free energy by the exchange of vortex filaments about a vorticity maximum. Recalling from Eq. (3.1) that vorticity is equivalent to charge density, the exchange of vortex filaments produces electric fields that drive current and dissipate energy according to Ohm's law. In the presence of an equilibrium magnetic field, reduced MHD equations (Strauss, 1976) provide a convenient description of this process. Like MHD, reduced MHD consists of an equation for Ohm's

law and a vorticity evolution equation that is essentially the curl of Eq. (4.3) without the small electron inertia terms. However, the mean magnetic field leads to dynamics that are nearly 2D, with the perturbed flow and magnetic field perpendicular to the mean field. Along the field there is an ohmic current and its driving electric field. The reduced MHD equations are

$$\rho \frac{d}{dt} \nabla_\perp^2 \frac{\Phi}{B_0} = B_0 \nabla_\parallel J_\parallel + \nabla_\perp A_\parallel \times \mathbf{z} \cdot \nabla_\perp J_\parallel, \quad (5.6)$$

$$\frac{d}{dt} A_\parallel = -B_0 \nabla_\parallel \frac{\phi}{B_0} - \eta J_\parallel, \quad (5.7)$$

where ρ is the plasma mass density, $\nabla_\perp^2 \Phi B_0^{-1}$ is the total vorticity, J_\parallel is the plasma current along the equilibrium field B_0 , A_\parallel is the magnetic vector potential of the perturbed field along B_0 , and η is the resistivity. The derivative d/dt includes advection by the equilibrium flow $\bar{u}(x) = -B_0^{-1} \nabla \Phi_0 \times \mathbf{b}$ and fluctuating flow $-B_0^{-1} \nabla \phi \times \mathbf{b}$, where \mathbf{b} is the unit vector along B_0 . Note that the left-hand side of Eq. (5.6) is identical in form to the neutral-fluid case [Eq. (3.2)]; the right-hand side is the curl of the Lorentz force. The first and second terms of Ohm's law are the inductive and electrostatic electric fields of the Lorentz gauge.

For the Kelvin Helmholtz instability magnetic-field fluctuations are negligible, allowing terms with A_\parallel to be dropped (Chiueh *et al.*, 1986). The parallel current gradient of the vorticity equation couples to resistive dissipation, introducing the stabilizing magnetic-shear effect discussed above. Dropping the nonlinearity and combining these equations by eliminating J_\parallel , we obtain the vorticity equation

$$\begin{aligned} \left(\frac{\partial}{\partial t} + ik_y \bar{u}(x) \right) \left(\frac{\partial^2}{\partial x^2} - k_y^2 \right) \frac{\phi_{k_y}}{B_0} - ik_y \frac{d^2 \bar{u}}{dx^2} \frac{\phi_{k_y}}{B_0} \\ = \frac{B_0^2}{\rho \eta L_s^2} k_y^2 x^2 \frac{\phi_{k_y}}{B_0}, \end{aligned} \quad (5.8)$$

where Eq. (5.4) and the slab reduction [Eq. (5.5)] have been used. The last term of Eq. (5.8) is the sink associated with ohmic dissipation. Unlike dissipation in neutral fluids [Eq. (3.2)], which is negligible at high Reynolds number, this sink becomes weak when dissipation (plasma resistivity) is large, because a weaker parallel current is induced when resistivity is large. The dissipation is also large when x is large, forming a quadratic eigenmode potential well. At $x=0$, the location of the rational surface, the electric field has no component along B_0 , and there is no parallel current or ohmic dissipation. The effect of dissipation on the instability depends on how the instability eigenmode varies with x . If the fluctuation must extend to large x in order to draw free energy from the flow shear, the growth rate will be reduced. This happens either because the fluctuation structure is broad or because the mean vorticity peaks at $x \neq 0$ (fluctuations grow in the region of maximum vorticity). However, even a narrow structure centered on $x=0$ is stabilized by magnetic shear if η is sufficiently small or k_y is large.

Numerical evaluation of Eq. (5.8) for a model flow profile $\bar{u}(x) = V_0 \tanh(x/L_E)$ indicates that the mode is stabilized for all wave numbers of the system if the dissipative term is larger than the drive term (last term of the left-hand side) at $x \cong L_E$ for k_y evaluated at the minimum poloidal wave number of the system (Chiueh *et al.*, 1986; Sugama and Wakatani, 1991). Thus stability requires

$$\frac{d^2\bar{u}/dx^2}{\bar{u}} \cong \frac{1}{L_E^2} < \left(\frac{B_0^2 k_{\min}}{\rho V_0 \eta L_s^2} \right)^{1/2} = (\text{Lu})^{1/2} (\text{Al})^{1/2} a^{-1} L_s^{-1}, \quad (5.9)$$

where $\text{Lu} = \mu_0 a v_A / \eta$ is the Lundquist number, $\text{Al} = v_A / V_0$ is the Alfvén number, and k_{\min} is taken to be the inverse minor radius a^{-1} . This condition is cited by Burrell (1997), but $V_0 k_{\min}$ is replaced by $\Delta\omega_D$, the turbulence decorrelation rate. Equation (5.9) omits a multiplier of order unity and thus is not a precise threshold criterion, but it does identify the vicinity of the instability threshold. Because the stabilizing dissipative term of Eq. (5.8) is quadratic in x , it dominates the driving term at large x . A necessary condition for instability is that the stabilizing term become weak at some value of x , i.e., that $S_M = B_0^2 k_y x^2 / \rho \eta L_s^2 - d^2\bar{u}/dx^2$ change sign in the domain of x . This is equivalent to the instability criterion of Eq. (3.4), which for barotropic instability requires that $S_R = \beta - \partial^2\bar{u}/\partial y^2$ change sign in the flow domain (the meanings of x and y are exchanged in the standard notations of plasma and atmospheric literature). Comparison of these criteria indicates that the planetary rotation gradient β and magnetic shear $B_0^2 k_y x^2 / \rho \eta L_s^2$ play comparable roles in stabilizing flow shear instability. For typical tokamak parameters, Eq. (5.9) is satisfied and the Kelvin-Helmholtz modes are stable.

2. Instabilities in a nonuniform magnetic field

In Sec. II.C it was pointed out that flow shear can stabilize certain plasma collective modes. The criterion of Eq. (2.33) is too simple to provide a predictive stabilization threshold, in large part because it fails to account for inhomogeneities such as magnetic shear. In the presence of magnetic shear, each unstable mode has a different eigenmode structure, resulting in a different interaction with the flow shear inhomogeneity. Hence, in contrast to turbulent decorrelation [Eq. (2.17)], there is no single criterion for the effect of flow shear on linear stability. In this subsection the effect of flow shear on several instabilities is described.

The drift wave is an electrostatic fluctuation involving perturbations of the flow and electron density that is closely related to the atmospheric Rossby wave. Advection of the mean density by the perturbed $E \times B$ flow induces wave propagation at a rate known as the diamagnetic flow speed. In a neutrally stable drift wave, the rapid motion of electrons along the magnetic-field line enforces a Boltzmann condition, $n_e = n_0 e \phi / T_e$, making the perturbed density proportional to the potential. Dis-

sipative electron effects [e.g., Landau damping (Krahl and Trivelpiece, 1973), other resonances, and collisions] shift the phase of the density perturbations relative to the potential and destabilize the wave. Dissipation of ion motion along the field lines (e.g., Landau damping and viscosity) damps wave motion and opposes the instability. A basic model for unstable drift waves in the presence of flow shear and magnetic shear in a slab geometry is given by Carreras *et al.* (1992):

$$\frac{d}{dt} (1 - \rho_s^2 \nabla_{\perp}^2) \phi + U_D \frac{\partial \phi}{\partial y} + D_0 \frac{\partial^2 \phi}{\partial y^2} - L_n D_0 \left[\nabla_{\perp} \left(\frac{\partial \phi}{\partial y} \right) \times \mathbf{z} \right] \cdot \nabla_{\perp} \phi - \frac{C_s^2}{v_i} \nabla_{\parallel}^2 \phi = 0. \quad (5.10)$$

In Eq. (5.10), $d/dt = \partial/\partial t - B_0^{-1} \nabla \Phi \times \mathbf{z} \cdot \nabla$ is the advective derivative of the equilibrium $E \times B$ flow, $\rho_s = (T_e m_i)^{1/2} / e B_0$ is the ion radius of gyration in the magnetic field (evaluated at the electron temperature), $C_s = (T_e / m_i)^{1/2}$ is the ion sound speed, $U_D = C_s \rho_s L_n^{-1}$ is the diamagnetic flow speed, $L_n^{-1} = n_0^{-1} dn_0 / dx$ is the inverse scale length of the equilibrium density, D_0 is the strength of the electron dissipation coupling, producing both the destabilizing term $D_0 \partial^2 \phi / \partial y^2$ and the nonlinearity (Terry and Horton, 1982), v_i is the collisional dissipation rate of parallel ion momentum, and ϕ has been normalized by $T_e / |e|$ (T_e is the electron temperature times the Boltzmann constant). The flow profile is assumed to be stable; hence the curvature term is neglected. The first and last terms are almost identical to the first and last terms of Eq. (5.8). Here there is the addition of $d\phi/dt$, from dn_e/dt (with $n_e = n_0 e \phi / T_e$), and the magnetic-shear damping term arises from parallel ion motion instead of parallel current. (Parallel momentum is modeled by the equation $n_0 v_i u_{\parallel} = -C_s^2 \nabla_{\parallel} n_i$, describing the balance of collisional drag with parallel ion pressure. This equation couples to ion momentum through parallel compression of the flow.)

Under linearization and a Fourier transform in y and t , Eq. (5.10) becomes an eigenmode equation in x , the direction of inhomogeneity of both the mean flow and the parallel damping term. In the absence of the mean flow, the least stable eigenmode peaks about the rational surface with a width that is determined from the balance of the time derivative of vorticity and the parallel damping term, yielding $\Delta = (\omega \rho_s^2 v_i L_s^2 / C_s^2 k_y^2)^{1/4} \cong \rho_s (L_s / L_n)^{1/2} (v_i / k_y U_D)^{1/2}$. With linear flow shear, $-B_0^{-1} \nabla \Phi \times \mathbf{z} = U_y(x) = U_y(0) + x U_y'(0)$, the peak of the eigenmode structure is shifted off the rational surface by the linear inhomogeneity of the flow shear. The shift S is proportional to the shear strain rate ω_s normalized to the drift-wave propagation frequency Doppler shifted by the mean flow speed at the rational surface, i.e., $S = k_y U_y'(0) \Delta / [\omega - k_y U_y(0)] \cong \omega_s / k_y U_D$. The shift forces the eigenmode into a region of stronger parallel damping, causing a reduction of growth rate. In the expression for the growth rate, flow shear enters as an additive reduction to the linear instability drive. Complete

stabilization occurs when the shear term is larger than the difference of the drive term and the parallel damping term:

$$\omega_s > 2k_y U_D \frac{\rho_s}{W} \left[\frac{k_y^2 D_0}{k_y U_D} - \frac{\rho_s^2}{\sqrt{2W^2}} \right]^{1/2}, \quad (5.11)$$

where W is the mode width Δ evaluated at $\omega = k_y U(0) + k_y U_D$. The factor $\rho_s/W \sim (L_n/L_s)^{1/2}$ and the term in brackets are both considerably less than unity, indicating that the mode is stabilized at a flow shear strength far below the linear stability estimate of Eq. (2.33), which yields $\omega_s > k_y U_D$. However, Eq. (5.11) is comparable to the nonlinear suppression criterion, Eq. (2.17), because saturated turbulence adjusts to make the turbulence decorrelation rate essentially equal to the growth rate, particularly for long wavelengths ($k_y \rho_s < 1$) where there is little dispersion.

Ion-temperature-gradient modes are a drift-wave instability believed to be an important source of turbulence in tokamaks. Free energy for the instability is provided by the ion temperature gradient. At the instability threshold, where the temperature gradient scale length just exceeds a critical value, the gradient free energy is accessed through a resonance of the mode with the guiding-center motion of individual ions under the drifts produced by the gradient and curvature of the magnetic field. Correct modeling of the threshold requires kinetic theory. Well above the instability threshold, the mode frequency becomes larger than the frequency of drift motion, and fluid equations can be used to model the instability and the turbulence it drives (Lee and Diamond, 1987). The spatial structure of the fluctuations has different forms in a slab and a torus. Moreover, in toroidal geometry, there are two branches, one whose structure is like that of a slab, and one whose structure is uniquely toroidal, with a tendency for the fluctuations to be much larger at $\theta=0$ than at $\theta=\pi$. Because of these and other complexities, there are numerous models and growth-rate calculations for ion-temperature-gradient modes (for a review, see Horton, 1999).

In the ion-temperature-gradient mode, flow shear is destabilizing at weak levels and becomes stabilizing when it is stronger. This feature is related to the effective eigenmode potential and is most easily illustrated using a fluid model (Wang, Diamond, and Rosenbluth, 1992). In addition to vorticity and parallel flow equations, the fluid model has an ion pressure evolution equation,

$$\frac{d}{dt} (1 - \nabla_\perp^2) \phi + U_D \left[1 + \left(\frac{1 + \eta_i}{T} \right) \nabla_\perp^2 \right] \frac{\partial \phi}{\partial y} + \nabla_\parallel u_\parallel = 0, \quad (5.12)$$

$$\frac{d}{dt} u_\parallel = -\nabla_\parallel \phi - \nabla_\parallel p, \quad (5.13)$$

$$\frac{d}{dt} p + U_D \left(\frac{1 + \eta_i}{T} \right) \frac{\partial \phi}{\partial y} + \frac{\Gamma}{T} \nabla_\parallel u_\parallel = 0, \quad (5.14)$$

where ϕ , u_\parallel , and p are normalized by T_e/e , C_s , and $n_o T_e$, spatial scales are normalized by ρ_s , $T = T_e/T_i$,

$\eta_i = d \ln T_i / d \ln n_o$, and Γ is the ratio of specific heats. Under linearization, the derivative d/dt includes advection by the equilibrium flow $\bar{u}(x) = -B_0^{-1} \nabla \Phi_0 \times \mathbf{z}$. The drift terms (those with U_D dependence) come from $E \times B$ advection of the equilibrium pressure in the ion momentum and pressure evolution. When $\eta_i > 1$ the instability is driven primarily by the temperature gradient contribution to the pressure gradient.

In Eq. (5.12) the parallel compression term $\nabla_\parallel u_\parallel$ couples the dynamics of parallel ion motion to the vorticity. Unlike the prior example, in which the parallel motion was purely dissipative, here parallel motion is driven by the pressure, which through the advection of the mean pressure gradient drives the instability. Consequently larger values of ∇_\parallel^2 away from the rational surface produce stronger drive. However, this tendency is limited by the parallel electric field in Eq. (5.13), which acts as a dissipative sink in this model. At sufficiently large distances from the rational surface this dissipation overcomes the drive, and the fluctuation structure becomes evanescent. This feature is evident in the behavior of the growth rate as a function of the radial eigenmode number in the $\bar{u}=0$ case. The eigenmode number is a measure of the rms displacement from the rational surface. With increasing eigenmode number, the growth rate first increases as the coupling to the pressure drive becomes stronger, and then decreases as the dissipation associated with the parallel electric field overcomes the gradient drive (Terry *et al.*, 1988).

When flow shear with a linear profile is added to the equations, it shifts the fluctuation structure further from the rational surface. Thus weak shear can enhance the coupling to the pressure drive and thereby increase the growth rate, while stronger shear favors compressional damping and lowers the growth rate (Hamaguchi and Horton, 1992; Wang, Diamond, and Rosenbluth, 1992). Strong shear also introduces a wave absorption resonance that further damps fluctuations (Wang, Diamond, and Rosenbluth, 1992). Kinetic treatments of the ion-temperature-gradient instability in slab geometry show the same behavior, with a growth rate that increases with weak shear and decreases with stronger shear (Staebler and Dominguez, 1991; Wang, Diamond, and Rosenbluth, 1992). In toroidal geometry, flow shear strongly affects eigenmodes because of their large radial extent (Connor, Taylor, and Wilson, 1993). In simulation of ion-temperature-gradient turbulence in toroidal geometry the shear flow is typically generated self-consistently by the Reynolds stress. When the shear strain rate is larger than the linear growth rate, there is a significant reduction of turbulence and a tenfold reduction of transport (Waltz, Kerbel, and Milovich, 1994). The effect of shear flow on the ion-temperature-gradient mode has also been investigated experimentally in a linear plasma device (Song and Sen, 1994). This mode, which appears as a quasicohherent feature in the fluctuation spectrum, was observed to increase in amplitude with weak shear and decrease with stronger shear. This behavior was attributed to the fact that the same external control, i.e., the voltage on an rf heating grid, affects

both the ion-temperature-gradient drive and the flow shear. It was postulated that the rf voltage favors the ion-temperature-gradient drive at lower values and the generation of sheared flow at higher values. Complete stabilization of the mode required considerably larger flow shear than the theoretically predicted values.

The resistive interchange instability is a pressure-driven interchange mode that is closely related to the Rayleigh-Taylor-instability. It is unstable when the pressure gradient is parallel to the curvature of the equilibrium magnetic field. The field-line curvature therefore acts as an effective gravity. The instability is described by the reduced MHD equations, Eqs. (5.6) and (5.7), and is damped by the dissipation of parallel current excited by the flow, just as with the Kelvin-Helmholtz instability. Pressure couples to the vorticity evolution through the pressure interchange torque (Sugama and Wakatani, 1991), $\kappa \times \nabla p \cdot \mathbf{z}$, where κ is the curvature of magnetic-field lines. With this term the vorticity equation is

$$\rho \frac{d}{dt} \nabla_{\perp}^2 \frac{\Phi}{B_0} = B_0 \nabla_{\parallel} J_{\parallel} - \kappa \frac{\partial p}{\partial y}. \quad (5.15)$$

As with the Kelvin-Helmholtz instability, the interchange mode is dominantly electrostatic, allowing the Lorentz term involving the inductive field A_{\parallel} to be dropped. The parallel current is governed by the right-hand side of Ohm's law, Eq. (5.7). A simple pressure evolution equation, $dp/dt = -(dp_0/dr) \partial/\partial y (\phi/B_0)$, describing advection of perturbed pressure by the equilibrium flow and advection of the equilibrium pressure by the perturbed flow, closes the system. The linear eigenmode equation is like the Kelvin-Helmholtz eigenmode equation, Eq. (5.8), with the addition of the curvature drive:

$$\begin{aligned} & [-i\omega + ik_y \bar{u}(x)] \left(\frac{\partial^2}{\partial x^2} - k_y^2 \right) \frac{\phi_{k_y}}{B_0} - ik_y \frac{d^2 \bar{u}}{dx^2} \frac{\phi_{k_y}}{B_0} \\ &= \frac{B_0^2}{\rho \eta L_s^2} k_y^2 x^2 \frac{\phi_{k_y}}{B_0} - \frac{\kappa k_y^2}{\rho [-i\omega - ik_y \bar{u}(x)]} \frac{\phi_{k_y}}{B_0} \frac{dp_0}{dr}, \end{aligned} \quad (5.16)$$

where the temporal Fourier transform has been introduced. The advective pressure response in the denominator of the curvature drive complicates the eigenmode structure; hence a simple characterization of the effect of flow shear is not possible. Clearly large flow shear weakens the curvature drive, but large shear flow also triggers the Kelvin-Helmholtz instability. There is a regime where flow shear stabilizes the resistive interchange instability, but the system is Kelvin-Helmholtz stable (Sugama and Wakatani, 1991; Tajima *et al.*, 1991; Carreras *et al.*, 1993). For smaller resistivity, Kelvin-Helmholtz stability is possible with stronger flow shear, and the resistive interchange mode is stable at larger values of the curvature. The real part of the stabilized interchange eigenmode remains centered at the rational surface, but the eigenfunction develops a significant imaginary part (Sugama and Wakatani, 1991). The

eigenfunction can be modeled as a shifted Gaussian with an imaginary shift proportional to the flow shear magnitude (Carreras *et al.*, 1995).

The above examples demonstrate that strong (Kelvin-Helmholtz-stable) flow shear frequently stabilizes collective plasma instabilities. Unlike the nonlinear decorrelation process of Sec. II, the details and mechanism vary from case to case. Hence there is no universal criterion for stabilization, and in some cases flow shear, particularly weak flow shear, can be destabilizing. Moreover, the ideal of a collective linear mode in the presence of a prescribed flow shear, though convenient for analysis and interpretation, is not generally realized in plasmas. A variety of numerical studies in which the fluctuations are allowed to act on the shear flow through the mechanisms of Sec. IV show that there is a strong feedback, and the effect of flow shear on fluctuations must be treated self-consistently (Carreras, Lynch, and Garcia, 1991; Ware *et al.*, 1992; Guzdar *et al.*, 1993; Waltz, Kerbel, and Milovich, 1994). The feedback mechanisms of these simulations are nonlinear, also indicating that the effect of flow shear on fluctuations likely involves some combination of the physics of linear stabilization and nonlinear decorrelation.

3. Shear straining in a torus

Observations of fluctuation suppression in tokamaks are consistent with the shear suppression criterion, Eq. (2.17), provided it is modified for the tokamak geometry. In this section, the $E \times B$ shearing rate appropriate for tokamak fluctuations is derived. Consider a sheared poloidal flow driven by the $E \times B$ drift of a radial electric field in a torus. For the Fourier transform of toroidal and poloidal angles introduced just prior to Eq. (5.2), the rate of poloidal advection is

$$\omega_{E \times B} = -\frac{E_r}{B_{\phi}} \frac{im}{r}. \quad (5.17)$$

A wide class of fluctuations are sufficiently localized in the vicinity of the rational surface that the expression $m = qn$, which is precisely true only on a rational surface, remains approximately true over the radial extent of the fluctuation. Using this and the definition of q in Eq. (5.3), we obtain the advection rate $\omega_{E \times B} = -in(E_r/RB_{\theta})$. The shear straining rate is the difference of advection rates at two radial locations separated by a radial correlation length Δr ,

$$\omega_s = \frac{\Delta r}{\Delta \hat{\phi}} \frac{\partial}{\partial r} \left(\frac{E_r}{RB_{\theta}} \right), \quad (5.18)$$

where $\Delta \hat{\phi} = \Delta \varphi / 2\pi = (in)^{-1}$ is the toroidal correlation length (wavelength) normalized by 2π . The difference has been expanded in a Taylor series, retaining only the first term. From Eq. (5.18) the shearing rate depends on variations of both the radial electric field and the poloidal magnetic field.

In a torus, the flux surfaces need not have circular cross sections, and a radial coordinate that uniquely

identifies individual flux surfaces is advantageous. Such a coordinate can be defined from the poloidal flux through a toroidal annulus of width dr and radius $2\pi R$ in the toroidal symmetry plane,

$$d\psi = 2\pi R B_\theta dr, \quad (5.19)$$

where ψ is the flux coordinate. The toroidal symmetry plane is the plane of $\theta=0$ and $\theta=\pi$, i.e., the plane in which a bagel is sliced. A flux coordinate normalized by 2π is often used: $\hat{\psi} = \psi/2\pi$. In terms of the normalized flux coordinate, $\Delta r \partial/\partial r \rightarrow \Delta \hat{\psi} \partial/\partial \hat{\psi}$, and the shearing rate is

$$\omega_s = \frac{\Delta \hat{\psi}}{\Delta \hat{\phi}} \frac{\partial}{\partial \hat{\psi}} \left(\frac{E_r}{RB_\theta} \right). \quad (5.20)$$

This is the expression given by Burrell (1997) for the shearing rate in a tokamak. It is general, despite our use in the present context of the circular form of q [Eq. (5.3)]. An equivalent expression is given by Hahn and Burrell (1995) by transforming $E_r = -\partial\Phi_0/\partial r$ to flux coordinates. Under this transformation, $E_r = (\partial\Phi_0/\partial \hat{\psi}) d\hat{\psi}/dr = (\partial\Phi_0/\partial \hat{\psi}) RB_\theta$, and

$$\omega_s = \frac{\Delta \hat{\psi}}{\Delta \hat{\phi}} \frac{\partial^2}{\partial \hat{\psi}^2} (\Phi_0). \quad (5.21)$$

Since the mean electrostatic potential Φ_0 is constant on a flux surface, the shear parameter of Eq. (5.20), $\partial/\partial \hat{\psi}(E_r/RB_\theta)$, is also constant on a flux surface. Isolating which parts of an expression vary over a flux surface and which parts do not is important in addressing the origin of asymmetries with respect to θ . In the case of Eqs. (5.20) and (5.21), asymmetries in poloidal angle originate with the ratio of correlations $\Delta \hat{\psi}/\Delta \hat{\phi}$.

This ratio can be expressed in terms of the magnetic field and the major radius R (Burrell, 1997) as follows: From the flux coordinate definition, Eq. (5.19), $\Delta \hat{\psi}$ is related to a radial correlation by $\Delta r = (B_\theta R)^{-1} \Delta \hat{\psi}$. The toroidal correlation $\Delta \hat{\phi}$ is related to the correlation length L_\perp perpendicular to the magnetic field in a flux surface. The latter is determined from the perpendicular gradient in a flux surface, $L_\perp^{-2} = |\hat{\psi}^{-1} \nabla \hat{\psi} \times \nabla_\perp| = |\hat{\psi}^{-1} \nabla \hat{\psi} \times (\nabla - B^{-1} \mathbf{B} \cdot \nabla)|$. In terms of the Fourier transform of toroidal and poloidal angles,

$$L_\perp^{-1} = \left| \frac{in}{R} \left(1 - \frac{B_\phi}{B} \right) \hat{\phi} + \frac{im}{r} \left(1 - \frac{B_\theta}{B} \right) \hat{\theta} \right|, \quad (5.22)$$

where $\hat{\phi}$ and $\hat{\theta}$ are unit vectors in the toroidal and poloidal angles, respectively. In a tokamak the toroidal field component is an order of magnitude larger than the poloidal component. Therefore the second term of Eq. (5.22) dominates and $L_\perp^{-1} \cong m/r = nq/r = B_\phi/\Delta \hat{\phi} RB_\theta \cong B/\Delta \hat{\phi} RB_\theta$. Observations (Fonck *et al.*, 1992) and simulations (Parker, Lee, and Santoro, 1993; Waltz, Kerbel, and Milovich, 1994) indicate that to a good approximation $\Delta r \cong L_\perp$, from which

$$\frac{\Delta \hat{\psi}}{\Delta \hat{\phi}} \cong \frac{R^2 B_\theta^2}{B}. \quad (5.23)$$

Substituting Eq. (5.23) into the shear strain rate, Eq. (5.20) yields

$$\omega_s = \frac{R^2 B_\theta^2}{B} \frac{\partial}{\partial \hat{\psi}} \left(\frac{E_r}{RB_\theta} \right). \quad (5.24)$$

In this expression, the factor $R^2 B_\theta^2/B$ is not a constant along the flux surface. The magnitude of B varies as R^{-1} and $R = R_0 + r \cos \theta$ varies significantly from $\theta=0$ to $\theta = \pi$.

A variation of the shear straining rate from the outside midplane ($\theta=0$) to the inside midplane ($\theta=\pi$) is consistent with observations of fluctuations in the Doublet III-D (DIII-D) tokamak in the H mode (Burrell *et al.*, 1992; Doyle *et al.*, 1992) and for a core transport barrier (Burrell, 1997). In the latter the shear straining rate is calculated to increase by a factor of 7 from the inside midplane to the outside midplane. Scattered light from a far-infrared laser diagnostic indicates that density fluctuations are larger at the inside midplane than at the outside midplane. This observation is striking because the outside midplane is a region of unfavorable magnetic-field curvature and therefore enhanced susceptibility to interchange-driven turbulence. In the absence of flow shear, the outside midplane generally has stronger fluctuation activity. This poloidal asymmetry is also reflected in the spatial and temporal behavior of the transport barrier induced by biased probes. The rise in the total number of electrons and electron kinetic energy associated with flow-shear-induced suppression commences at the outside midplane (Jachmich *et al.*, 1998). The factor E_r/RB_θ in the derivative is also significant in understanding other observations. In a type of enhanced confinement mode called the VH mode, the H -mode transport barrier broadens inward to include a larger plasma volume, as indicated by the region of fluctuation reduction and steepened pressure gradient. In some cases the confinement improvement covers all of the plasma volume. Shear in the $E \times B$ velocity E_r/B is significant only in the outer part of the region of improved confinement, whereas shear in E_r/RB_θ extends over the entire region of improved confinement (Lao *et al.*, 1996).

B. Effect of flow shear on transport fluxes

The fluctuation-induced transport fluxes of density and heat, Eqs. (2.8) and (2.9), depend on the amplitudes of turbulent fluctuations $\tilde{\phi}_{-\mathbf{k}}$, $\tilde{p}_{\mathbf{k}}$, and $\tilde{n}_{\mathbf{k}}$, but they also depend on the complex phase angle between each of the two fluctuations that compose the correlation. In terms of a phase representation of the complex Fourier fluctuation amplitudes, the heat flux can be written

$$\text{Re } Q_e = -B_0^{-1} \sum_{\mathbf{k}} k_y |\tilde{\phi}_{-\mathbf{k}}| |\tilde{p}_{\mathbf{k}}| \sin \alpha_{\mathbf{k}} \Theta_{\mathbf{k}}, \quad (5.25)$$

where the cross phase $\alpha_{\mathbf{k}}$ is defined as the difference of the phase angles of $\tilde{\phi}_{-\mathbf{k}}$ and $\tilde{p}_{\mathbf{k}}$ in the complex plane,

$$\exp(i\alpha_{\mathbf{k}}) \equiv \frac{\langle \tilde{\phi}_{-\mathbf{k}} \tilde{p}_{\mathbf{k}} \rangle}{|\tilde{\phi}_{-\mathbf{k}}| |\tilde{p}_{\mathbf{k}}|}, \quad (5.26)$$

and $\Theta_{\mathbf{k}}$ is the coherency (Bendat and Piersol, 1986). The coherency, defined by $\Theta_{\mathbf{k}} = |\tilde{\phi}_{-\mathbf{k}} \tilde{p}_{\mathbf{k}}| \{|\tilde{\phi}_{\mathbf{k}}|^2 |\tilde{p}_{\mathbf{k}}|^2\}^{-1/2}$, is a measure of noise. If the fluctuations are perfectly correlated but out of phase, $\Theta_{\mathbf{k}} = 1$ and $\alpha_{\mathbf{k}} = \pi$. We have discussed in Sec. II. B the effect of flow shear on turbulence amplitudes. Here its effect on the cross phase $\alpha_{\mathbf{k}}$ is discussed.

A simple illustration of the effect of flow shear on the cross phase can be drawn from the pressure evolution equation of the resistive interchange instability, given just prior to Eq. (5.16). If there is no flow, linearization yields

$$p_{\mathbf{k}} = \frac{\phi_{\mathbf{k}} k_y}{B_0} \frac{dp_0}{\omega} \frac{dr}{dr}. \quad (5.27)$$

The unstable root of the dispersion relation has a purely imaginary frequency (growth rate),

$$\omega = i\gamma_k = i \left(\frac{\kappa^2 k_y^2 L_s^2 \eta (dp_0/dr)^2}{B_0^2 \rho} \right)^{1/3}. \quad (5.28)$$

Therefore, for the linear instability, $(k_y/\omega) = -ik_y/\gamma_k$, and $\alpha_{\mathbf{k}} = -\pi/2$. The flux $\text{Re } Q_e = \sum_k |\tilde{\phi}_{\mathbf{k}}|^2 [k_y^4 (dp_0/dr) \rho B_0^{-4} \kappa^{-2} L_s^{-2} \eta^{-1}]^{1/3}$ is positive, and heat is transported outward (the coherency $\Theta_{\mathbf{k}}$ has been ignored). If there is an equilibrium flow and advection dominates the pressure response ($k_y U_y \gg \omega$), the pressure is given by

$$p_{\mathbf{k}} = - \frac{\phi_{\mathbf{k}}}{B_0} \frac{k_y}{k_y U_y(x)} \frac{dp_0}{dr}. \quad (5.29)$$

If the frequency of advection $k_y U_y$ is real, the cross-phase angle is $\alpha_{\mathbf{k}} = \pi$, and there is zero transport. This illustration only suggests how flow affects the cross phase because it relies on gross simplifications. The flow $U_y(x)$ extends from the rational surface, and the correlation $\langle \tilde{\phi}_{-\mathbf{k}} \tilde{p}_{\mathbf{k}} \rangle$ therefore samples the eigenmode. Because the eigenmode becomes complex in the presence of flow shear, the phase angle is neither π nor $\pi/2$. Moreover, at finite amplitude, the nonlinear pressure response must also be considered, and the eigenmode itself is nonlinear. These effects decrease the phase factor $\sin \alpha_{\mathbf{k}}$ from its maximum value of unity in the case of the linearly unstable mode, but quantifying the decrease is difficult and requires approximation.

Analytic studies of the effects of flow shear on the cross phase have been largely limited to resistive interchange turbulence. The first discussion (Carreras *et al.*, 1995) included the turbulent diffusivity D in the advection of pressure, representing the pressure equation as $[ik_y U_y(x) - D \partial^2 / \partial x^2] p_{\mathbf{k}} = -ik_y B_0^{-1} \phi_{\mathbf{k}} dp_0/dr$. This equation was inverted heuristically,

$$\text{Im} \frac{ik_y}{[ik_y U_y(x) - D \partial^2 / \partial x^2]} \rightarrow \frac{-D/2W^2}{(k_y^2 U_y^2 + D^2/4W^4)^{1/2}} = \sin \alpha_{\mathbf{k}}, \quad (5.30)$$

accounting for the eigenmode width W in the turbulent diffusion, but not accounting for the shifted, complex eigenmode structure in the form of the flow shear term. A subsequent study (Ware *et al.*, 1996) dealt with the nonlinear eigenmode problem in a more consistent fashion. This study also considered a renormalized model (Carreras, Garcia, and Diamond, 1987), i.e., one in which the advection of vorticity and pressure was replaced by an amplitude-dependent viscous diffusion operator and a turbulent pressure diffusivity, respectively. The nonlinear eigenmode problem was solved approximately, using an eigenfunction ansatz with an undetermined mode width and imaginary shift. Moments were taken in order to determine the mode width, the shift, the magnitudes of the turbulent viscosity and diffusivity, and the appropriate form of the operator inversion in Eq. (5.30). The cross phase in the weak shear limit was found to be

$$\sin \alpha_{\mathbf{k}} = - \left(1 - \frac{5k_y^2 U_y'(0)^2 \Delta_{\mathbf{k}}^6}{4D^2} \right), \quad (5.31)$$

where D is the turbulent pressure diffusivity, $U_y'(0)$ is the flow shear rate at the rational surface, $\Delta_{\mathbf{k}} = W(\mu/W^2 \gamma_k)^{1/6}$ is the nonlinear mode width, γ_k is the linear growth rate [Eq. (5.28)], μ is the turbulent viscosity, and $W = [\rho \eta^2 L_s^4 \kappa (dp_0/dr) B_0^{-4} k_y^{-2}]^{1/6}$ is the linear mode width. Both Eqs. (5.30) and (5.31) indicate that in the limit of no flow, $\sin \alpha_{\mathbf{k}} = -1$, as in the case of the linear instability with no flow, while nonzero flow decreases the value of $\sin \alpha_{\mathbf{k}}$, independent of any amplitude effects. Both results yield a reduction of cross phase, independent of the sign of the flow shear. Flow curvature has also been examined in the weak limit (Kelvin-Helmholtz stable) and was found to reduce the cross phase (Ware *et al.*, 1996).

An extension of the resistive interchange model shows that in circumstances in which the conduction of heat along the magnetic field is important in the turbulent dynamics, shear flow can lead to a marked decrease in the particle flux with almost no reduction in the heat flux (Ware *et al.*, 1998). The effect is sensitively dependent on the relationship between flow shear and the cross phase through the inversion of the relevant advective operators, indicated heuristically by Eq. (5.30). To address both heat and particle transport the pressure equation is split into two equations, one for density and one for temperature. Temperature fluctuations are subject to heat conduction along the magnetic field, carried by rapidly streaming electrons. The parallel thermal conductivity goes as the square of the electron thermal speed divided by the electron collision frequency. In the density equation, parallel dissipation involves the propagation of sound waves, with an effective diffusivity that scales as the square of the sound speed divided by the ion

collision rate. This diffusivity is smaller than the parallel thermal conductivity by the square root of the electron-to-ion mass ratio and is easily smaller than the linear and nonlinear time scales in the density evolution. The same is not true for the temperature evolution. In the edge of fusion plasmas it is possible to have a regime in which the temperature evolution, $[U_y(x)\partial/\partial y - \mathbf{u}\cdot\nabla - \chi_{\parallel}\nabla_{\parallel}^2]T = -B_0^{-1}\partial\phi/\partial y dT_0/dr$, is dominated by the balance of the thermal conduction with the advection of the mean temperature, even in the presence of a mean shear flow. Under such a circumstance there is no effect of flow shear on the cross phase. In the density equation, $[U_y(x)\partial/\partial y - \mathbf{u}\cdot\nabla]n = -B_0^{-1}\partial\phi/\partial y dn_0/dr$, flow shear diminishes cross phase as discussed in the previous paragraph. This effect provides an explanation for the observed behavior of heat and particle transport in edge shear flows in the Continuous Current Tokamak (Tynan *et al.*, 1996) and the Madison Symmetric Torus Reversed-Field Pinch (Craig *et al.*, 1997). In both cases, shear flows induced by biased probes produced a marked decrease in particle transport with virtually no change in the heat flux. The heat and particle fluxes calculated from the model for the parameters of these devices show the same features (Ware *et al.*, 1998). In contrast, the edge plasmas of the TEXTOR tokamak have a higher mean density, leading to a parallel thermal conduction rate that is smaller than the turbulence decorrelation rate and shear strain rate. There, a reduction of both the temperature fluctuations and the heat flux is observed (Boedo *et al.*, 1998).

Measuring the cross phase is difficult because two fluctuations must be measured simultaneously in the same spatial location. Such measurements are most frequently carried out with Langmuir probes, from which the fluctuations in plasma density and potential can be inferred. Langmuir probe measurements do not directly measure the fluctuating plasma potential $\tilde{\phi}_{\mathbf{k}}$. They require assumptions about temperature fluctuations, which are often not measured, in order to infer the potential fluctuations. This limitation should be borne in mind in assessing Langmuir probe data. A reciprocating Langmuir probe has been employed to measure the cross phase and fluctuation amplitudes of the particle flux in DIII-D (Moyer *et al.*, 1995). To accommodate a probe, colder pre-*H*-mode and *H*-mode plasmas were produced by limiting auxiliary heating to a short neutral beam pulse that triggered the *H* phase. Several aspects of these measurements are of interest. The particle flux is observed to decrease much more dramatically than the fluctuations, which remain at finite amplitude. The flux is reduced by 1–2 orders of magnitude over a range of radial positions in which the flow shear varies from strongly positive to strongly negative. There is no peaking of the particle flux even where the flow shear goes through zero. In qualitative agreement with shear suppression, the amplitudes $\tilde{\phi}_{-\mathbf{k}}$ and $\tilde{n}_{\mathbf{k}}$, normalized to their pre-*H*-mode values, are larger in the region of zero flow shear than outside it, where shear is large. The fact that the flux remains small suggests that the cross phase

is near an integer multiple of π . Indeed, a direct measurement of the phase angle at this location reveals that $\alpha_{\mathbf{k}}$ changes from $\pi/2$ to $-\pi$ in going from the pre-*H*-mode to the *H* mode. This establishes that the cross phase can be modified independently of the amplitudes. It also suggests that the cross phase is sensitive to features of the flow other than its shear, e.g., the flow curvature. The cross phase has also been measured in an *H* mode induced by external biasing, again using Langmuir probes (Boedo *et al.*, 1998). In the region where the flow shear changes sign, the cross phase causes the particle flux to shift from outward to inward.

VI. FLOW SHEAR AND ENHANCED PLASMA CONFINEMENT

The importance of confinement in fusion devices has encouraged the discovery of numerous modes of operation with improved confinement (Carreras, 1997). Strong flow shear is present in those enhanced-confinement modes that have a universal character, i.e., that are reproducible under diverse conditions and occur in a large variety of distinct magnetic confinement configurations. It is also conjectured to be present in other enhanced-confinement modes (Carreras, 1997). Although observational details remain to be understood, particularly those that relate to how transport barriers are generated, flow-shear-induced suppression of turbulence and transport is the leading explanation for the improvement of confinement. This follows from the observed temporal and spatial coincidence of transport reduction with the region of strong flow shear; from numerous features of the reduction that are in agreement with theory, as discussed in previous sections; and, importantly, from the requisite universality of the flow shear suppression mechanism. Other explanations have lacked this universality. This section reviews the salient features of enhanced confinement in fusion devices.

A. Tokamak

The most extensive body of knowledge on enhanced-confinement operation comes from the tokamak. In this device, transport barriers are either formed spontaneously or induced by external means. Moreover, they occur in both the core and the edge regions of the plasma.

1. Spontaneous edge transport barrier

The spontaneous formation of a transport barrier in the plasma edge is generally regarded as a transition to the *H* mode. The *H* mode is remarkable for its universality. Every auxiliary heated divertor tokamak since 1982 has reproducibly created *H* modes (auxiliary heating and divertors are discussed in subsequent paragraphs). References to the extensive number of diverted tokamaks reporting *H* mode can be found in the reviews of Stambaugh *et al.* (1990), Groebner (1993), and Burrell (1997). The *H* mode has also been achieved in other tokamaks and in nontokamak magnetic confinement devices. Other modes of tokamak operation involving en-

hanced confinement in conjunction with edge processes, such as radiation, have been reported. These are peculiar to individual machines (Lazarus *et al.*, 1985; Ongena *et al.*, 1993; Messiaen *et al.*, 1997) and thus lack the universality of the H mode.

The general properties of the H mode, outlined in Sec. II. D, occur in all discharges and devices, providing an operational definition of the H mode. The underlying physical process is robust, and while affected by the complexities and highly variable conditions of the plasma edge, it transcends these conditions as a universal phenomenon. The universal aspects of the H mode are

(1) The requirement of heating power to the plasma above a threshold. Heating power increases the heat flux through the edge, which has been linked to the transition. It also increases the edge temperature.

(2) The existence of a transition or bifurcation to a new plasma state as manifested by changes in the profiles of temperature and density and local heat and particle fluxes. The transition occurs when a threshold value of plasma heating or edge temperature is reached.

(3) The presence of strong $E \times B$ flow shear.

(4) The other features described in Sec. II. D, such as confinement time increase and H_α decrease.

The H mode occurs over a wide range of plasma conditions. In particular,

(1) The heating power required for the transition can be provided by any of an assortment of techniques with widely varying effects on the energy distributions and temperatures of electrons and ions. The H mode has been produced with the injection of energetic neutral beams, a method employed in numerous devices; with the injection of rf power at the electron cyclotron resonance (Hoshino *et al.*, 1989), the ion cyclotron resonance (Steinmetz *et al.*, 1987), and the lower hybrid resonance (Tsuji *et al.*, 1990); and by ohmic heating (Osborne *et al.*, 1990). Ohmic (resistive) heating is associated with the production and maintenance of plasma current. (For additional references on heating in the H mode see Burrell, 1997).

(2) While it is desirable to have edge control with regard to concentrations of impurities and neutrals, radiation, and the recycling of plasma particles through ionization and charge exchange, a particular form of control is not required. It can be achieved with either divertors or limiters, devices that lead to widely differing magnetic and electric fields in the plasma edge region. The divertor is a set of external magnetic-field coils that modifies the topology of the edge magnetic field, producing a singularity in the magnetic shear at the x point of the separatrix. The divertor channels heat and particle outflows away from the plasma-facing wall, thereby controlling the concentrations of impurity ion species and neutrals. In limiter discharges the plasma edge is manipulated by a material surface protruding inward from the walls. Limiter discharges tend to have a higher impurity content at the edge, and/or a higher concentration of neutrals, both of which cool the edge and make triggering the H mode more difficult. Consequently, di-

vertors are used routinely for H -mode plasmas, but the H mode also has been achieved with limiters (Odajima *et al.*, 1987; Sengoku *et al.*, 1987; Bush *et al.*, 1990; and Refs. 90–92 of Burrell, 1997).

(3) The transition power threshold varies from device to device. It is sensitive to the heating mechanism, whether a divertor or limiter is used, the location of the divertor, whether particle drifts are away from or toward the divertor, and other plasma parameters.

(4) The magnitude of the changes in profiles, confinement time, the time required for the transition to the H mode, and the other changes described in Sec. II. D all vary when plasma conditions are changed.

(5) The H mode occurs in the widely different magnetic geometries of nontokamak devices.

The large variability of plasma conditions associated with the H mode requires a physical mechanism of considerable generality. A variety of proposed models have been tied to a particular collective instability, geometry, or field topology. They did not have the requisite generality and failed in experimental comparisons. However, stable flow shear provides a universal mechanism for turbulence reduction. This mechanism applies under all the observed variations of the H mode. The identification of this mechanism does not mean that the H mode is fully understood. A predictive theory of the H mode that accounts for generation of shear flow under all of the variable circumstances of the transition does not at present exist.

2. Externally induced edge transport barrier

The external biasing technique discussed in Sec. IV. B. 2 produces an edge transport barrier by externally driving $E \times B$ flow shear. These transport barriers share many common features with the spontaneous H mode, including a bifurcation of the plasma equilibrium, the subsequent formation of steep gradients in the region of flow shear, a decrease in H_α emission, and an increase in plasma energy. Thus the edge transport barrier produced by external biasing is regarded as an induced H mode. Several aspects of induced H modes are noted here. Particle confinement is generally observed to increase, indicating a decrease in the particle flux. In some cases the energy confinement also increases, although weakly in comparison to the particle confinement (Weynants *et al.*, 1991). In other cases there is virtually no change in energy confinement (Tynan *et al.*, 1996; Craig *et al.*, 1997). Differences in the response of heat and particle fluxes to flow shear can be understood if collisional heat conduction along the magnetic field is important (see Sec. V. B). Where measured, the fluctuation levels of density and potential also decrease (Tynan *et al.*, 1992). The improvement of particle confinement with biasing can be obtained without the bifurcation (Weynants and Van Oost, 1993). This indicates that favorable changes in particle confinement are attributable to the flow shear and not simply changes in equilibrium that occur with bifurcation. In the reversed-field pinch, a bifurcation with biasing has not been observed (Craig

et al., 1997). In the biasing experiments, unlike the spontaneous H mode, the sign of the electric field can be varied from positive to negative. While the increases in particle confinement time differ for the two cases, there is an increase for both signs (Weynants *et al.*, 1991), consistent with shear suppression (Secs. II. B and V. B).

3. Spontaneous internal transport barriers

The existence of several distinct internal transport barriers has been reported. In many cases internal barriers have led to greater gains in confinement time than from the H mode alone. In the most notable internal barrier, ion thermal and particle transport rates fall to the irreducible minimum arising from collisions in a nonequilibrium plasma.

The internal barrier that has the most direct connection with the H mode is the VH mode (Jackson *et al.*, 1991; Greenfield *et al.*, 1993). The designation VH is for “very high,” a reference to the enhancement of confinement time by a factor of 2 beyond that of the H mode, as observed in DIII-D. The VH mode occurs as an inward expansion of the region of steepened density and temperature gradients, coinciding with an inward penetration of the region of strong flow shear, decreased ion thermal conductivity, and decreased density fluctuations. In the Joint European Torus (JET), the toroidal flow and its radial shear are observed to increase throughout the VH mode. The VH mode requires a quiescent H mode, free of coherent edge fluctuations known as edge-localized modes (ELM’s) that sometimes appear in the H mode. More recently, internal transport barriers with no connection to the H mode have been reported. In the JT-60U tokamak, a barrier forms spontaneously at an internal radial location, as manifested by a marked steepening of the gradients of ion temperature and electron density and the inferred decrease in the local ion thermal diffusivity (Koide *et al.*, 1994). The barrier formation temporally coincides with a large increase in the $E \times B$ flow due to poloidal rotation. This barrier is not created as an extension of the H mode. On the contrary, MHD activity driven at the barrier by a steepened pressure gradient can produce a heat pulse that propagates to the edge and triggers an H -mode transition.

The most impressive transport barrier from the standpoint of its effect on global confinement is a barrier that links favorable magnetic-shear configurations (Hugon *et al.*, 1992) with flow shear suppression. This barrier (Levinton *et al.*, 1995; Strait *et al.*, 1995; Koide *et al.*, 1997) has come to be referred to simply as an internal transport barrier (ITB). Internal transport barrier were first created in a magnetic-shear configuration in which the generalization of the magnetic winding number $q(r)$ decreased as a function of radius in the center of the tokamak. Between the center and the edge, q reached a minimum and increased further out. This type of q variation requires a current profile that peaks away from the center of the plasma cross section, and therefore tends to be transient because of inward current diffusion. In ITB’s, the turbulent diffusion of ion heat can

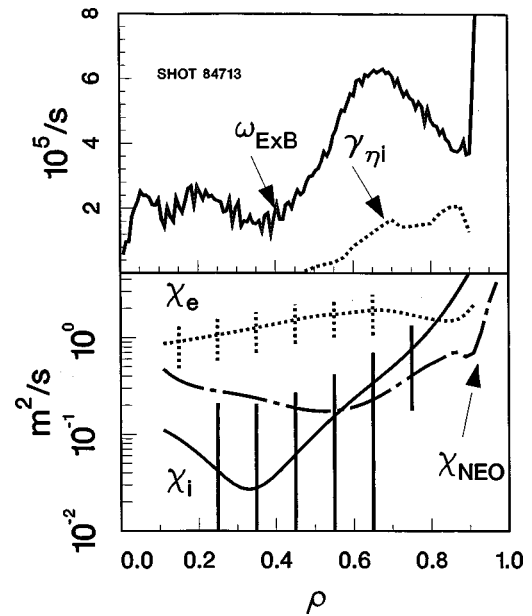


FIG. 12. Electron and ion thermal conductivities in a discharge with an internal transport barrier. The ion conductivity falls below a theoretical estimate for the collisional conductivity, indicating that turbulent losses are extremely small. For reference, the shear straining rate $\omega_{E \times B}$ is compared with $\gamma_{\eta i}$, the linear growth rate for the ion-temperature-gradient instability with zero flow shear. The latter is an estimate for the turbulent correlation rate. From Burrell, 1997.

diminish to the rate established by collisional processes. This is illustrated in Fig. 12, which shows the experimental ion and electron thermal conductivities compared with a standard theoretical prediction for the collisional conductivity. The measured conductivity is actually below the predicted collisional conductivity in the central region. (The standard theoretical expression used in making Fig. 12 overestimates the true collisional conductivity because it was not formulated for the steep gradients and strong electric field of the ITB and is not valid when the distance to the center of the plasma is comparable to a banana orbit width.) The comparison is taken as an indication that the turbulence-driven conductivity is smaller than the collision-driven conductivity. With heat and particles continually supplied by neutral beams, the pressure gradient can become so steep that global instabilities may set in. It is possible to tailor the plasma parameters so that pressure profile steepening is distributed over the entire plasma, locally avoiding pressure-gradient thresholds for instability, while achieving transport reduction throughout the plasma.

The negative magnetic shear in the core ($dq/dr < 1$), in conjunction with $q > 1$ throughout the plasma, reduces the growth rate of key instabilities and suppresses coherent core fluctuations known as sawtooth oscillations to an extent allowing a bifurcation of the plasma equilibrium to a new state with strong flow shear. The flow shear suppresses turbulence and transport as described in Sec. II. The transition or bifurcation that produces the flow shear is necessary for enhanced

confinement, and there is a heating or power input threshold required for the transition. However, the negative magnetic-shear configuration, while helpful, does not appear to be necessary (Koide *et al.*, 1996; Burrell *et al.*, 1998) if some other method is used for suppressing sawtooth oscillations. There is a temporal and spatial correlation between an estimate of the suppression parameter ε_s , Eq. (2.17), and the transport barrier. In the experiments, ε_s is not measured directly because the turbulence correlation time is typically not available. In its place, the instability growth time is used, calculated from kinetic linear stability codes in toroidal geometry that employ measured profiles for density, temperature, and current, but assume zero flow. Such codes accurately reproduce the linear behavior of a large number of plasma collective instabilities. The replacement of the turbulence correlation time with the linear growth time is based on the approximate equality of these times, which holds because turbulent energy transfer saturates the instability. Although the equality is not exact, experience indicates that the approximation is often quite good. Before the transition, the shear straining rate and linear growth rate are comparable. Immediately after the transition, and throughout the enhanced confinement mode, the shear straining rate exceeds the linear growth rate. Likewise the shear straining rate exceeds the linear growth rate in the regions where density fluctuations are suppressed and the transport fluxes are reduced. Ion transport is strongly reduced in all devices that have studied this enhanced-confinement mode, while electron transport has been modestly reduced in some cases and not significantly reduced in others. The weaker effect on electron transport is not understood.

There are other enhanced-confinement modes that involve transport reduction in the core. In the high internal inductance discharges of DIII-D, characterized by a transient highly peaked current profile, confinement improvement is correlated with an increased $E \times B$ flow shear (Lao *et al.*, 1993). The most intensively studied enhanced-confinement mode in the Tokamak Fusion Test Reactor (TFTR) was the supershot (Strachan *et al.*, 1987). This discharge was characterized by strongly peaked pressure profiles in the core. The plasma was heated with nearly zero-momentum input. From recent analysis and modeling, Ernst *et al.*, (1998) have argued that the steep ion pressure gradient produces a significant radial electric field [see Eq. (4.1)] and associated $E \times B$ shear flow. The flow shear is localized in the core, yielding enhanced confinement in that region. Outside the shear layer, confinement is degraded. Other enhanced-confinement modes that steepen profiles, such as the pellet enhanced-performance mode (Hugon *et al.*, 1992), may also produce a radial electric field in the region of a large pressure gradient (Carreras, 1997).

4. Externally induced internal transport barrier

Given the confinement improvements attained with core transport barriers, particularly when produced in combination with the H mode, a technique for externally inducing transport barriers is highly desirable. Ex-

ternally induced barriers offer the possibility of controlling transport, e.g., placing the barrier at desired locations to obtain turbulence-free operation, maintaining barriers in a steady state, or transiently weakening barriers to reduce pressure gradients or exhaust the helium ash of fusion. The CH mode (LeBlanc *et al.*, 1995) discussed in Sec. IV.B.3 represents an initial demonstration that externally induced transport barriers can be formed using injected rf waves to produce an internal flow shear layer. In the final experiments on the TFTR tokamak at Princeton Plasma Physics Laboratory, the formation of the CH mode was attempted on the larger, hotter TFTR plasma using an rf injection scheme similar to that of the PBX-M. The limited time available for the experiment before shutdown of the device did not permit adjustments and optimization. A flow shear layer was successfully created in the core, but the rf power was insufficient to reach the suppression threshold, as given by Eq. (2.17) (LeBlanc *et al.*, 1999). This result is encouraging and suggests that external transport control may be possible in fusion-grade plasmas.

B. Stellarator

The stellarator and its variants (torsatron, heliotron) are toroidal devices in which helical external current windings produce both toroidal and poloidal field components. It is thus possible to operate a stellarator with no plasma current, although in practice a plasma current may exist. Because the helical windings break toroidal symmetry, the radial electric field (as opposed to its radial derivative) has long been known to affect collisional transport rates in stellarators (Mynick and Hitchon, 1983). Notwithstanding, the H mode has been observed in the current-free Wendelstein 7-AS (W7-AS) stellarator (Erckmann *et al.*, 1993) and in the CHS torsatron/heliotron (Toi *et al.*, 1994). The observation of the H mode in stellarators is significant because it indicates that the physics of the H mode is not dependent on the high plasma currents of tokamaks and it suggests that the radial derivative of the radial electric field is important in stellarators, as in tokamaks. The stellarator evinces all the H -mode signatures of tokamaks. H_α and D_α (alpha line of deuterium) emissions drop at the transition, fluctuations drop, gradients steepen, and the confinement time rises. The increase in confinement time is weaker in a stellarator than it is in a tokamak. The maximal increase of 30% in W7-AS was attributed to the presence of a limiter, which in tokamaks is known to result in smaller confinement time increases. In W7-AS the poloidal rotation rate of the BIV impurity species also rises dramatically just preceding the H -mode transition. In a back transition to the L mode the poloidal rotation rate returns to its lower L -mode value. Flow shear, already sizable in the L mode, was not observed to increase in the CHS. In the CHS, however, the confinement improvement was only 15%. In W7-AS, the H mode occurs only for a narrow range of values of the inverse winding number [the generalization for stellara-

tors of q^{-1} from Eq. (5.3)]. For the observed range a velocity shear layer already exists prior to the transition, and neoclassical flow damping is minimum (Hirsch *et al.*, 1997). This narrow operational window is consistent with a suppression of transport by flow shear. However, the stellarator results overturn H -mode theories based on specific current profiles or the large magnetic shear at the edge of divertor tokamaks.

C. Reversed-field pinch

The reversed-field pinch (RFP) is a toroidal device in which the toroidal and poloidal magnetic fields are comparable in magnitude (Taylor, 1986). The radial profile of q decreases monotonically, starting at a few tens of percent in the core and decreasing through zero to a negative value of a few percent at the wall. In this configuration global tearing modes are unstable and dominate the core transport of heat and particles. The RFP thus differs from the tokamak in two significant ways, both of which have potential impact on suppression of turbulence by flow shear. First, the turbulence in the RFP is magnetic, whereas tokamak fluctuations are thought to be dominantly electrostatic. Second, the turbulence in the RFP is global in scale, whereas in the tokamak radial fluctuation scales are a few centimeters. The latter distinction is particularly important since flow shear in the H mode is confined to a narrow layer. These differences have led to strategies for confinement enhancement in the RFP that have focused on reducing the global magnetic turbulence by removing its free-energy source, the current gradient. The injection of current into the edge to flatten the current gradient has led to increases in confinement time by a factor of 4–5 (Sarff *et al.*, 1997).

Recent observations indicate that a sheared $E \times B$ flow is present in plasmas of the RFX experiment (Antoni *et al.*, 1997) and the Madison Symmetric Torus (MST; Chapman, Almagri, *et al.*, 1998; Chapman, Chiang, *et al.*, 1998). In the MST, a shear flow occurs with a pulsed current drive technique and is generated spontaneously in other discharges labeled enhanced-confinement discharges. The contribution of flow shear to confinement enhancement in the pulsed current drive discharges has not been assessed precisely because the current flattening effect is also present. In enhanced-confinement plasmas there is no current drive and the confinement time increases by as much as a factor of 3 relative to a standard case with no flow shear and no current drive. Both temperature and particle confinement times increase. Like the H mode, the flow shear is confined to a narrow layer of approximately 1-cm width in the edge. The presence of flow shear is correlated temporally and spatially with a reduction in fluctuations. The enhanced-confinement phase is initiated with a sawtooth crash, after which fluctuations of the magnetic field and electrostatic potential decrease. The decrease occurs over a broad frequency range that includes the unstable global tearing modes. The spatial region of suppression extends throughout the edge, but suppression is

most pronounced in the region of flow shear. Some steepening of the temperature and density gradients in the edge is observed or inferred. These observations complement the studies of confinement changes in the reversed-field pinch with biasing (Craig *et al.*, 1997).

The observation of turbulence suppression with flow shear in the RFP raises issues that have not been confronted in tokamak research, including the effect of a narrow shear layer on global fluctuations and the generation of flow by a magnetic Reynolds stress of turbulence that is predominantly nonpropagating. Initial work on the effect of a narrow flow shear layer in the external region of a tearing mode indicates that localized external flow shear can suppress a global tearing mode, provided it is sufficiently strong (Hegna *et al.*, 1998). However, there is also electrostatic edge turbulence in the RFP, and its suppression may lower the edge resistivity, indirectly diminishing tearing-mode instability. The magnetic Reynolds stress is typically zero in the RFP, as expected for global tearing modes, but becomes very large in sawtooth events (Fiksel, 1998). The latter are precursors for the enhanced-confinement phase. Flow in the RFP is mostly toroidal, and, unlike the tokamak, there is no significant neoclassical viscosity. These properties suggest flow generation and transition processes that differ in crucial ways from those of other devices.

D. Linear magnetic configurations

Linear devices represent the greatest variation of geometry from that of the tokamak, where flow-shear-induced transport barriers were first observed. In linear devices, magnetic-field lines may terminate on material surfaces, e.g., the end plates of a cylindrical vacuum vessel, and plasma can be lost by axial motion.

The tandem mirror is a cylindrical device with an axial magnetic field whose strength increases toward the cylinder ends. Particles are trapped in the magnetic mirror thus formed, but only those with velocities along the field that are not sufficient to overcome the mirror barrier. End cells with electrostatic potentials inhibit the loss of particles that escape the magnetic mirror. The H mode has been achieved on a tandem mirror by biasing an annular limiter placed midway along the cylinder axis (Sakai, Yasaka, and Itatani, 1993). The transport barrier so formed arrests radial losses, but not axial losses. In the H mode, neutral emissions abruptly decrease, the bulk density and energy rise, fluctuations decrease, and gradients steepen in the region of $E \times B$ flow shear. The confinement time increases by a factor of 2.5. The voltage-current characteristic of the limiter exhibits a bifurcation like that of tokamak biasing experiments, with a sharp drop in current for a given voltage just above the bifurcation threshold. Also, as observed in other experiments, the reduction of transport begins with the flow shear created before the bifurcation, indicating that the transport reduction is intrinsic to the flow shear and not the bifurcation. The standard interpretation of the bifurcation in tokamaks involves the nonlinear dependence of the neoclassical viscosity on flow speed. Because the

neoclassical viscosity is intrinsic to toroidal geometry (Sec. IV. B), the mechanics of the bifurcation in mirrors remains to be understood.

Another linear device is the Z pinch. The Z pinch is cylindrical, but the magnetic field is azimuthal, created by the axial plasma current (Freidberg, 1982). The Z -pinch configuration represents a solution of the ideal MHD equilibrium model, either for a steady state or under implosion by the radial Lorentz force produced by a large axial current. The Z pinch is susceptible to a number of rapidly growing Alfvén-time-scale instabilities. Following up on experimental indications of improved performance in the presence of flow, Shumlak and Hartman (1995) found that a sheared axial flow stabilizes the $m=1$ kink mode, provided the equilibrium is stable to the $m=0$ mode and the flow shear strength dU_z/dr exceeds $0.1kV_A$. (U_z is the axial equilibrium flow and k and m are the axial and azimuthal mode numbers.) If the pressure profile does not satisfy the precondition for $m=0$ stability, stabilization of ideal MHD modes requires supersonic flows as large as Mach 4 (Arber and Howell, 1996a). It has also been argued that flow shear stabilizes the Rayleigh-Taylor instability in imploding Z -pinch plasmas (Shumlak and Roderick, 1998). Given the existence of certain numerical issues (Arber and Howell, 1996b; Shumlak and Hartman, 1996) and the indirect connection between infinitesimal-amplitude linear stability analyses and experimental conditions, further experimental work is needed to ascertain whether flow shear can provide the benefits for the Z pinch that exist with the tokamak.

VII. TRANSITION TO ENHANCED-CONFINEMENT STATES

A. Bifurcation of plasma state

Sections II and IV effectively treated as independent the suppression of turbulence by flow shear and the generation of flow shear by a variety of mechanisms, including turbulence. In reality, the two processes are coupled and must be treated self-consistently. For illustration, consider a closed set of equations, taken from prior sections, that describes some of the couplings:

$$\frac{\partial \xi}{\partial t} + u_E(x) \frac{\partial \xi}{\partial y} + \bar{u}_{xi} \frac{\partial \xi}{\partial x} + \bar{u}_{yi} \frac{\partial \xi}{\partial y} = \sigma_\xi, \quad (7.1)$$

$$u_E(x) = \frac{E_r}{B_\phi} = \frac{1}{B_\phi Z_i e n_i} \frac{\partial}{\partial x} p_i - \langle u_{yi} \rangle, \quad (7.2)$$

$$\frac{\partial \langle u_{yi} \rangle}{\partial t} = - \frac{\partial}{\partial x} \langle \bar{u}_{xi} \bar{u}_{yi} \rangle - \mu_\theta \langle u_{yi} \rangle, \quad (7.3)$$

$$\frac{\partial p_i}{\partial t} + \frac{\partial}{\partial x} Q_i = \hat{P}_i. \quad (7.4)$$

Equation (7.1) is the equation for turbulent fluctuations [Eq. (2.12)], and in this system includes both ion flow $\bar{\mathbf{u}}$ and ion pressure p_i . Each fluctuation has a source σ_ξ , and the shear flow $u_E(x)$ is a poloidal $E \times B$ flow with shear in the radial (x) direction. The $E \times B$ flow is deter-

mined by Eq. (7.2) [Eq. (4.1) divided by the magnetic field]. The magnetic field is taken as toroidal. For simplicity, there is no mean toroidal flow. The poloidal ion flow is governed by Eq. (7.3) [Eq. (4.4) without magnetic fluctuations]. The mean pressure p_i is governed by Eq. (7.4) [Eq. (2.34)], where the ion heat flux Q_i is the correlated product of fluctuations of the ion flow and pressure, $Q_i = \langle \bar{u}_{xi} \bar{p}_i \rangle$, and \hat{P}_i is the external input power density to the ions.

In systems of equations such as Eqs. (7.1)–(7.4), quantities feed back on themselves through the couplings. For example, (1) from Eqs. (7.2), (7.1), and (7.4), ∇p_i drives $u_E(x)$, $u_E(x)$ suppresses $\bar{\mathbf{u}}$ and \bar{p}_i , lower values of $\bar{\mathbf{u}}$ and \bar{p}_i reduce Q_i , reduced Q_i increases ∇p_i , which further drives $u_E(x)$; (2) when poloidal flow dominates the pressure force equation (7.2), $\langle \bar{u}_{xi} \bar{u}_{yi} \rangle$ drives $\langle u_{yi} \rangle$, which drives $u_E(x)$, and through Eq. (7.1), $u_E(x)$, determines the value of $\partial/\partial x \langle \bar{u}_{xi} \bar{u}_{yi} \rangle$. The feedbacks of Eqs. (7.1)–(7.4) are nonlinear and spatiotemporal and give rise to the striking phenomenon of dynamic transitions between different mean states of the system. These transitions are generally referred to as bifurcations because small changes in an externally controlled parameter lead to abrupt and large changes in the character of the plasma state.

Bifurcations have been observed in the external bias-driven H mode in tokamaks, stellarators, and mirrors, where the bifurcation is driven by increasing the bias voltage and is evident in both the I - V curve of the electrode and the plasma equilibrium. In a reversed-field pinch, biasing leads to improved confinement, but a bifurcation has not been observed. A bifurcation occurs in the spontaneous H mode, in the spontaneous enhanced-confinement mode of the RFP, in the internal transport barrier, and in the core barrier in JT-60U. These bifurcations are induced by increasing the input heating power. From the above statement it is evident that bifurcated states entail fluctuation suppression, but suppression is not always accompanied by bifurcation. Backward transitions can also be induced by reversing the direction of changes in the external parameter that controls the transition. Hysteresis is generally evident, i.e., the threshold values of the control parameter are different for forward and backward transitions.

This section describes aspects of the phenomenology and modeling of transitions in order to illustrate the rich nonlinear dynamics that underlie transport barriers in fusion plasmas. The current state of transition modeling is primitive and heuristic. At present, no transition theory captures every relevant detail of experimental transitions, making it difficult to assess their validity. Nevertheless, a variety of transition models have been disproved by experiment, or their dominant processes found to be of marginal importance. Other models, including some discussed here, have known shortcomings, but may include physics of importance in the actual transition.

B. Transition modeling

Analytic transition models can be separated into two-step and single-step models. In two-step models, flow is

first driven through a bifurcation that relies on the nonlinear variation of the neoclassical poloidal flow damping with flow speed. In the second step there is suppression of turbulence, profile steepening, and increased confinement. These result from the increased flow speed that accompanies the bifurcation, but do not contribute causally to the bifurcation. In single-step models, flow generation and turbulence suppression evolve as integral parts of the transition and cannot be separated. Nonlinear poloidal flow damping is not required. Single-step transitions are divided into first- and second-order critical transitions. Transitions have recently been reported in the direct numerical simulation of edge fluid models (Rogers, Drake, and Zeiler, 1998). It has not been ascertained how these results compare with theoretical models.

1. Two-step transition models

When a radial electric field and $E \times B$ flow are externally driven, as in biased electrode experiments, the transition is intrinsically a two-step process (Cornelis *et al.*, 1994). A two-step scenario has also been proposed for the H -mode and internal barrier transitions, invoking a plasma drive mechanism for flow shear generation (Shaing and Crume, 1989; Shaing *et al.*, 1998). Because these models rely on nonlinear poloidal flow damping for bifurcation, they apply only to situations in which the dissipation is dominated by poloidal flow dynamics.

The transition observed in biased electrode experiments was modeled with the ion momentum and electric-field equations [Eqs. (4.3) and (4.1)] using experimental data to supply equilibrium quantities, such as the pressure gradient, at any desired time during the transition (Cornelis *et al.*, 1994). These two equations combine to yield a radial Ohm's law with an effective radial conductivity that depends on neoclassical flow damping. The Ohm's law is obtained by first noting that an equilibrium plasma current flows in the radial direction in response to a current injected into the plasma from the electrode. The plasma current enters the ion momentum balance [Eq. (4.3)] through the $J \times B$ force. The other contributors to the balance are the neoclassical viscous damping and ion-neutral friction, yielding

$$\frac{1}{n_i} (J_r \hat{\mathbf{r}} \times \mathbf{B}) = \frac{\nabla \cdot \tilde{\Pi}}{n_i} + m_i v_{i0} \mathbf{u}_i. \quad (7.5)$$

where $n_i^{-1} \nabla \cdot \tilde{\Pi}$ can be cast as the neoclassical viscous force $m_i \mu_\theta u_{\theta i}$ and v_{i0} is the ion-neutral damping rate. This equation can be solved for \mathbf{u}_i and substituted into the equation for the radial electric field [Eq. (4.1)] to yield Ohm's law. The conductivity is equal to a linear combination of the neoclassical flow-damping rate and the ion-neutral collision rate. As noted in Sec. IV. B. 2, the neoclassical flow-damping rate μ_θ has a maximum value at $u_\theta = u_{Ti} B_\theta / B_\phi$ (see the dotted curve in Fig. 1 of Shaing and Crume, 1989). Above this critical flow, which corresponds to the critical electrode current and bias voltage, the neoclassical viscosity drops, leading to a larger flow and smaller electrode current. Cornelis *et al.*

(1994) compare measured and predicted radial electric-field profiles, using a variety of theoretical models for the neoclassical viscosity. All agree qualitatively with the experimental data, but there are distinct quantitative differences.

The two-step model for a spontaneous H -mode transition invokes ion-orbit loss to drive a radial electric field within a banana orbit of the separatrix (Sec. IV. B.4). Through orbit squeezing, the width of the banana orbit depends on the $E \times B$ flow shear, becoming smaller as the shear increases. If, through a similarity relation, the flow shear is proportional to the flow, the torque supplied by orbit loss is maximum for zero flow and falls to zero at higher flow speeds due to the squeezing effect. The torque goes as $v_{*i} (v_{*i} + \alpha^4 u_{pm}^4)^{-1/2} \exp[-(v_{*i} + \alpha^4 u_{pm}^4)^{1/2}]$, where v_{*i} is the rate at which ions are collisionally scattered across the separatrix from a trapped orbit to an untrapped orbit, α is the form factor that relates the flow shear to the flow speed (Shaing and Crume, 1989), and $u_{pm} = (u_{Ti} B_\theta)^{-1} [u_\theta B_\phi - (Z_i e n_i)^{-1} \nabla p_i]$ is the poloidal flow, normalized and adjusted by the pressure contribution in the radial momentum balance equation. The collision rate v_{*i} is normalized to the bounce rate, or inverse time for an ion to move between the turning points in the magnetic mirror. For an ion to be trapped in the mirror field, and therefore have a banana orbit, v_{*i} must be less than unity, i.e., the ion must not scatter from its trapped orbit before reaching a turning point. The neoclassical viscous force is linear at small flow velocities, where it behaves like a standard viscous drag. Above $u_E = u_{Ti} B_\theta / B_\phi \approx 1$, it turns over and falls to zero. The viscosity also has an overall proportionality to the collision rate v_{*i} , because the drag involves collisional friction between untrapped and trapped ions.

The steady-state $E \times B$ flow is determined from the balance of the applied torque and the viscous force. When the collision rate v_{*i} is large, the torque and the drag balance at a small flow speed, in the parameter region where the viscous force is linear in flow speed. This balance corresponds to the L mode. As the collision rate decreases, three solutions become possible. One continues the branch with small flow speed and two occur for a larger flow speed, in the parameter region where the viscous force becomes weaker with increasing flow speed. The branch with the largest flow speed is stable (as is the L -mode branch) and represents the H mode. At still weaker collision rates, the H -mode branch is the only solution yielding a steady flow. The appearance of the H -mode branch allows for a bifurcation of the equilibrium to a state with large flow shear.

In this transition model, the transport barrier is formed within approximately one poloidal gyroradius (ion banana width) [Eq. (4.6)] of the separatrix or limiter. The width of the barrier region is squeezed by $E \times B$ flow, so the poloidal gyroradius is an upper limit. For electric-field generation, v_{*i} must be less than unity, and the poloidal Mach number should change from less than one to greater than one as the plasma goes from L mode to H mode. Experimental data on the H -mode

transition have been examined for evidence of these features. While the model reproduces qualitative features of the H mode, there are serious quantitative discrepancies related to these theoretical constraints. Measurement of u_{pm} before and after the transition shows that it passes through the critical value of unity, consistent with theory (Burrell *et al.*, 1992). However, the barrier width does not change under variation of the poloidal field and can be as large as six times the poloidal gyroradius. The normalized collision rate v_{*i} is more than an order of magnitude larger than unity in JFT-2M (Ida *et al.*, 1990) and can vary from 1 to 14 in DIII-D (Carlstrom and Groebner, 1996).

A two-step transition theory has also been proposed for the transition to the internal transport barrier in TFTR (Shaing *et al.*, 1998). The ion-electron flux difference created by the large toroidal ripple of TFTR (Sec. IV.C) is invoked to create a radial electric field in the core. Although the plasma rotation is principally toroidal, the dominant dissipation process is the damping of poloidal flow. Like two-step edge bifurcation models, the nonlinear variation with flow of the neoclassical poloidal viscosity produces the bifurcation. The internal transport barrier transition in TFTR produces a rapid poloidal spinup with a subsequent return to pretransition rotation rates on a slightly longer time scale (Bell *et al.*, 1998). (As the flow relaxes, the pressure gradient, steepened by suppression of the heat flux, takes over as the driving mechanism for the radial field.) Because two-step transitions are governed by the nonlinearity of the poloidal flow damping, the decay of the flow transient is predicted to occur over a collisional relaxation time, which is much longer than that observed in TFTR.

2. First-order critical transition theory

In first- and second-order critical transition models, the suppression of turbulence by $E \times B$ flow shear is an integral part of the transition dynamics. In analogy with the Landau theory of phase transitions (Landau and Lifshitz, 1980), the flow shear is the order parameter. In the simplest first-order model (Hinton, 1991), equilibrium balances from Eqs. (4.1) and (4.3) are combined with a model for the heat flux that incorporates shear suppression heuristically. The radial electric field is governed by Eq. (4.1) with the poloidal flow term dominating the right-hand side, $E_r = -u_\theta B_\phi$. The poloidal flow is governed by Eq. (4.3) from a balance of terms that make up the anisotropic pressure force $(n_i)^{-1} \nabla \cdot \vec{\Pi}$. Using the standard neoclassical evaluation of $\nabla \cdot \vec{\Pi}$ (Hinton and Hazeltine, 1976), we find that the flow is proportional to the ion temperature gradient, $u_\theta = -(eB)^{-1} \mu \partial T / \partial r$, where the dimensionless constant of proportionality μ is given by $\mu = 1.7 + \mu_1 (v_{*i})^{-2}$ and μ_1 is a constant less than unity. This model does not invoke nonlinear variation of the flow damping above the poloidal sound speed. The radial shear in u_θ , which directly relates to the $E \times B$ flow shear, is given by

$$\frac{\partial u_\theta}{\partial r} = - \frac{4\mu_1}{eB(v_{*i})^2 T} \left(\frac{\partial T}{\partial r} \right)^2, \quad (7.6)$$

where the additional temperature-gradient factor arises from the dependence of v_{*i} on the temperature, and the second derivative of T is assumed to be smaller than the radial variation of v_{*i} that enters through the temperature gradient.

The local heat flux [Eq. (2.9)] is modeled by the expression

$$Q = Q_n + \frac{Q_f}{1 + \gamma_f (\partial u_\theta / \partial r)^2}, \quad (7.7)$$

where Q_n is the neoclassical (collisional) heat flux, Q_f is the fluctuation-induced heat flux in the absence of flow shear effects, and the denominator is a model representation of shear suppression with γ_f a constant. For illustration, assume a Fick's law variation for the fluxes Q_n and Q_f , making both linear functions of the temperature gradient. The fluctuation-induced heat flux dominates the collisional heat flux when there is no shear flow, so the linear rise of Q_f with the temperature gradient is steeper than that of Q_n . The shear suppression factor introduces additional dependence on the temperature gradient through Eq. (7.6), yielding

$$Q = Q_n + \frac{Q_f}{1 + \lambda_f (\partial T / \partial r)^4}, \quad (7.8)$$

where $\lambda_f = \gamma_f (4\mu_1 / eBT)^2 (v_{*i})^{-4}$. For reasonable values of the parameters λ_f and Q_n / Q_f , the net variation of the total local heat flux is as follows. For $\partial u_\theta / \partial r < \lambda_f^{-1/4}$, the local heat flux is dominated by the fluctuation-induced flux with negligible shear suppression, $Q \cong Q_f$. For gradients just larger than $\lambda_f^{-1/4}$, the total local heat flux decreases with increasing gradient as a result of shear suppression. At still larger gradients the suppression of the fluctuation-induced flux is so strong that the local heat flux goes as the collisional flux, $Q \cong Q_n$. This behavior is shown in Fig. 13.

The transition is manifested as a discontinuity of the temperature gradient. The discontinuity appears when the temperature gradient is determined by equating the local heat flux [Eq. (7.8)] to the heat flux at the boundary of the local region under consideration. When the auxiliary heating power is low, the boundary flux is low. Equating Eq. (7.8) with a small boundary flux yields a temperature gradient from the linear part of Eq. (7.8) where $Q \cong Q_f$. The boundary flux has a critical value when it is equal to the local heat flux at its maximum, where flow shear begins to suppress the fluctuation-induced heat flux. For a boundary flux slightly above the critical value, the intersection shifts discontinuously to the part of Eq. (7.8) where $Q \cong Q_n$, and the gradient is much larger than g_1 . The flow shear also changes discontinuously as the boundary heat flux passes through the critical value. The temperature profile is determined by equating Q with the boundary heat flux at each point and integrating from the edge inward. If the boundary flux at the edge is above the critical value, the boundary flux deeper in the plasma falls below the critical value,

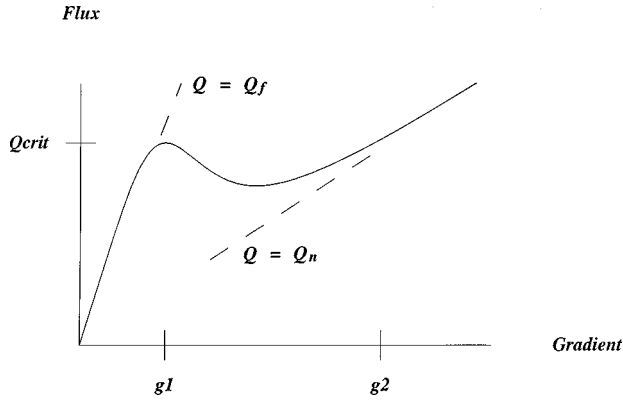


FIG. 13. Local heat flux as a function of the temperature gradient in a model for first-order critical transitions. For small values of the gradient the flux is dominated by turbulence ($Q = Q_f$). For larger gradients, flow shear suppresses turbulent heat transport and approaches the collisional heat flux Q_n asymptotically. The temperature gradient is determined by equating the local flux [Eq. (7.8)] with a boundary flux at the edge of the local region. When the boundary flux just exceeds Q_{crit} , the gradient shifts from g_1 to a value near g_2 . Adapted from Hinton, 1991.

and the gradients inside that point correspond to the part of the local flux curve where $Q \cong Q_f$ and $\partial T/\partial r < g_1$. A steep temperature gradient and strong flow shear thus form in an edge region, as in the H mode.

This transition is analogous to the first-order critical transition occurring, for example, between the liquid and gas phases of a fluid (Landau and Lifshitz, 1980). The order parameter can be chosen to be either the temperature gradient or the flow shear. The temperature parameter of the Landau phase transition is replaced by the boundary heat flux. As the boundary flux passes through the critical value, the order parameter jumps discontinuously. Figure 14 gives a schematic representation of this behavior. The jump in flow shear is analogous to the presence of latent heat in the liquid/gas phase transition. Characteristic of first-order phase transitions, there is hysteresis (Hinton, 1991). When the boundary heat flux is reduced from a large value through the critical point (H - L transition), the stable equilibrium on the $Q \cong Q_n$ part of Eq. (7.7) remains stable down to the minimum of Q . For lower values, the gradient shifts discontinuously to smaller values where $Q \cong Q_f$. The critical flux for the back transition is thus lower than the critical flux for the forward transition.

An extension of the Hinton (1991) model incorporates both the particle and heat flux, yielding profiles for both density and temperature (Hinton and Staebler, 1993). Time-dependent effects associated with inward motion of the critical point in the L - H and VH transitions have also been modeled (Staebler *et al.*, 1994). A first-order transition model has been developed for the internal transport barrier transition (Diamond *et al.*, 1997). The local heat flux is replaced by an equation for the fluctuation energy. (These models do not account for the cross-phase effects of Sec. V.C, so the heat flux is simply proportional to the fluctuation energy.) The local

fluctuation strength in the absence of flow shear has a spatial variation to account for the stabilizing effect of magnetic shear. The shear suppression factor is equivalent to that of Eq. (7.7). The poloidal flow is governed by the balance of pressure force and flow damping as in Hinton (1991), but the density profile is evolved instead of the temperature profile. This leads to an equation like Eq. (7.6), with $\partial n/\partial r$ replacing $\partial T/\partial r$. The transition begins in the core where the fluctuation energy is minimum because of magnetic-shear stabilization and works its way outward until it stops at a position where the flow damping lowers the flow shear below the suppression threshold.

3. Second-order critical transition theory

A second-order critical transition is possible when the Reynolds stress is larger than the ion pressure term in the ion momentum balance (Diamond *et al.*, 1994). The Reynolds stress drives a sheared poloidal flow against the dissipation of neoclassical flow damping. The sheared poloidal flow produces $E \times B$ flow shear, which reduces fluctuations. The magnitude of the Reynolds stress depends on both the fluctuation energy and the flow shear. Two basic equilibrium states are possible under this coupling. There is a state in which the Reynolds stress is too weak to overcome the flow damping. Any perturbation of the flow decays to zero. The fluctuation energy is large because there is no flow shear. In the other state, the Reynolds stress is sufficient to drive a steady flow, whose shear suppresses turbulence. A transition to the second state represents a diversion of free energy from fluctuations into the mean flow, through the Reynolds stress.

A dynamical model for the second-order transition is derived from the poloidal momentum equation, Eq. (4.4), and an equation for the turbulent energy evolution. The latter is constructed from an appropriate turbulent amplitude equation by multiplying by the amplitude and taking an average over a suitable statistical ensemble. Equation (7.1) is a generic amplitude equation and Eq. (5.10) is a specific example for drift-wave turbulence. A statistical closure is applied so that the nonlinearity is proportional to the square of the turbulent energy. This process is detailed for Eq. (5.10) in Carreras *et al.* (1992). The form of the energy equation is

$$\frac{1}{2} \frac{\partial E}{\partial t} = \gamma_0 E - \alpha_1 E^2 - \alpha_2 U E, \quad (7.9)$$

where E is the fluctuation energy of the linearly unstable, energy-containing modes, and U is the square of a uniform mean flow shear strength in the region of the unstable modes. The first term on the right-hand side is the linear instability term, describing injection of energy at the rate γ_0 . The second term represents spectral transfer of energy away from the unstable modes into damped modes at the rate $\alpha_1 E$. In a steady state without flow shear, the turbulent energy is fixed by the balance of the injection rate with the spectral transfer rate,

yielding $E = \gamma_0 / \alpha_1$. The third term describes shear suppression, lowering the steady-state turbulent energy when U is nonzero. Specific forms for γ_0 , α_1 , and α_2 are given in Diamond *et al.* (1994) for a variety of turbulence models.

An equation for U is obtained by taking a radial derivative of the poloidal ion momentum balance and multiplying by the radial derivative of the mean poloidal flow. This equation must also be closed in order to express the Reynolds stress as a function of U and E . The equation for U is

$$\frac{1}{2} \frac{\partial U}{\partial t} = -\mu U + \alpha_3 U E, \quad (7.10)$$

where μ is the poloidal flow-damping rate and α_3 is a constant. The first term on the right-hand side is the neoclassical flow-damping rate, modeled in the linear regime below the poloidal sound speed, and the second term is the closure of the Reynolds stress. The definition of the Reynolds stress [Eq. (2.11)] directly leads to linear scaling with fluctuation energy. The linear dependence on U reflects the fact that the asymmetry required for a nonzero Reynolds stress can be induced by the flow shear (as it shears and tilts fluctuations). For example, consider the Reynolds stress of the linear eigenmode of the drift-wave equation (5.10). The eigenmode is (Carreras *et al.*, 1992)

$$\begin{aligned} \phi_k = \phi_0 \exp\left(\frac{1+i}{\sqrt{2}} \frac{\xi_k^2}{W_k^2}\right) \exp\left[\frac{-1}{2\sqrt{2}W_k^2}(x-\xi_k)^2\right] \\ \times \exp\left[\frac{-i}{2\sqrt{2}W_k^2}(x+\xi_k)^2\right], \end{aligned} \quad (7.11)$$

where W_k is the mode width Δ evaluated at the oscillation frequency $\omega = k_y U(0) + k_y U_D$, and $\xi_k = \Delta^3 S / 2\rho_s^2$ is proportional to the flow shear. The other parameters were defined in Sec. V.A.2. When the flow shear is zero, $\xi_k = 0$, and the radially symmetric Gaussian gives a zero Reynolds stress. The asymmetry induced by ξ_k leads to a nonzero Reynolds stress, whose radial derivative is (Terry *et al.*, 1994)

$$\begin{aligned} \frac{\partial}{\partial x} \langle \bar{u}_x \bar{u}_y \rangle = C_s^2 \rho_s^2 \frac{\partial}{\partial x} \sum_{k_y} \left\langle -ik_y \phi_{-k} \frac{\partial \phi_k}{\partial x} \right\rangle \\ = C_s^2 \rho_s^2 \sum_{k_y} k_y \xi_k \Delta^{-3} |\phi_0|^2, \end{aligned} \quad (7.12)$$

where ϕ_k and ϕ_0 are dimensionless potentials under the normalization by $T_e / |e|$ introduced with Eq. (5.10). The factor ξ_k leads to the linear scaling with respect to U of the third term of Eq. (7.10). Equation (7.12) is a manifestation of the radial symmetry breaking required for a nonzero Reynolds stress, as discussed in Sec. IV.B.1.

Equations (7.9) and (7.10) have fixed points given by (1) $E = \gamma_0 / \alpha_1$, $U = 0$ and (2) $E = \mu / \alpha_3$, $U = (\gamma_0 - \alpha_1 \mu / \alpha_3) / \alpha_2$. The first fixed point corresponds to an L -mode state with no flow shear and a fluctuation energy given by the balance of linear growth rate and spec-

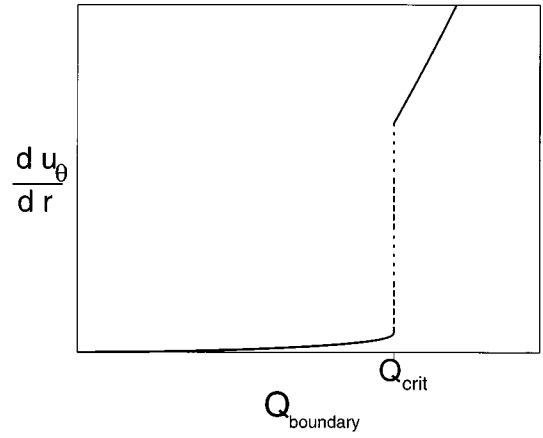


FIG. 14. First-order critical transition with dU_θ/dr as the critical parameter and Q_{boundary} as the effective temperature in the Landau theory. The order parameter is discontinuous at Q_{crit} .

tral transfer rate. It is stable when $\gamma_0 < \alpha_1 \mu / \alpha_3$. The second fixed point has finite flow shear and a suppressed fluctuation energy and thus corresponds to the H mode. It is stable for $\gamma_0 > \alpha_1 \mu / \alpha_3$. The control parameter can be taken as the linear growth rate γ_0 , which increases when auxiliary heating is applied and gradients are steepened by the deposited power. (It could also be taken as the damping rate μ , which decreases when auxiliary heating is applied and the edge temperature is increased.) When the control parameter γ_0 increases, the L -mode fixed point becomes unstable and the system transits to the stable H -mode fixed point. The flow shear increases from zero to its H -mode value as the fluctuation energy drops from its L -mode value to the reduced H -mode value.

The flow shear is continuous across the transition, as can be seen by evaluating the H -mode flow $U = (\gamma_0 - \alpha_1 \mu / \alpha_3) / \alpha_2$ at the transition threshold $\gamma_0 = \alpha_1 \mu / \alpha_3$. The derivative of U with respect to γ_0 is discontinuous. This behavior is analogous to second-order critical transitions in the Landau theory. The order parameter can be chosen to be $U^{1/2} \approx du_\theta/dr$. The growth rate is the effective temperature parameter. The transition, illustrated in Fig. 15, can be directly compared to the first-order transition of Fig. 14, as both have the same order parameter, and the temperature parameters are directly related through the dependence of the turbulent heat flux on the instability drive γ_0 . As a second-order transition, there is no hysteresis in the transition threshold. However, the rate at which the system transits from one fixed point to the other is different in the forward and backward transitions (see Fig. 2 of Diamond *et al.*, 1994).

Second-order transition dynamics have been invoked to explain the transient poloidal spinup in the internal transport barrier transition (Newman *et al.*, 1999). The Reynolds stress generates a flow that initiates shear suppression and the steepening of the pressure gradient. As the pressure gradient increases, it becomes the primary driver of the radial electric field and the flow relaxes to its pretransition state. Both the spinup and relaxation

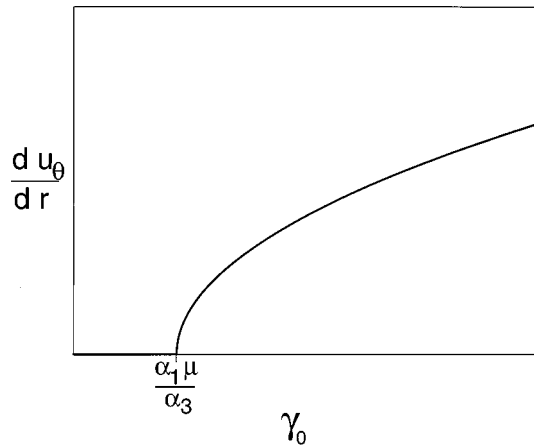


FIG. 15. Second-order phase transition associated with shear generated by the Reynolds stress. There is no discontinuity of the order parameter $dU_\theta/dr \approx U^{1/2}$, but its slope is discontinuous at the critical value of the effective temperature parameter.

are driven by the Reynolds stress and occur on similar time scales, as observed in experiment. A transient spike in the poloidal flow also occurs in models that include stabilizing flow curvature as the dominant agent for turbulence suppression (see Fig. 2 in Terry *et al.*, 1994). Both cases illustrate a reciprocity principle intrinsic to Reynolds stress-driven transitions. Whenever there is sufficient shear to suppress fluctuations, the Reynolds stress as modified by the shear is of sufficient magnitude to modify the flow shear. Even in first-order transitions, this holds for a few turbulent correlation times before reduced fluxes have steepened the pressure gradient to the point where it can dominate the radial force balance. Thus second-order transition dynamics are likely to apply on short time scales, with first-order transition dynamics entering on longer time scales of the pressure evolution. Second-order transition dynamics also play a role in bifurcation models based on Galerkin projections for quasicohherent nonlinear evolution close to a stability threshold (Beyer and Spatschek, 1996), complementing treatments that assume fully developed turbulence. Second-order transitions have elements in common with temporally and spatially evolving Reynolds stress-driven atmospheric flows such as the quasibiennial oscillation (Holton and Lindzen, 1972; Plumb, 1977).

C. Transient phenomena

Fluctuation activity does not cease after transition. In addition to residual small-scale turbulence, the H mode has a class of fluctuations known as edge-localized modes (ELM's). There are several types of ELM's distinguished by gross features, including amplitude, frequency, and temporal characteristics relating to intermittent behavior. Large-amplitude ELM's can eject a fraction of the particles and heat stored in the plasma edge region without terminating the plasma discharge. They thus provide some control of edge gradients. In the future they may be useful in removing helium ash from a

burning plasma. Under some circumstances ELM's behave as a transient return to L mode. This has led to modeling studies of ELM's based on limit-cycle solutions of transition models like the ones presented in this section. It is also possible that ELM's are a global instability driven by the steep gradients caused by transport reduction. While ELM's are an important issue in the use of transport barriers in fusion plasmas, they are beyond the scope of this review. A discussion of ELM's can be found in Itoh and Itoh (1996).

VIII. GENERALIZATION TO RELATED SYSTEMS

Previous sections have presented extensive experimental, analytical, and computational work describing the suppression of turbulence and transport by $E \times B$ flow shear in fusion plasmas. As is apparent from the generality of Sec. II, shear suppression is a universal feature of advection of turbulence by stable, sheared mean flow. In this section generalizations and applications to nonplasma systems are considered. As in fusion plasmas, turbulence in these systems is approximately 2D, and the generalization carries over directly. The effect of stable flow shear on turbulent decorrelation in fully 3D systems remains to be investigated.

A. Coherent vortices in navier-stokes turbulence

Suppression of turbulent vorticity transport by flow shear leads to spatial intermittency in decaying 2D Navier-Stokes turbulence (Terry, 1989; Terry, Newman, and Mattor, 1992). Intermittency manifests itself as the emergence of coherent vortices in simulations that initialize homogeneous turbulence from a Gaussian random distribution of vorticity with no mean flow (McWilliams, 1984). As the turbulence decays under a hyperviscous damping, certain eddies emerge as coherent vortices, avoiding mixing by ambient fluctuations and persisting for a large number of eddy turnover times. The vortices are patches of intense localized vorticity characterized by a particular variation within the vortex of a quantity called the Gaussian curvature. The Gaussian curvature is the difference of the mean squared shear stress, $(\partial V/\partial x - \partial U/\partial y)^2 + (\partial U/\partial x + \partial V/\partial y)^2$, and the mean squared vorticity. (Here U and V are the total flow velocities in the x and y directions.) The Gaussian curvature is strongly positive in the vortex core and strongly negative in the edge. Contours of Gaussian curvature for a coherent vortex are shown in Fig. 16. Because the coherent vortices avoid transferring their vorticity into the turbulent cascade, they persist long after ambient turbulence has been viscously dissipated through its cascade to the Kolmogorov scale (Sec. II.A.1). A central question in the physics of intermittency is what physical process or processes permit a coherent vortex to avoid the turbulent mixing that causes eddies to decay in an eddy turnover time. One such process is shear suppression of turbulence. Localized vorticity fluctuations have a flow profile in which flow shear is largest at their edges. Those whose initial vorticity is

sufficiently more intense than ambient fluctuations have an edge flow shear that satisfies Eq. (2.17), and ambient turbulence and its transport of vorticity are suppressed. Those whose initial vorticity is comparable to that of ambient turbulence cannot suppress ambient turbulence. They participate in the cascade of energy to the Kolmogorov scale and decay in an eddy turnover time.

The interaction of an intense symmetric vortex with the ambient turbulence can be described by a two-time scale analysis of the Navier-Stokes equation. The origin of a polar coordinate system is placed at the center of the vortex. With a Fourier-Laplace transform of the turbulent vorticity $\xi(r, \theta, t)$,

$$\xi_{n,\gamma} = \int_0^\infty dt \exp(-\gamma t) \int_0^{2\pi} d\vartheta \exp(in\vartheta) \xi(r, \vartheta, t). \quad (8.1)$$

the $n=0$ component is the symmetric vortex and $n \geq 1$ is the turbulence. Turbulent vorticity fluctuations will be referred to as eddies. The $n=0$ component evolves on a slow time scale under the action of turbulent mixing. On a rapid time scale the vortex can be treated as stationary. The evolution of the turbulence is identical to that of Sec. II.B.3 and is given by Eq. (2.29),

$$\begin{aligned} [\gamma_n - i(r-r_0)n(\bar{u}/r)_r] \xi_{n,\gamma} - \frac{1}{r} \frac{\partial}{\partial r} \left(r D_n \frac{\partial \xi_{n,\gamma}}{\partial r} \right) \\ + \frac{n^2}{r^2} D_n \xi_{n,\gamma} = \frac{-in}{r} \phi_{n,\gamma} \frac{\partial \Xi}{\partial r}, \end{aligned} \quad (8.2)$$

where the terms on the left-hand side are defined after Eq. (2.29), the source is the turbulent advection of the vortex vorticity Ξ , and ϕ is the turbulent stream function, related to the turbulent vorticity in the usual way with $\nabla^2 \phi \rightarrow r^{-1} \partial / \partial r (r \partial \phi_{n,\gamma} / \partial r) - n^2 r^{-2} \phi_{n,\gamma} = \xi_{n,\gamma}$. The vortex flow has been Taylor expanded about a point r_0 in the region near its edge where shear is strongest. Only the linear variation is retained. The turbulent velocity is $\mathbf{u} = -\nabla \phi \times \mathbf{z}$, where \mathbf{z} is the unit vector perpendicular to the plane of variation. The slow-scale vortex evolution equation is

$$\frac{\partial \Xi}{\partial t} + \frac{1}{r} \frac{\partial}{\partial r} \left[r \int_{-i\infty+\gamma_0}^{i\infty+\gamma_0} d\gamma' \sum_n \left(\frac{-in}{r} \phi_{-n,-\gamma'} \xi_{n,\gamma'} \right) \right] = 0, \quad (8.3)$$

where the integral is the inverse Laplace transform of the turbulent vorticity flux, and the overbar on Ξ indicates an average over the rapid time scale.

Equation (8.2) is solved by inverting the operator of the left-hand side using a Green's function,

$$\xi_{n,\gamma}(r) = \int dr' G_n(r|r') \frac{-in}{r'} \phi_{n,\gamma} \frac{\partial \Xi}{\partial r'} = 0, \quad (8.4)$$

where $G_n(r|r')$ is the solution of

$$\begin{aligned} D_n \frac{1}{r} \frac{\partial}{\partial r} \left(r \frac{\partial G_n}{\partial r} \right) - \gamma_n G_n + i\Omega'_n(r-r') G_n \\ - \frac{n^2}{r^2} D_n G_n = \delta(r-r'), \end{aligned} \quad (8.5)$$

and $\Omega'_n = n(\bar{u}/r)_r = n \partial(\bar{u}/r) / \partial r|_{r_0}$ is the shear strain rate. When Eq. (8.4) is substituted into Eq. (8.3), an equation is obtained that describes the mixing of the vortex vorticity by the turbulence through an effective eddy viscosity D_v :

$$\frac{\partial \Xi}{\partial t} - \frac{1}{r} \frac{\partial}{\partial r} \left(r D_v \frac{\partial \Xi}{\partial r} \right) = 0, \quad (8.6)$$

$$\begin{aligned} D_v = - \int_{-\infty+\gamma_0}^{i\infty+\gamma_0} d\gamma' \int dr' \sum_n \left(\frac{n^2}{rr'} \right) G_n(r|r') \\ \times \langle \phi_{-n,-\gamma'}(r) \phi_{n,\gamma'}(r') \rangle. \end{aligned} \quad (8.7)$$

Note that D_v is an integral operator and quantities to its right are understood to have $r \rightarrow r'$. From Eq. (8.7) the rate at which the vortex vorticity is mixed depends on the turbulence level $|\phi_{n,\gamma'}|^2$. The Green's function also depends on the turbulent amplitude through the turbulent diffusivity D_n , and on the shear straining of turbulence by the shear of the vortex flow through Ω'_n .

When the vortex flow has weak shear, the Green's function is dominated by the turbulent diffusivity and $G_n \sim D_n^{-1}$. This combines with the $|\phi|^2$ factor to make the vortex mixing rate go as the eddy turnover time ($\partial^2 D_v / \partial r^2 \sim nu/r \sim n^2 r^{-2} \phi$). In this case the vortex is indistinguishable from a turbulent eddy and it decays, like all eddies, on the eddy turnover time scale. When the vortex flow has strong shear, the Green's function is determined by the balance of the large shear strain rate $\Omega'_n(r-r')$ and the turbulent diffusivity. As described in Sec. II.B, this balance is achieved by a reduction of the radial scale, yielding $\tau_s = \tau_N$ [Eq. (2.16)] in the region of flow shear. The Green's function is thus proportional to τ_s , i.e., $G_n \propto \Omega'_n{}^{-1}$, giving a reduction in the magnitude of D_v . Consequently the vortex survives for many eddy turnover times. Moreover, the radial scale of ambient turbulence is reduced [Eq. (2.15)]. This means that diffusion of turbulence at the vortex periphery into the vortex is confined to a narrow layer whose width is given by Eq. (2.32). These features are reflected in the solution of D_v , obtained from asymptotic boundary layer analysis in the limit of strong shear, or $\varepsilon_s^{-1} = a^3 \Omega'_n / D_n \gg 1$, where a is the radius of the vortex. The effective viscosity D_v is given by

$$\begin{aligned} D_v \sim \int d\gamma \sum_n \left(\frac{-in^2 |\phi_{n,\gamma}|^2}{r^2} \right) \frac{S \Omega'_n{}^{-1}}{(r-r_0)^{1/4} (a-r_0)^{3/4}} \\ \times \exp \left[\frac{2}{3} \left(\frac{-i\Omega'_n}{D_n} \right)^{1/2} (r-r_0)^{3/2} \right], \end{aligned} \quad (8.8)$$

$(\varepsilon_s^{-1} \gg 1),$

where S is a weakly varying structure function of order unity. Due to phase mixing in summing the exponential of a complex argument, the effective viscosity is dominated by $n=1$. Moreover, the real part of the argument of the exponential makes D_v different from zero only within a narrow exponential layer of thickness $(D_n/\Omega'_n)^{1/3}$ at the vortex edge. Stronger vortices (rela-

tive to ambient fluctuations) have a larger value of ε_s^{-1} and therefore a smaller effective viscosity. For turbulence to mix the vortex, it must diffuse into the vortex, extending the edge layer inward. This process is greatly slowed by the weakness of the viscosity and its localization within a narrow layer.

The condition $\varepsilon_s = D_n/a^3 \Omega_n' < 1$ is dimensionally equivalent to the condition that the vortex vorticity exceed the rms turbulent vorticity,

$$\frac{\Xi_0}{\langle \xi^2 \rangle^{1/2}} > 1, \quad (8.9)$$

where the rms average is computed for an ensemble of fluctuations in the vicinity of the vortex and Ξ_0 is the vortex vorticity at $r=0$. Equation (8.9) indicates that a vorticity fluctuation becomes coherent if it lies in the tail of the vorticity probability distribution function. For decaying turbulence, fluctuations initially in the core of the probability distribution function, distinguished by $\Xi_0/\langle \xi^2 \rangle^{1/2} < 1$, decay as part of the Kolmogorov cascade. Fluctuations in the tail ($\Xi_0/\langle \xi^2 \rangle^{1/2} > 1$) decay at a far slower rate, causing the tail probability to become enhanced with time. A Kolmogorov cascade with no coherent vortices implies a Gaussian probability distribution function. Thus an initial Gaussian distribution function will evolve so that its core remains Gaussian while its tail develops an enhanced non-Gaussian feature. This type of evolution is observed in intermittent turbulence. (Interactions between two coherent vortices, which also affect the probability distribution function, have not been treated.)

The observed Gaussian curvature profile in the region of a coherent vortex directly indicates that the shear suppression criterion $\varepsilon_s < 1$ is satisfied. The Gaussian curvature of the vortex flow is $C_v = r^2 n^{-2} \Omega_n'^2 - \Xi^2$, while the total Gaussian curvature is

$$C_T = \frac{r^2 \Omega_n'^2}{n^2} - (\Xi^2 + \langle \xi^2 \rangle). \quad (8.10)$$

The turbulent vorticity is included in Eq. (8.10) to account for the total squared vorticity. It is of importance near $r=a$, where the vortex vorticity is zero. (The vanishing of vorticity at the vortex radius is implicit in the stipulation that the vortex be localized.) The turbulent shear stress is not included in Eq. (8.10) because it is dominated by the vortex shear stress in the edge, and fluctuations are small near the center. The observed negative Gaussian curvature near the centers of the coherent vortices (McWilliams, 1984) reflects the fact that $r^2 \Omega_n'^2 n^{-2}$ vanishes there. At the edge, Ξ^2 vanishes and positive Gaussian curvature implies that $a^2 \Omega_n'^2 n^2 > \langle \xi^2 \rangle \approx D_n^2 a^{-4}$, reproducing $\varepsilon_s < 1$.

The emergence of coherent vortices in 2D decaying Navier-Stokes turbulence thus provides an example of shear suppression in a neutral fluid and at the same time the elucidation of one mechanism responsible for intermittency in fluid turbulence.

B. Transport of stratospheric constituents

The atmosphere contains many trace gases and particulates, which while advected by flows as passive sca-

lars, play a crucial role in the other processes. Ozone and chlorofluorocarbons (CFC's) are examples. The transport of constituents is an important factor in their local concentrations. Significant transport occurs from convection in large-scale circulations and flow patterns. These flows are more coherent than turbulent, and the associated transport and mixing can be described by a process referred to as chaotic mixing (Pierrehumbert, 1991). Turbulence, though often not the dominant agent, also plays an important role in constituent transport. Turbulence is responsible for flattening constituent concentration gradients after wave-breaking instabilities in regions descriptively called surf zones (McIntyre and Palmer, 1984). Many observations do not resolve the turbulent fluctuations but their presence is inferred by other means. For example, global modeling of constituent concentrations using transport codes requires turbulent diffusivities to reproduce observed concentrations.

1. Meridional transport across zonal flows

Localized barriers to meridional (north-south) transport of constituent concentrations are commonly ascribed to regions in the stratosphere with steep concentration gradients. The gradients can arise from a variety of processes, e.g., when rapid advection brings regions of lowered constituent concentration into immediate proximity with regions of elevated concentration. There is a transport barrier if the gradients persist where they would normally be mixed by dynamical processes. Such barriers are widely attributed to the stabilization of wave breaking, which otherwise leads to robust transport across the gradients. Wave breaking is stabilized by the gradient of potential vorticity, a quantity derived from the total vorticity and the vertical stratification of the atmosphere (Andrews, Holton, and Leovy, 1987). Some persistent steep gradients are observed where the *flow shear* is maximum and not the potential-vorticity gradient. These maxima do not coincide because they are proportional to first and second derivatives of the mean flow, respectively. If there is ambient turbulence in regions of strong shear, the shear will create a transport barrier if it is strong enough to impede turbulent mixing across the gradient.

There is evidence for a barrier coincident with maximum flow shear that impedes the turbulent transport of stratospheric constituents from the tropics to higher latitudes. Pronounced constituent gradients near $\pm 20^\circ$ latitude are evident in all seasons, not just the winter when the potential-vorticity mechanism is in force. The location of the gradients corresponds to the edges of a zonal flow known as the equatorial jet. The equatorial jet is a stratospheric flow confined to tropical latitudes, generally between $\pm 20^\circ$. The flow is fairly uniform between those latitudes, and changes abruptly beyond them over $\sim 5^\circ - 10^\circ$. Flow shear du/dy is therefore weak except at $\pm 20^\circ$, where it is strong. The equatorial jet does not extend into the troposphere. Contours of volcanic aerosol show poleward spreading beyond $\pm 20^\circ$ in the troposphere, but distinct gradients form at $\pm 20^\circ$ at higher el-

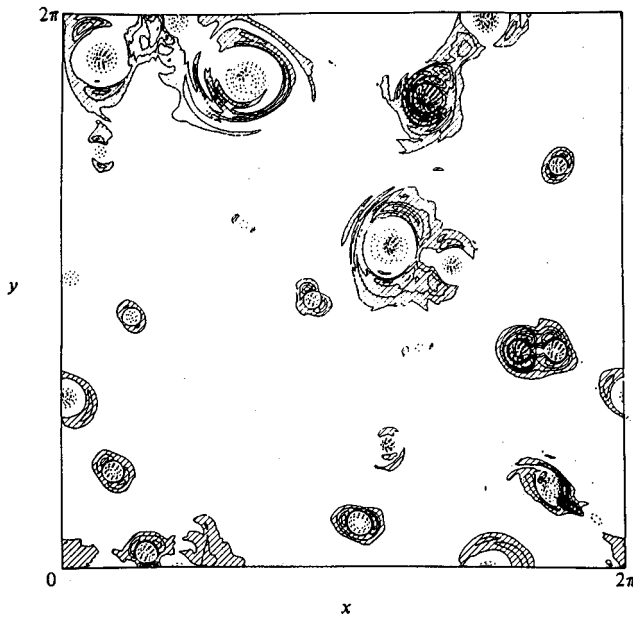


FIG. 16. Contours of Gaussian curvature for coherent vortices in simulations of decaying two-dimensional Navier-Stokes turbulence. The vortices consist of a central region of negative Gaussian curvature surrounded by a region of positive Gaussian curvature. Away from the vortices, the value of the Gaussian curvature fluctuates near zero. From McWilliams, 1984.

evations in the stratosphere (Trepte and Hitchman, 1992; Hitchman, McKay, and Trepte, 1994). The effect is particularly striking when large quantities of aerosols are injected into the atmosphere after a major volcanic eruption in the tropics. Aerosols injected into the stratosphere by Mt. Pinatubo in June of 1991 spread rapidly poleward, within a band between $\pm 20^\circ$ and along the equator. Figure 17 shows the global distribution of stratospheric aerosols a little more than a month after eruption. A near homogenization of aerosol concentrations in the equatorial direction is already evident. Concentrations are nearly uniform within the tropical band between $\pm 20^\circ$ and have steep gradients northward and southward. The persistence of these gradients is illustrated in the temporal record of aerosol concentrations following the eruption of Nevado del Ruiz in November of 1985. Figure 18 shows that these gradients persisted for four years after the eruption. (Eruptions of Mt. Kelut in 1990 and Mt. Pinatubo in 1991, which saturated the instruments, appear in the latter part of the record.) The steep concentration gradients closely coincide with the zone of steepest flow shear, as indicated in Fig. 6 of Trepte, Veiga, and McCormick (1993).

Zonal flows known as the Arctic and Antarctic winter polar vortices occur over the wintertime poles. These vortices extend from the poles to approximately 60° , with a zone of strong shear at the edge. The catalytic ozone depletion cycle of late winter leads to reduced and elevated concentrations of O_3 and ClO, respectively, in the polar regions. These concentrations are quite uniform over the poles, implying mixing, but have sharp gradients at the edge of the polar vortex, suggesting a

barrier to mixing and transport toward the equator. Hartmann *et al.* (1989) and Proffitt *et al.* (1989) note that the steep gradients occur in the region of maximum flow shear, which is distinctly poleward of the maximum potential-vorticity gradient (see Fig. 20 of Hartmann *et al.*, 1989). Similar features are evident in the data of Tuck (1989), collected in instrumented aircraft flights over the Arctic and Antarctic regions. In some cases fluctuations also appear to be smaller in the region of large flow shear (see Plate 5b of Tuck, 1989). These observations are anecdotal but suggestive, indicating that further analysis is warranted.

2. β -plane model of meridional transport

Transport in situations like those of the prior subsection has been studied numerically with the quasigeostrophic β -plane model [Eq. (3.20)] (Shepherd, 1987; Ware *et al.*, 1995, 1999). In these studies a mean zonal flow with meridional shear was specified as a model for flows such as the equatorial jet and polar winter vortices. For computational simplicity, the mean flow profile was a one-period sinusoid, allowing periodic boundary conditions in both zonal and meridional directions. The turbulence was initialized and allowed to decay, or driven by an external force. In the simulations, turbulence is not driven by the mean flow because β is chosen sufficiently large relative to the second derivative of the mean flow to make the flow barotropically stable, as represented in the condition of Eq. (3.4). The largest scales of the turbulence were smaller than the meridional scale of the mean flow by a factor of ~ 5 . This turbulence is representative of fluctuations created by wave breaking or driven by other processes, such as waves propagating upward from the troposphere.

Shepherd (1987) observed a reduction in turbulent vorticity where the zonal mean flow had maximum shear, but provided no explanation. The shear suppression criterion $\varepsilon_s < 1$ was not a part of the analysis or interpretation, and it is difficult to determine how strongly it was satisfied. In Ware *et al.* (1999), parameters were chosen to make ε_s as small as 0.1 in the region of maximum shear. Figure 19 shows the mean flow profile and values of ε_s across the jet. (Large fluctuations of ε_s arise from scatter in the turbulent correlation time.) The vorticity contours are shown in Fig. 20(a). There is a near absence of turbulence where $\varepsilon_s < 1$ and strong turbulence elsewhere. For comparison, Fig. 20(b) shows vorticity contours for a case with no jet ($\varepsilon_s \rightarrow \infty$). There the turbulence is isotropic as expected. Figures 19 and 20 represent steady turbulence driven by an external force. Similar results were reported for damped turbulence. Ware *et al.* (1995, 1999) also examined passive scalar transport using tracer particles and calculating an effective spatial diffusivity from the separation of pairs of tracer particles as a function of time. Consistent with Fig. 20(a), the diffusivity was minimum where ε_s was minimum. The diffusivity decreased with jet amplitude for fixed mean flow scale length ($\sim \varepsilon_s^{-1}$). Above a critical amplitude, however, the jet became unstable

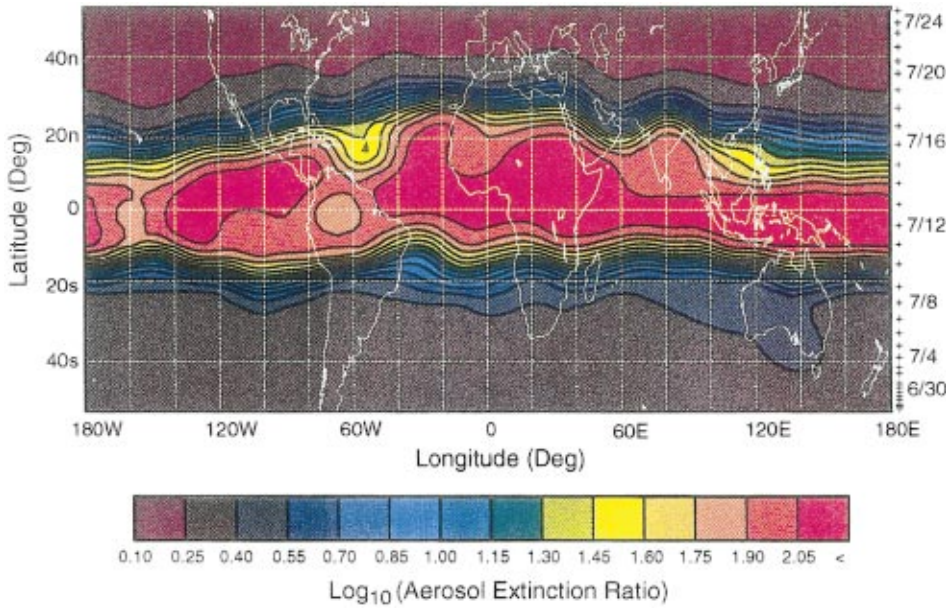


FIG. 17. Distribution of stratospheric aerosols approximately one month after the eruption of Mt. Pinatubo. Aerosol concentration is nearly homogeneous along the equator with sharp gradients around $\pm 20^\circ$ latitude. From Trepte, 1993 [Color].

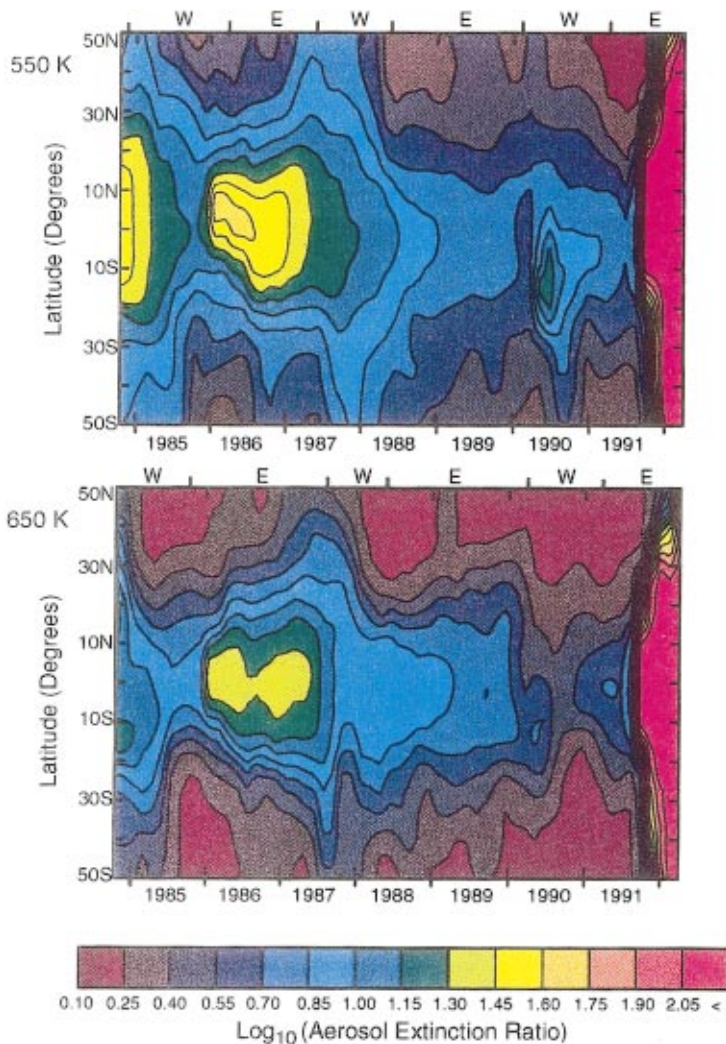


FIG. 18. Zonal averages of aerosol concentration at two altitudes in the stratosphere during the years 1985–1991. Large increases associated with the eruption of Nevado del Ruiz in November of 1985 persisted for years within the latitudes bounded by $\pm 20^\circ$ but did not spread poleward beyond these latitudes in any significant way. From Trepte, 1993 [Color].

($\partial^2 \bar{u} / \partial y^2 > \beta$), and the diffusivity rose abruptly. Above the instability threshold diffusivities in the zonal and meridional directions were comparable, while below the threshold the meridional diffusivity was much smaller than the zonal diffusivity.

C. Shear flow in self-organized criticality

The suppression of transport by flow shear has been observed in systems with self-organized criticality (SOC; Newman *et al.*, 1996). In such systems, a local flux induces transport at adjacent locations, leading in some cases to extended avalanche-like transport events whose correlation length and time exceed those of the fluctuation spectrum. Systems with self-organized criticality are not limited to flows, but have been used to model transport in granular media such as sandpiles (Bak, Tang, and Weisenfeld, 1987, Nagel, 1992), networks, and even seismic faults. By adopting appropriate generalizations for flow shear, systems with self-organized criticality have provided the greatest potential to date for application of the notion of shear suppression to dynamical systems.

The paradigm of self-organized criticality was introduced to plasma physics to model the global transport caused by small-scale fluctuations in terms of a universal process transcending particular collective instabilities (Diamond and Hahn, 1995). In these models, transport organizes itself on a hierarchy of spatial scales, ranging from the fluctuation scale, which may be limited by the magnetic field to a gyroradius, to the system size. The organizing principle is a “bucket-brigade” effect linking discrete cells of spatially localized fluctuation activity. The arrival of transported material at a cell location induces local instability by pushing the gradient above its local instability threshold. The resulting instability transports the incident material to the next cell. If the local instability in each cell transports more than the incident material, the chain of transport events can grow in space and time and can become global in nature. Such large-scale avalanche-like events lead to a characteristic frequency spectrum subrange with a power-law decay of f^{-1} . The fact that individual cells transport more than the incident material leads to a profile that is subcritical, i.e., the gradient is below the instability threshold, except during sporadic transport events.

A model realization of self-organized criticality is the sandpile automaton (Bak, Tang, and Weisenfeld, 1987; Nagel, 1992). Transport of sand down the pile is forced by grains of sand randomly falling from above. When the sandpile gradient becomes too steep locally, sand slides down the pile. The process is modeled using a grid to track the amount of sand in each cell. At each time step, if the difference in the amount of sand between each cell and its neighbor exceeds a threshold, a fixed amount of it is removed from the cell and transported to the neighboring site. If the difference does not exceed the critical threshold, no sand is transported. The process is governed by the simple prescription:

$$\text{If } Z_n(t) \geq Z_{\text{crit}}$$

$$\begin{aligned} h_n(t+1) &= h_n(t) - N_f, \\ h_{n+1}(t+1) &= h_{n+1}(t) + N_f, \end{aligned} \quad (8.11)$$

where $h_n(t)$ is the amount of sand in the n th cell at time t , $Z_n(t) = h_n(t) - h_{n+1}(t)$ is the local gradient, Z_{crit} is the critical gradient, and N_f is the amount of sand transported between adjacent cells in one time unit. A sample parameter set is $Z_{\text{crit}} = 8$, $N_f = 3$, and $Z_n(t_0) = 7$. If a grain of sand (one unit) is added to site n , the threshold gradient is exceeded and three grains of sand are passed to the next site. If adjacent sites are also near threshold, it is apparent that sites $n-1$ and $n+1$ could exceed the threshold at the next time step. In this way a single grain of externally incident sand can initiate a transport event that unfolds over many time steps and affects many sites both uphill and downhill from the initial site. On the other hand, if the same sample parameter set applies to a site n whose neighboring sites $n-1$ and $n+1$ are well below the threshold, the removal of three grains from site n to $n+1$ may be the extent of the event. There is therefore a hierarchy of events, from those that affect only adjacent sites to those that affect the entire sandpile.

Shear flow can be introduced into the sandpile automaton as a flow transverse to the sandpile gradient with shear in the gradient direction (Newman *et al.*, 1996). The spatial grid of cell sites must now be two dimensional, describing, for example, a conical sandpile on a planar surface. At the top and bottom of the sand pile the sand flows at constant speed transverse to the gradient in opposite directions. Connecting these flows is an intermediate region where the flow is sheared, matching the oppositely directed flows at top and bottom, and passing through zero in the middle. The flow is added to the dynamics in the time advance step after moving any falling grains to their new positions. The sheared flow is observed to dramatically decrease the number of large-scale transport events, i.e., events involving sites across the entire shear zone. If the incident sand flux is the same for sandpiles with and without flow, the net transport of sand over time will be the same in both cases. Consequently in the sheared case there is an increase in small-scale events to compensate for the decrease in large-scale events. The diffusivity changes functional form as a result of the flow shear, although there is not a marked decrease in its magnitude. The mechanism for the decrease of large-scale events is the simple decorrelation of these events by the flow shear.

IX. CONCLUSIONS

A. Summary

The suppression of turbulence and turbulent transport by stable flow shear is a robust process in plasmas and neutral fluids. The physical mechanism is the acceleration of turbulent decorrelation by mean flow shear, and it is in force whenever $\tau_s < \tau_N < \tau_D$, where τ_s , τ_N , and τ_D are the shear straining time, turbulent correlation time, and domain time, respectively. This hierarchy of

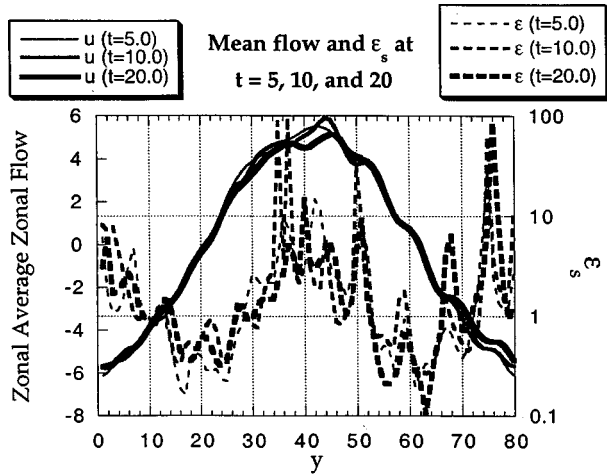


FIG. 19. Meridional profiles of a zonally averaged zonal flow and the shear suppression parameter ε_s in a simulation of geostrophic turbulence in a beta plane. According to the predictions of Sec. II, when the shear suppression parameter is less than unity, as it is in the regions of maximum flow shear, turbulence is suppressed. From Ware *et al.*, 1999.

time scales distinguishes the physics of shear suppression from rapid-distortion theory, which holds when $\tau_s \leq \tau_D < \tau_N$. With the domain time shorter than the turbulent correlation time in rapid-distortion theory the dynamical equations can be linearized. The distinction between the theory of shear suppression and rapid-distortion theory is apparent in the analysis of the Fourier-Laplace expansion of the inverted advective operator for turbulence in a simple background flow with unidirectional plane shearing (Sec. II.B.3). These two theories emerge as the long-time and short-time asymptotic limits. As such the theory of shear suppression is a nonlinear extension of rapid-distortion theory. The dynamical importance of the turbulent correlation time in the theory of shear suppression causes the turbulence to adjust itself (as in slowly changing turbulence) to bring the shear straining time and correlation time into balance, $\tau_s = \tau_N$. This is accomplished by a reduction in the cross-shear scale length to make τ_N as small as τ_s . If the driving source remains invariant across the shear flow, the decrease in τ_N directly leads to a decrease in the turbulent energy, hence to a suppression of turbulence.

The suppression of turbulence in shear flows has been observed in plasma experiments and in simulations of magnetically confined plasmas. It is a robust property of analytic theory ranging from simple dimensional scaling analysis to more rigorous asymptotic theory. As a dynamic phenomenon in fusion plasmas, this process is unusually universal. It occurs in regions of the plasma ranging from the edge to the core. These are regions in which the turbulence dramatically changes character because of different driving mechanisms and parameters, such as temperature (which can range over three orders of magnitude). This process also occurs in numerous plasma confinement devices, with widely varying geometries, magnetic topologies, and plasma conditions. The flow shear can arise from a variety of mechanisms, ex-

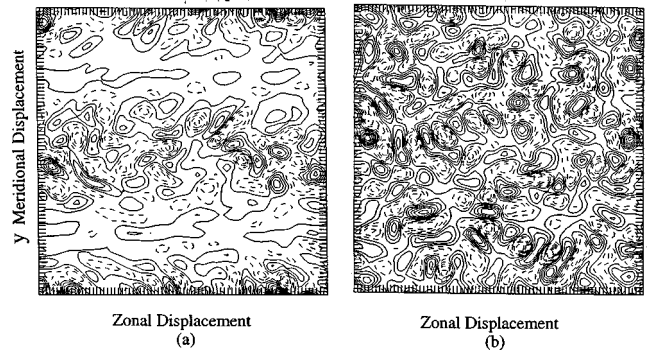


FIG. 20. Contours of constant vorticity in simulations of externally driven beta-plane turbulence, (a) with no mean zonal flow, and (b) with the mean zonal flow of Fig. 19. Suppression of the turbulence in the regions where $\varepsilon_s < 1$ is clearly evident. From Ware *et al.*, 1999.

ternal and internal. Moreover, shear suppression occurs in hydrodynamics and in more general transporting systems with self-organized criticality.

The use of flow shear to create transport barriers in fusion plasmas represents a major breakthrough in the ability to achieve fusion in magnetically confined plasmas. The seemingly irreducible transport associated with small-scale turbulence, driven by the large gradients of temperature and density in fusion plasmas, has long been an impediment to magnetic fusion. With flow shear, transport in some cases has been reduced to the absolute minimum associated with Coulomb collisions that occur because of thermal motion. A variety of present-day records have been set in magnetic fusion devices—for fusion power produced, fusion power efficiency, and confinement time—utilizing flow-shear-induced transport barriers.

The effect of flow shear in plasmas is not limited to the way it accelerates the nonlinear decorrelation process. Though the mechanisms are less general, flow shear can stabilize a variety of collective instabilities in fusion plasmas. Flow shear affects the complex phase angle between an advected fluctuation and the advecting flow. This produces a reduction factor in the transport flux that is independent of amplitude reduction. Flow shear also disrupts large-scale transport events in systems with self-organized criticality.

Shear flow is generated in plasmas by a variety of mechanisms in what is often a very complicated fashion. The radial electric field required for the $E \times B$ flow can be driven externally by probes or internally by the pressure gradient, by ion flows in the toroidal and poloidal directions, or by differential charge loss. The ion flows, in turn, are driven by the Reynolds stress, by injected *rf* waves, or by asymmetries in the transport flux. The creation of shear flows in plasmas by internal mechanisms that are themselves modified by the flow shear and its associated reduction in transport has led to a new picture of the magnetically confined plasma as a self-regulated state. Shear suppression gives this state the curious feature that increases in free energy, in the form of greater external heat input, can lead to lower turbu-

lence and steeper gradients, rather than the opposite. The complicated nonlinear connections between internally generated flow shear, turbulence, and profiles of the mean quantities that drive turbulence and transport lead to bifurcations of the plasma state, the most universal being the transition from the L to the H mode.

At present, studies of shear suppression outside plasma physics have been limited but promising. These include a demonstration that flow shear in the edge of intense vortices in Navier-Stokes turbulence allows these vortices to greatly reduce or effectively eliminate the mixing of vorticity by ambient turbulence. This process provides an explanation for intermittency in decaying 2D Navier-Stokes turbulence and explains in a natural way the observed evolution of probability distribution functions and the Gaussian curvature. Shear suppression also affects geostrophic turbulence and its transport of constituents in the stratosphere. The observed presence of transport barriers in regions of strong flow shear at the edges of the equatorial jet and polar winter vortices may be associated with this mechanism. Systems with self-organized criticality are more general than the hydrodynamic flows of the Navier-Stokes equations and the related atmospheric turbulence models. The existence of a form of shear suppression in these systems, affecting the large-scale correlated transport events, represents an application to the broadest class of dynamical systems considered to date.

B. Open questions

This review has examined the suppression of turbulence by flow shear, assuming flows that are stable, 2D, and steady on time scales that are long compared to the turbulent correlation time. What occurs under other conditions is, in many cases, an open question. For example, unstable shear flows drive turbulence rather than suppress it. However, if the instability is intermittent, driving and suppression may occur intermittently, leading to some reduction of turbulent energy in a time-average sense relative to a steady instability process. This situation ultimately applies to the stratosphere when the mean flow is periodically unstable to wave-breaking events, although if the time between wave-breaking events is longer than the turbulent correlation time, the flow can be treated as stable. Intermittent stability may also account for the reduction of turbulence observed in certain 3D atmospheric boundary-layer flows (Smedman, Bergström, and Högström, 1995). In general, 3D dynamics complicate the picture presented in this review. While flow shear may accelerate the decorrelation of eddies whose vorticity is not aligned with the flow, leading to a suppression of vorticity, aligned eddies are stretched and their vorticity is amplified. Alignment (or lack thereof) is itself a product of the turbulence, making it difficult to anticipate what role shear suppression ultimately plays in 3D shear flows.

Of recent interest, *unsteady* zonal flows (i.e., toroidally and poloidally symmetric flows) arise in simulations of ion-temperature-gradient turbulence in toka-

maks (Sec. V.A.2) and are observed to lead to lower turbulent energy and transport (Lin *et al.*, 1998). Although this effect has been attributed to a suppression of turbulence by the shear in the zonal flows (Diamond *et al.*, 1998), the zonal flows are incoherent and appear in simulations to decorrelate on a time scale that is comparable to that of the turbulence. Other effects may also play a role, such as diminished efficiency of spectral transfer with zonal flows.

The suppression of turbulence by flow shear in plasmas generally involves turbulence excited by a collective instability. It is relatively easy to determine the effect of flow shear on the linear stability. How it affects saturated turbulence in an inhomogeneous magnetic field is more difficult to assess because the saturated state may involve nonlinear changes in the eigenmode structure. The nature of shear suppression in externally driven turbulence has not been explored beyond simple dimensional analysis. It was assumed in Sec. II.B that flow-wise scales are not affected by the flow shear. The validity of this assumption depends on how incompressibility is maintained under the forcing, an issue that has not been examined.

There is a wide consensus within the magnetic fusion research community that flow shear is responsible for the transport barriers observed in experiment. At present there is no consensus on the mechanism responsible for generation of the shear flow. Despite the large number of mechanisms described in Sec. IV, none has been shown to be invalid or inoperative. This statement even applies to externally driven flow shear, where although there is clearly an external current as described in Secs. IV.B and VII.B.1, there are discrepancies between the observational details and model predictions, and the measurements do not account for all the forces, e.g., the Reynolds stress. Considerable work remains to be done, especially in measuring quantities of relevance to the proposed mechanisms and in producing predictive (as opposed to heuristic) models of flow generation. The same statements also apply to transition modeling. Again there are a large number of models (Sec. VII.B), none of which has been shown to be invalid.

Open questions remain concerning the details of transport suppression in fusion experiments. For example, in the internal transport barrier, the suppression of the ion heat and particle fluxes appears to be stronger in many cases than the suppression of the electron heat fluxes. This difference is not understood. Moreover, certain experiments, particularly those with probe-induced H modes, have temperature fluctuation and heat flux reductions with flow shear, while similar experiments in other tokamaks do not. This difference may be accounted for by the variation of the parallel thermal conduction from device to device, but has yet to be demonstrated. The existence of transport barriers in plasmas necessarily involves a reduction in plasma transport. Yet most theoretical work on shear suppression treats only the amplitude reduction, and not the effect of flow shear on the cross phase (Sec. V.B). Theories that describe the latter have been restricted to a weak-flow-shear regime,

which is not likely the regime of experiments. While flow shear has been shown to reduce the cross phase, a number of experimental observations relating to the cross phase have yet to be explained. These include observations of a reduction of the cross phase with little or no accompanying reduction of amplitudes and observations that fluxes can change sign in transport barriers.

C. Future directions

Despite the widely held view that flow shear is responsible for the transport barriers observed in fusion experiments, the evidence is inferred in experiments with highly complex dynamics, complicated geometries, and many variables, few of which can be externally controlled. A simple, direct demonstration of shear suppression, ideally in a controlled neutral-fluid experiment, is a desirable direction for future work. In a neutral fluid, the number of collective modes is limited, there is a single unequivocal flow velocity (as opposed to a plasma in which each charge species has its own flow and flow dynamics), and the geometry can be simple because it does not have to confine an ionized gas. The constraints of a stable shear flow and 2D turbulent dynamics could be realized in a rotating soap film with grid-generated turbulence or in a differentially rotating tank with a turbulent Rayleigh-Bénard flow. Such an experiment could not only verify the general mechanism of shear suppression, but measure scalings and spectra, and examine the effect of different forcing mechanisms.

Much work remains to be done in measuring quantities of importance to shear suppression in fusion experiments. This is particularly true of the Reynolds stress. This paper has presented numerous parallels between plasmas and neutral fluids, which in many cases lead to strikingly similar expressions and effects. In neutral fluids the Reynolds stress not only leads to turbulent viscosities, but it generates a number of geophysical flows such as the quasibiennial oscillation (Holton and Lindzen, 1972; Plumb, 1977). The importance of the Reynolds stress as a flow generation mechanism in neutral fluids suggests that it should not be ignored in plasma turbulence. Indeed, all of the measurements of the Reynolds stress in plasmas have indicated that its magnitude is sufficient for it to contribute to observed flows. Measurement of the Reynolds stress in fusion plasmas is very difficult but is crucial to a detailed understanding of transport barrier physics.

Shear suppression has the potential for leading to future fusion reactors whose size is manageable and whose costs are competitive with other nonfossil forms of future energy generation. Although record confinement parameters have been achieved with flow-shear-induced transport barriers, these barriers are transient. The internal transport barrier requires a hollow current profile, which is not maintained in a steady state because of inward current diffusion. Moreover, the confinement is so good in these discharges that pressure gradients steepen to the point where they can become unstable to global, MHD instabilities that can terminate the discharge. The

development of techniques to produce steady and controllable shear flow is crucial if flow shear suppression is to provide the confinement needed in future steady-state fusion reactors. A better understanding is also needed of the requirements of flow generation in reactor regimes, the availability of enhanced-confinement modes in reactors, and the scaling of transition thresholds to reactor parameters.

Finally, some speculations are offered for non plasma situations, other than those described in Sec. VIII, in which shear suppression might apply. The Earth's turbulent boundary layer has already been mentioned in connection with observations of suppression when a jet forms near a land/sea interface (Smedman, Bergström, and Högström, 1995). The process of shear suppression may apply to wall flows during the transient period of laminarity after bursts of turbulent eddy formation at the wall. A form of shear suppression has already been invoked in the turbulent boundary layer above an undulating surface (Hunt, Leibovich, and Richards, 1988). The ocean has phenomena that possibly relate to shear suppression. These include gulf stream rings and Mediterranean salt lenses (meddies). Both are long-lived coherent vortical flows that sequester elevated concentrations of heat and, in the case of meddies, salinity. These concentrations are subject to outward diffusion by ambient turbulence and mixing and their longevity may suggest a transport barrier. Astrophysics may also present situations in which shear suppression applies, particularly in relationship to the differential rotation of Keplerian motion.

ACKNOWLEDGMENTS

The author acknowledges helpful conversations with J. A. Boedo, K. Burrell, J. D. Callen, B. A. Carreras, B. E. Chapman, P. H. Diamond, P. Durbin, E. Fernandez, G. Fiksel, C. Forest, R. Gatto, T. S. Hahm, A. B. Hassam, C. C. Hegna, M. H. Hitchman, R. A. Moyer, P. Moin, D. E. Newman, S. C. Prager, W. C. Reynolds, J. Sarff, L. Smith, A. S. Ware, and S. Zweben. This work was supported by the U.S. Department of Energy under Grant No. DE-FG02-89ER-53291 and by the Vilas Trustees.

REFERENCES

- Andrews, D. G., J. R. Holton, and C. B. Leovy, 1987, *Middle Atmosphere Dynamics* (Academic, Orlando).
- Antoni V., D. Desideri, E. Martinez, G. Serianni, and L. Tramontin, 1997, *Phys. Rev. Lett.* **79**, 4814.
- Arber, T. D., and D. F. Howell, 1996a, *Phys. Plasmas* **3**, 554.
- Arber, T. D., and D. F. Howell, 1996b, *Phys. Rev. Lett.* **76**, 2198.
- ASDEX Team, 1989, *Nucl. Fusion* **29**, 1959.
- Askinazi, L. G., V. E. Golant, S. V. Lebedev, L. S. Levin, V. A. Rozhansky, and M. Tendler, 1993, *Phys. Fluids B* **5**, 2421.
- Azouni, M. A., E. W. Bolton, and F. H. Busse, 1986, *Geophys. Astrophys. Fluid Dyn.* **34**, 301.

- Bak, P., C. Tang, and K. Weisenfeld, 1987, *Phys. Rev. Lett.* **59**, 381.
- Batchelor, G. K., and I. Proudman, 1954, *Q. J. Mech. Appl. Math.* **7**, 83.
- Belcher, S. E., T. M. J. Newley, and J. C. R. Hunt, 1993, *J. Fluid Mech.* **249**, 557.
- Bell, R. E., F. M. Levinton, S. H. Batha, E. J. Synakowski, and M. C. Zarnstorff, 1998, *Phys. Rev. Lett.* **81**, 1429.
- Bendat, J. S., and A. G. Piersol, 1986, *Random Data, Analysis and Measurement Procedures* (Wiley, New York).
- Bender, C. M., and S. A. Orszag, 1978, *Advanced Mathematical Methods for Scientists and Engineers* (McGraw-Hill, New York).
- Berk, H. L., and A. A. Galeev, 1967, *Phys. Fluids* **10**, 441.
- Berry, L. A., E. F. Jaeger, and D. B. Batchelor, 1999, *Phys. Rev. Lett.* **82**, 1871.
- Beyer, P., and K. H. Spatschek, 1996, *Phys. Plasmas* **3**, 995.
- Biglari, H., P. H. Diamond, and P. W. Terry, 1990, *Phys. Fluids B* **2**, 1.
- Biglari, H., M. Ono, P. H. Diamond, and G. G. Craddock, 1991, in *Radio-Frequency Power in Plasmas, 9th Topical Conference*, Charleston, edited by D. B. Batchelor (American Institute of Physics, New York), p. 376.
- Boedo, J. A., D. Gray, S. Jachmich, R. Conn, G. Van Oost, and R. R. Weynants, 1998, *Nucl. Fusion*, in press.
- Boutros-Ghali, T., and T. H. Dupree, 1981, *Phys. Fluids* **24**, 1839.
- Brower, D. L., W. A. Peebles, and N. C. Luhmann, 1987, *Nucl. Fusion* **27**, 2055.
- Brown, R. A., 1980, *Rev. Geophys. Space Phys.* **18**, 683.
- Burrell, K. H., 1994, *Plasma Phys. Controlled Fusion* **36**, A291.
- Burrell, K. H., 1997, *Phys. Plasmas* **4**, 1499.
- Burrell, K. H., M. E. Austin, C. M. Greenfield, L. L. Lao, B. W. Rice, G. M. Staebler, and B. W. Stallard, 1998, *Plasma Phys. Controlled Fusion* **40**, 1585.
- Burrell, K. H., *et al.*, 1990, *Phys. Fluids B* **2**, 1405.
- Burrell, K. H., *et al.*, 1992, *Plasma Phys. Controlled Fusion* **34**, 1859.
- Burrell, K. H., *et al.*, 1995, *Plasma Physics and Controlled Nuclear Fusion Research, 1994* (International Atomic Energy Agency, Vienna), Vol. 1, p. 221.
- Burrell, K. H., *et al.*, 1996, *Plasma Phys. Controlled Fusion* **38**, 1313.
- Bush, C. E., *et al.*, 1990, *Phys. Rev. Lett.* **65**, 424.
- Callen, J. D., 1977, *Phys. Rev. Lett.* **24**, 1540.
- Carlstrom, T. N., and R. J. Groebner, 1996, *Phys. Plasmas* **3**, 1867.
- Carreras, B. A., 1997, *IEEE Trans. Plasma Sci.* **25**, 1281.
- Carreras, B. A., L. Garcia, and P. H. Diamond, 1987, *Phys. Fluids* **30**, 1488.
- Carreras, B. A., V. E. Lynch, and L. Garcia, 1991, *Phys. Fluids B* **3**, 1438.
- Carreras, B. A., V. E. Lynch, L. Garcia, and P. H. Diamond, 1993, *Phys. Fluids B* **5**, 1491.
- Carreras, B. A., V. E. Lynch, L. Garcia, and P. H. Diamond, 1995, *Phys. Plasmas* **2**, 2745.
- Carreras, B. A., L. W. Owen, R. Maingi, P. K. Mioduszewski, T. N. Carlstrom, and R. J. Groebner, 1998, *Phys. Plasmas* **5**, 2623.
- Carreras, B. A., K. Sidikman, P. H. Diamond, P. W. Terry, and L. Garcia, 1992, *Phys. Fluids B* **4**, 3115.
- Chandrasekhar, S., 1961, *Hydrodynamic and Hydromagnetic Stability* (Dover, New York).
- Chang, Z., and J. D. Callen, 1992, *Phys. Fluids B* **4**, 1766.
- Chapman, B. E., A. F. Almagri, J. K. Anderson, C.-S. Chiang, D. Craig, G. Fiksel, N. E. Lanier, S. C. Prager, J. S. Sarff, M. R. Stoneking, and P. W. Terry, 1998, *Phys. Plasmas* **5**, 1848.
- Chapman, B. E., C.-S. Chiang, S. C. Prager, J. S. Sarff, and M. R. Stoneking, 1998, *Phys. Rev. Lett.* **80**, 2137.
- Charlton, L. A., B. A. Carreras, V. E. Lynch, K. L. Sidikman, and P. H. Diamond, 1994, *Phys. Plasmas* **1**, 2700.
- Chen, X. L., and P. J. Morrison, 1990, *Phys. Fluids B* **2**, 495.
- Chiueh, T., P. W. Terry, P. H. Diamond, and J. E. Sedlak, 1986, *Phys. Fluids* **29**, 231.
- Connor, J. W., J. B. Taylor, and H. R. Wilson, 1993, *Phys. Rev. Lett.* **70**, 1803.
- Cornelis, J., R. Sporcken, G. Van Oost, and R. R. Weynants, 1994, *Nucl. Fusion* **34**, 171.
- Costley, A. E., P. Cripwell, and G. Vayakis, 1993, in *Local Transport Studies in Fusion Plasmas*, edited by J. D. Callen, G. Gorini, and E. Sindoni (Editrice Compositori, Bologna), p. 223.
- Craddock, G. G., and P. H. Diamond, 1991, *Phys. Rev. Lett.* **67**, 1535.
- Craig, D., *et al.*, 1997, *Phys. Rev. Lett.* **79**, 1865.
- Das, A., S. Mahajan, P. Kaw, A. Sen, S. Benkadda, and A. Verga, 1997, *Phys. Plasmas* **4**, 1018.
- Diamond, P. H., and T. S. Hahm, 1995, *Phys. Plasmas* **2**, 3640.
- Diamond, P. H., and Y. B. Kim, 1991, *Phys. Fluids B* **3**, 1626.
- Diamond, P. H., V. B. Lebedev, D. E. Newman, B. A. Carreras, T. S. Hahm, W. M. Tang, G. Rewoldt, and K. Avinash, 1997, *Phys. Rev. Lett.* **78**, 1472.
- Diamond, P. H., Y.-M. Liang, B. A. Carreras, and P. W. Terry, 1994, *Phys. Rev. Lett.* **72**, 2565.
- Diamond, P. H., M. N. Rosenbluth, F. L. Hinton, M. Malkov, J. Fleischer, and A. Smolyakov, 1998, in *Fusion Energy 1998* (International Atomic Energy Agency, Vienna), in press.
- Dominguez, R. R., and G. M. Staebler, 1993, *Phys. Fluids B* **5**, 3876.
- Doyle, E. J., P. Gohil, R. J. Groebner, T. Lehecka, N. C. Luhmann, M. A. Mahdavi, T. H. Osborne, W. A. Peebles, and R. Philipona, 1993, *Plasma Physics and Controlled Nuclear Fusion Research, 1992* (International Atomic Energy Agency, Vienna), Vol. 1, p. 235.
- Dritschel, D. G., 1989, *J. Fluid Mech.* **206**, 193.
- Dupree, T. H., 1972, *Phys. Fluids* **15**, 334.
- Durst, R. D., R. J. Fonck, J. S. Kim, S. F. Paul, N. Bretz, C. Bush, Z. Chang, and R. Hulse, 1993, *Phys. Rev. Lett.* **71**, 3135.
- Eliassen, A., and E. Palm, 1960, *Geofysike Publikationer* **22**, 1.
- Erckmann, V., *et al.*, 1993, *Phys. Rev. Lett.* **70**, 2086.
- Ernst, E. R., *et al.*, 1998, *Phys. Plasmas* **5**, 665.
- Fiksel, G., 1998, private communication.
- Fonck, R. J., N. Bretz, G. Cosby, R. Durst, E. Massucato, R. Nazikian, S. Paul, S. Scott, W. Tang, and M. Zarnstorff, 1992, *Plasma Phys. Controlled Fusion* **34**, 1993.
- Freidberg, J. P., 1982, *Rev. Mod. Phys.* **54**, 801.
- Garcia, L., P. H. Diamond, B. A. Carreras, and J. D. Callen, 1985, *Phys. Fluids* **28**, 2137.
- Gibson, A., and the JET Team 1998, *Phys. Plasmas* **5**, 1839.
- Greenfield, C. M., *et al.*, 1993, *Plasma Phys. Controlled Fusion* **35**, B263.
- Groebner, R. J., 1993, *Phys. Fluids B* **5**, 2343.
- Groebner, R. J., K. H. Burrell, and R. P. Seraydarian, 1990, *Phys. Rev. Lett.* **65**, 3015.

- Groebner, R. J., P. Gohil, K. H. Burrell, T. H. Osborne, R. P. Seraydarian, and H. St. John, 1989, in *Proceedings of the 16th European Conference of Controlled Fusion and Plasma Physics* (European Physical Society, Petit-Lancy), Vol. I, p. 245.
- Guzdar, P. N., J. F. Drake, D. McCarthy, A. B. Hassam, and C. S. Liu, 1993, *Phys. Fluids B* **5**, 3712.
- Hahm, T. S., and K. H. Burrell, 1995, *Phys. Plasmas* **2**, 1648.
- Hamaguchi, S., and W. Horton, 1992, *Phys. Fluids B* **4**, 319.
- Hartmann, D. L., K. R. Chan, B. L. Gary, M. R. Schoeberl, P. A. Newman, R. L. Martin, M. Loewenstein, J. R. Podolske, and S. E. Strahan, 1989, *J. Geophys. Res.* **94**, 11625.
- Hasegawa, A., and K. Mima, 1977, *Phys. Rev. Lett.* **39**, 205.
- Hasegawa, A., and M. Wakatani, 1987, *Phys. Rev. Lett.* **59**, 1591.
- Hassam, A. B., 1991, Comments, *Plasma Phys. Controlled Fusion* **14**, 275.
- Hassam, A. B., T. M. Antonsen, J. F. Drake, and C. S. Liu, 1991, *Phys. Rev. Lett.* **66**, 309.
- Hassam, A. B., and J. F. Drake, 1993, *Phys. Fluids B* **5**, 4022.
- Hazeltine, R. D., 1989, *Phys. Fluids B* **1**, 2031.
- Hegna, C. C., *et al.*, 1998, in *Fusion Energy 1998* (International Atomic Energy Agency, Vienna), in press.
- Hidalgo, C., *et al.*, 1997, *J. Plasma Fusion Res.* **1**, 96.
- Hinton, F. L., 1991, *Phys. Fluids B* **3**, 696.
- Hinton, F. L., and R. D. Hazeltine, 1976, *Rev. Mod. Phys.* **48**, 239.
- Hinton, F. L., and G. M. Staebler, 1993, *Phys. Fluids B* **5**, 1281.
- Hirsch, M., *et al.*, 1997, in *Fusion Energy 1996* (International Atomic Energy Agency, Vienna), Vol. 2, p. 315.
- Hirshman, S., and D. Sigmar, 1981, *Nucl. Fusion* **21**, 1079.
- Hitchman, M. H., M. McKay, and C. R. Trepte, 1994, *J. Geophys. Res.* **99**, 20689.
- Holton, J. R., and R. S. Lindzen, 1972, *J. Atmos. Sci.* **29**, 1076.
- Horton, W., 1999, *Rev. Mod. Phys.* **71**, 735.
- Hoshino, K. *et al.*, 1989, *Phys. Rev. Lett.* **63**, 770.
- Hugon, M., *et al.*, 1992, *Nucl. Fusion* **32**, 33.
- Hunt, J. C. R., and D. J. Carruthers, 1990, *J. Fluid Mech.* **242**, 497.
- Hunt, J. C. R., D. J. Carruthers, and J. C. H. Fung, 1991, in *New Perspectives in Turbulence*, edited by Lawrence Sirovich (Springer, New York), p. 55.
- Hunt, J. C. R., S. Leibovich, and K. J. Richards, 1988, *Q. J. R. Meteorol. Soc.* **114**, 1435.
- Ida, K., 1998, *Plasma Phys. Controlled Fusion* **40**, 1429.
- Ida, K., S. Hidekuma, Y. Miura, T. Fujita, M. Mori, K. Hoshino, N. Suzuki, T. Yamauchi, and the JFT2-M Group 1990, *Phys. Rev. Lett.* **65**, 1364.
- Isler, R. C., *et al.*, 1992, *Phys. Fluids B* **4**, 2104.
- ITER Confinement Database and Modelling Working Group 1997, *Plasma Phys. Controlled Fusion* **39**, B115.
- Itoh, K., and S.-I. Itoh, 1996, *Plasma Phys. Controlled Fusion* **38**, 1.
- Itoh, S.-I., and K. Itoh, 1988, *Phys. Rev. Lett.* **60**, 2276.
- Jachmich, S., G. Van Oost, R. R. Weynants, and J. A. Boedo, 1998, *Plasma Phys. Controlled Fusion* **40**, 1105.
- Jackson, G. L., *et al.*, 1991, *Phys. Rev. Lett.* **67**, 3098.
- Jackson, J. D., 1975, *Classical Electrodynamics* (Wiley, New York).
- Kim, J., K. H. Burrell, P. Gohil, R. J. Groebner, Y.-B. Kim, H. E. St. John, R. P. Seraydarian, and M. R. Wade, 1994, *Phys. Rev. Lett.* **72**, 2199.
- Kim, Y. B., P. H. Diamond, H. Biglari, and J. D. Callen, 1991, *Phys. Fluids B* **3**, 384.
- Kimura, H., and the JT-60 Team 1996, *Phys. Plasmas* **3**, 1943.
- Koide, Y., and the JT-60 Team 1997, *Phys. Plasmas* **4**, 1623.
- Koide, Y., T. Takizaka, S. Takeji, S. Ishida, M. Kikuchi, Y. Kamada, T. Ozeki, Y. Neyatani, H. Shirai, M. Mori, and S. Tsuji-Iio, 1996, *Plasma Phys. Controlled Fusion* **38**, 1011.
- Koide, Y., *et al.*, 1994, *Phys. Rev. Lett.* **72**, 3662.
- Kolmogorov, A. N., 1941, *Dokl. Akad. Nauk SSSR* **30**, 301.
- Kraichnan, R. H., 1959, *J. Fluid Mech.* **5**, 497.
- Krall, N. A., and A. W. Trivelpiece, 1973, *Principles of Plasma Physics* (McGraw-Hill, New York).
- Kuo, H. L., 1963, *Phys. Fluids* **6**, 195.
- LaBombard, B., and B. Lipschultz, 1987, *Nucl. Fusion* **27**, 81.
- La Haye, R. J., C. M. Greenfield, R. J. Groebner, A. W. Hyatt, J. T. Scoville, 1993, *Nucl. Fusion* **33**, 349.
- La Haye, R. J., T. H. Osborne, C. L. Rettig, C. M. Greenfield, A. W. Hyatt, and J. T. Scoville, 1995, *Nucl. Fusion* **35**, 988.
- Landau, L. D., and E. M. Lifshitz, 1980, *Statistical Physics, Part I* (Pergamon, Oxford).
- Lao, L. L., *et al.*, 1993, *Phys. Rev. Lett.* **70**, 3435.
- Lao, L. L., *et al.*, 1996, *Phys. Plasmas* **3**, 1951.
- Lazarus, E. A., *et al.*, 1985, *Nucl. Fusion* **25**, 135.
- LeBlanc, B., *et al.*, 1995, *Phys. Plasmas* **2**, 741.
- LeBlanc, B. P., R. E. Bell, S. Bernabei, J. C. Hosea, R. Majeski, M. Ono, C. K. Phillips, J. H. Rogers, C. Schilling, C. H. Skinner, and J. R. Wilson, 1999, *Phys. Rev. Lett.* **82**, 331.
- Lee, G. S., and P. H. Diamond, 1987, *Phys. Fluids* **29**, 3291.
- Lehnert, B., 1966, *Phys. Fluids* **9**, 1367.
- Lesieur, M., 1997, *Turbulence in Fluids* (Kluwer Academic, Dordrecht/Boston/London).
- Levinton, F. M., *et al.*, 1995, *Phys. Rev. Lett.* **75**, 4417.
- Liewer, P. C., 1985, *Nucl. Fusion* **25**, 543.
- Lin, C. C., 1955, *The Theory of Hydrodynamic Stability* (Cambridge University Press, Cambridge).
- Lin, Z., T. S. Hahm, W. W. Lee, W. M. Tang, and R. B. White, 1998, *Science* **281**, 1835.
- Matsumoto, H., *et al.*, 1992, *Plasma Phys. Controlled Fusion* **34**, 615.
- Matthews, P. G., D. T. Anderson, F. S. B. Anderson, J. L. Shoet, and J. N. Talmadge, 1993, *Phys. Fluids B* **5**, 4061.
- Mazzucato, E., *et al.*, 1996, *Phys. Rev. Lett.* **77**, 3145.
- McCarthy, D. R., J. F. Drake, P. N. Guzdar, and A. B. Hassam, 1993, *Phys. Fluids B* **5**, 1188.
- McIntyre, M. C., and T. N. Palmer, 1984, *J. Atmos. Terr. Phys.* **46**, 825.
- McWilliams, J., 1984, *J. Fluid Mech.* **146**, 21.
- Messiaen, A. M., *et al.*, 1997, *Phys. Plasmas* **4**, 1690.
- Morris, R. C., M. G. Haines, and R. J. Hastie, 1996, *Phys. Plasmas* **3**, 4513.
- Moyer, R. A., *et al.*, 1995, *Phys. Plasmas* **2**, 2397.
- Mynick, H. E., and W. N. G. Hitchon, 1983, *Nucl. Fusion* **23**, 1053.
- Nagel, S. R., 1992, *Rev. Mod. Phys.* **64**, 321.
- Newman, D. E., B. A. Carreras, P. H. Diamond, and T. S. Hahm, 1996, *Phys. Plasmas* **3**, 1858.
- Newman, D. E., B. A. Carreras, D. Lopez-Bruna, and P. H. Diamond, 1999, *Plasma Phys. Control. Fusion* (in press).
- Newman, D. E., P. W. Terry, P. H. Diamond, and Y.-M. Liang, 1993, *Phys. Fluids B* **5**, 1140.
- Odajima, K., *et al.*, 1987, *Plasma Physics and Controlled Nuclear Fusion Research, 1986* (International Atomic Energy Agency, Vienna), Vol. 1, p. 151.

- Ohdachi, S., T. Shoji, K. Nagashima, H. Tamai, Y. Miura, H. Baeda, H. Toyama, and JFT2-M Group, 1994, *Plasma Phys. Controlled Fusion* **36**, A201.
- Ongena, J., *et al.*, 1993, *Plasma Physics and Controlled Fusion Research, 1992* (International Atomic Energy Agency, Vienna), Vol. 1, p. 725.
- Ono, M., *et al.*, 1997, *Plasma Phys. Controlled Fusion* **39**, A361.
- Or, A. C., and F. H. Busse, 1987, *J. Fluid Mech.* **174**, 313.
- Osborne, T. H., *et al.*, 1990, *Nucl. Fusion* **30**, 2023.
- Parker, S. E., W. W. Lee, and R. A. Santoro, 1993, *Phys. Rev. Lett.* **71**, 2042.
- Pedlosky, Joseph, 1979, *Geophysical Fluid Dynamics* (Springer, New York).
- Petty, C. C., *et al.*, 1995, *Phys. Plasmas* **2**, 2342.
- Pierrehumbert, R. T., 1991, *Phys. Fluids A* **3**, 1250.
- Plumb, R. A., 1977, *J. Atmos. Sci.* **34**, 1847.
- Prager, S. C., 1990, *Plasma Phys. Controlled Fusion* **32**, 903.
- Proffitt, M. H., *et al.*, 1989, *J. Geophys. Res.* **94**, 16797.
- Rechester, A. B., and M. N. Rosenbluth, 1978, *Phys. Rev. Lett.* **40**, 38.
- Reynolds, W. C., and S. C. Kassinos, 1995, *Proc. R. Soc. London, Ser. A* **451**.
- Ritz, Ch. P., R. D. Bengtson, S. J. Levinson, and E. J. Powers, 1984, *Phys. Fluids* **27**, 2956.
- Ritz, Ch. P., H. Lin, T. L. Rhodes, and A. J. Wootton, 1990, *Phys. Rev. Lett.* **65**, 2543.
- Ritz, Ch. P., *et al.*, 1989, *Phys. Rev. Lett.* **62**, 1844.
- Rogers, B. N., J. F. Drake, and A. Zeiler, 1998, *Phys. Rev. Lett.* **81**, 4396.
- Rosenbluth, M. N., and F. L. Hinton, 1998, *Phys. Rev. Lett.* **80**, 724.
- Sakai, O., Y. Yasaka, and R. Itatani, 1993, *Phys. Rev. Lett.* **70**, 4071.
- Sarff, J. S., N. E. Lanier, S. C. Prager, and M. R. Stoneking, 1997, *Phys. Rev. Lett.* **78**, 62.
- Savill, A. M., 1987, *Annu. Rev. Fluid Mech.* **19**, 531.
- Sengoku, S., *et al.*, 1987, *Phys. Rev. Lett.* **59**, 450.
- Shaing, K. C., A. Y. Aydemir, W. A. Houlberg, and M. C. Zarnstorff, 1998, *Phys. Rev. Lett.* **80**, 5353.
- Shaing, K. C., and E. C. Crume, 1989, *Phys. Rev. Lett.* **63**, 2369.
- Shaing, K. C., E. J. Crume, and W. A. Houlberg, 1990, *Phys. Fluids B* **2**, 1492.
- Shaing, K. C., and S. P. Hirshman, 1989, *Phys. Fluids B* **1**, 705.
- Shepherd, T. G., 1987, *J. Fluid Mech.* **183**, 467.
- Shumlak, U., and C. W. Hartman, 1995, *Phys. Rev. Lett.* **75**, 3285.
- Shumlak, U., and C. W. Hartman, 1996, *Phys. Rev. Lett.* **76**, 2199.
- Shumlak, U., and N. F. Roderick, 1998, *Phys. Plasmas* **5**, 2384.
- Smedman, A.-S., H. Bergström, and U. Högrström, 1995, *Boundary-Layer Meteorol.* **76**, 211.
- Song, B., and A. K. Sen, 1994, *Phys. Rev. Lett.* **72**, 92.
- Springer, T. E., 1969, *Phys. Rev. Lett.* **22**, 1770.
- Staebler, G. M., and R. R. Dominguez, 1991, *Nucl. Fusion* **31**, 1891.
- Staebler, G. M., F. L. Hinton, J. C. Wiley, R. R. Dominguez, C. M. Greenfield, P. Gohil, T. K. Kurki-Suonio, and T. H. Osborne, 1994, *Phys. Plasmas* **1**, 909.
- Stambaugh, R. D., S. M. Wolfe, R. J. Hawryluk, J. H. Harris, H. Bigrari, S. C. Prager, R. J. Goldston, R. J. Fonck, T. Ohkawa, B. G. Logan, and E. Oktay, 1990, *Phys. Fluids B* **2**, 2941.
- Steinmetz, K., *et al.*, 1987, *Phys. Rev. Lett.* **58**, 124.
- Strachan, J., *et al.*, 1987, *Phys. Rev. Lett.* **58**, 1004.
- Strait, E. J., *et al.*, 1995, *Phys. Rev. Lett.* **75**, 4421.
- Strauss, H. R., 1976, *Phys. Fluids* **19**, 134.
- Stringer, T. E., 1969, *Phys. Rev. Lett.* **22**, 1770.
- Sugama, H., and M. Wakatani, 1991, *Phys. Fluids B* **3**, 1110.
- Tajima, T., W. Horton, P. J. Morrison, J. Schutkeker, K. Kamimura, K. Mima, and Y. Abe, 1991, *Phys. Fluids B* **3**, 938.
- Taylor, J. B., 1986, *Rev. Mod. Phys.* **58**, 741.
- Taylor, R. J., M. L. Brown, B. D. Fried, H. Grote, J. R. Liberati, G. J. Morales, P. Pribyl, D. Darrow, and M. Ono, 1989, *Phys. Rev. Lett.* **63**, 2365.
- Tendler, M., and V. Rozhansky, 1992, *J. Nucl. Mater.* **196–198**, 912.
- Tennekes, H., and J. L. Lumley, 1972, *A First Course in Turbulence* (MIT, Cambridge, MA).
- Terry, P. W., 1989, *Physica D* **37**, 542.
- Terry, P. W., and P. H. Diamond, 1985, *Phys. Fluids* **28**, 1419.
- Terry, P. W., P. H. Diamond, B. A. Carreras, and K. Sidikman, 1994, in *New Ideas in Tokamak Confinement*, San Diego, edited by M. N. Rosenbluth (AIP, New York), p. 109.
- Terry, P. W., G. Fiksel, H. Ji, A. F. Almagri, M. Cekic, D. J. Den Hartog, P. H. Diamond, S. C. Prager, J. S. Sarff, W. Shen, M. Stoneking, and A. S. Ware, 1996, *Phys. Plasmas* **3**, 1999.
- Terry, P. W., and W. Horton, 1982, *Phys. Fluids* **25**, 491.
- Terry, P. W., J. N. Leboeuf, P. H. Diamond, D. R. Thayer, J. E. Sedlak, and G. S. Lee, 1988, *Phys. Fluids* **31**, 2920.
- Terry, P. W., D. E. Newman, and N. Mattor, 1992, *Phys. Fluids A* **4**, 927.
- Toi, K., *et al.*, 1994, *Plasma Phys. Controlled Fusion* **36**, A117.
- Townsend, A. A., 1976, *The Structure of Turbulent Shear Flow* (Cambridge University, Cambridge, England).
- Trepte, C. R., 1993, Ph.D. thesis (University of Wisconsin-Madison).
- Trepte, C. R., and M. H. Hitchman, 1992, *Nature (London)* **335**, 626.
- Trepte, C. R., R. E. Veiga, and M. P. McCormick, 1993, *J. Geophys. Res.* **98**, 18563.
- Tsuji, S., *et al.*, 1990, *Phys. Rev. Lett.* **64**, 1023.
- Tuck, A. F., 1989, *J. Geophys. Res.* **94**, 11687.
- Tuck, A. F., *et al.*, 1992, *J. Geophys. Res.* **97**, 7883.
- Tynan, G. R., J. Liberati, P. Pribyl, R. J. Taylor, and B. Wells, 1996, *Plasma Phys. Controlled Fusion* **38**, 1301.
- Tynan, G. R., L. Schmitz, R. W. Conn, R. Doerner, and R. Lehmer, 1992, *Phys. Rev. Lett.* **68**, 3032.
- Tynan, G. R., *et al.*, 1994, *Phys. Plasmas* **1**, 3301.
- Vershkov, V. A., 1989, *J. Nucl. Mater.* **162–164**, 195.
- Wagner, F., *et al.*, 1982, *Phys. Rev. Lett.* **49**, 1408.
- Wagner, F., *et al.*, 1984, *Phys. Rev. Lett.* **53**, 1453.
- Waltz, R. E., R. L. Dewar, and X. Garbet, 1998, *Phys. Plasmas* **5**, 1784.
- Waltz, R. E., G. D. Kerbel, and J. Milovich, 1994, *Phys. Plasmas* **1**, 2229.
- Waltz, R. E., G. D. Kerbel, J. Milovich, and G. W. Hammett, 1995, *Phys. Plasmas* **2**, 2408.
- Wang, X.-L., P. H. Diamond, and M. N. Rosenbluth, 1992, *Phys. Fluids B* **4**, 2402.
- Ware, A. S., P. H. Diamond, B. A. Carreras, J.-N. Leboeuf, and D. K. Lee, 1992, *Phys. Fluids B* **4**, 102.
- Ware, A. S., P. W. Terry, B. A. Carreras, and P. H. Diamond,

- 1998, *Phys. Plasmas* **5**, 173.
- Ware, A. S., P. W. Terry, P. H. Diamond, and B. A. Carreras, 1996, *Plasma Phys. Controlled Fusion* **38**, 1343.
- Ware, A. S., P. W. Terry, M. H. Hitchman, and D. E. Newman, 1995, "The Role of Shear Flow in Stratospheric Transport Barriers," in *Tenth Conference on Atmospheric and Oceanic Waves and Stability*, Big Sky, edited by J. J. Tribia (American Meteorological Society, Boston), p. 193.
- Ware, A. S., P. W. Terry, M. H. Hitchman, and D. E. Newman, 1999, "Tracer transport by β -plane turbulence in a large scale jet," University of Wisconsin, Center for Plasma Theory and Computation Report No. UW-CPTC 99-1.
- Weynants, R. R., and G. Van Oost, 1993, *Plasma Phys. Controlled Fusion* **35**, B177.
- Weynants, R. R., *et al.*, 1991, *Plasma Physics and Controlled Nuclear Fusion Research, 1990* (International Atomic Energy Agency, Vienna), Vol. 1, p. 473.
- Wootton, A. J., B. A. Carreras, H. Matsumoto, K. McGuire, W. A. Peebles, Ch. P. Ritz, P. W. Terry, and S. J. Zweben, 1990, *Phys. Fluids B* **2**, 2879.
- Zhang, Y. Z., and S. M. Majahan, 1992, *Phys. Fluids B* **4**, 1385.